

The global chemical properties of high-mass star forming clumps at different evolutionary stages

Yan-Jun Zhang^{1,2} · Jian-Jun Zhou^{1,3} · Jarken Esimbek^{1,3} · Yu-Xin He^{1,2} · Da-Lei Li^{1,2} ·
Xin-Di Tang^{1,3} · Wei-Guang Ji^{1,3} · Ye Yuan^{1,3} · Wei-Hua Guo^{1,2}

Received: 17 March 2016 / Accepted: 3 May 2016 / Published online: 17 May 2016
© Springer Science+Business Media Dordrecht 2016

Abstract A total of 197 relatively isolated high-mass star-forming clumps were selected from the Millimeter Astronomy Legacy Team 90 GHz (MALT90) survey data and their global chemical evolution investigated using four molecular lines, N₂H⁺ (1–0), HCO⁺ (1–0), HCN (1–0), and HNC (1–0). The results suggest that the global averaged integrated intensity ratios $I(\text{HCO}^+)/I(\text{HCN})$, $I(\text{HCN})/I(\text{HNC})$, $I(\text{N}_2\text{H}^+)/I(\text{HCO}^+)$, and $I(\text{N}_2\text{H}^+)/I(\text{HCN})$ are promising tracers for evolution of high-mass star-forming clumps. The global averaged column densities and abundances of N₂H⁺, HCO⁺, HCN, and HNC increase as clumps evolve. The global averaged abundance ratios $X(\text{HCN})/X(\text{HNC})$ could be used to trace evolution of high-mass star forming clumps, $X(\text{HCO}^+)/X(\text{HNC})$ is more suitable for distinguishing high-mass star-forming clumps in prestellar (stage A) from those in protostellar (stage B) and HII/PDR region (stage C). These results suggest that the global averaged integrated intensity ratios between HCN (1–0), HNC (1–0), HCO⁺ (1–0) and N₂H⁺ (1–0) are more suitable for tracing the evolution of high-mass star forming clumps. We also studied the chemical properties of the target high-mass star-forming clumps in each spiral arm of the Galaxy, and got results very different from those above. This is probably due to the relatively small sample in each spiral arm. For high-mass star-forming clumps in Sagittarius arm

and Norma-Outer arm, comparing two groups located on one arm with different Galactocentric distances, the clumps near the Galactic Center appear to be younger than those far from the Galactic center, which may be due to more dense gas concentrated near the Galactic Center, and hence more massive stars being formed there.

Keywords Astrochemistry · ISM: clouds · ISM: molecules · ISM: abundances · Stars: formation

1 Introduction

High-mass star formation and its early evolution are still poorly understood (Zinnecker and Yorke 2007; Tan et al. 2014), but chemical studies on the different evolutionary stages of high-mass star formation provide an important tool for understanding the underlying physical processes (e.g. Gerner et al. 2014). The chemical composition of molecular gas undergoing star formation is predicted to evolve due to the physical changes occurring during the star formation process. The changing physical conditions may lead to the production and destruction of different molecular species, and several theoretical models predict changing molecular abundances of low mass star forming molecular cores as they evolve from the prestellar to protostellar phase (Hoq et al. 2013). Despite the numerous dedicated studies of the chemical properties of high-mass star-forming objects, their chemical evolution is still rather poorly understood.

Many recent studies have focused on deeper understanding of the chemistry in the various evolutionary stages of high-mass star formation. Sanhueza et al. (2012) se-

✉ Y.-J. Zhang
zhangyanjun@xao.ac.cn

¹ Xinjiang Astronomical Observatory, Chinese Academy of Sciences, Urumqi 830011, P.R. China

² University of the Chinese Academy of Sciences, Beijing 100080, P.R. China

³ Key Laboratory of Radio Astronomy, Chinese Academy of Sciences, Urumqi 830011, P.R. China

lected 92 infrared dark cloud (IRDC) clumps and classified them into quiescent, intermediate, active, and red clumps. They found that column densities of N_2H^+ , HNC, HN^{13}C , HCO^+ , H^{13}CO^+ , HCN, HC_3N , HNCO , and SiO, but not that of C_2H , increase with evolution, and N_2H^+ and HCO^+ abundances also increase with evolution. $\text{N}_2\text{H}^+/\text{HCO}^+$ and $\text{N}_2\text{H}^+/\text{HNC}$ abundance ratios could act as chemical clocks, increasing with clump evolution. Hoq et al. (2013) selected 333 sources from the Millimeter Astronomy Legacy Team 90 GHz (MALT90) survey, which included 59 quiescent, 95 protostellar and 179 HII/ photodissociation region (PDR) clumps, and investigated the chemical evolution of those clumps using the N_2H^+ (1–0), HCO^+ (1–0), H^{13}CO^+ (1–0), HCN (1–0), and HNC (1–0) molecular lines. They found that both N_2H^+ and HCO^+ abundances increased as a function of evolutionary stage, whereas the integrated intensity ratios of N_2H^+ (1–0) to HCO^+ (1–0) showed no discernable trend. The HCN (1–0) to HNC (1–0) integrated intensity ratios showed marginal evidence of increase as the clumps evolved. Miettinen (2014) studied the chemical properties of 12 IR-dark and 22 IR-bright clumps using the MALT90 survey data. He found that the abundances of SiO, HNCO , and HCO^+ were higher in IR-bright clumps than IR-dark sources, reflecting a possible evolutionary trend. However, the opposite trend was found for C_2H and N_2H^+ abundances. $\text{N}_2\text{H}^+/\text{HNC}$ and HCO^+/HNC abundance ratios appeared to increase as the clumps evolved.

We note that the aforementioned studies do not always yield fully consistent results. For example, Gerner et al. (2014) and Sanhueza et al. (2012) suggested that $\text{N}_2\text{H}^+/\text{HCO}^+$ abundance ratio could act as a chemical clock for high-mass star formation, whereas Hoq et al. (2013) found that $\text{N}_2\text{H}^+/\text{HCO}^+$ abundance ratio shows no discernable trend from quiescent to protostellar, and to HII/PDR stage. HCN/HNC abundance ratios of IRDC, HMPO (high-mass protostellar object), HMC (hot molecular core) obtained by Gerner et al. (2014) were between 0.3 and 0.6, whereas the median HCN/HNC abundance ratios for IR-dark and IR-bright clumps obtained by Miettinen (2014) were 3.17 and 1.84. One possible reason may be that these studies were based on single point data or beam averaged peak data, which is not suitable for tracing chemical evolution of complete high-mass star forming regions, because the same telescope with the same beam may obtain different chemical compositions for the same source at different distances by single point observation. Therefore, it is essential to obtain a sample of relatively isolated high-mass star forming regions at different stages, and study their global physical and chemical properties by mapping observation.

In this paper, we selected 197 relatively isolated high-mass clumps at different evolutionary stages from all the MALT90 survey data and studied their chemical evolution. The goal was to characterize their global chemical properties and find chemical clocks tracing their evolution. Section 2 briefly describes the archival data, which include the MALT90 survey, APEX Telescope Large Area Survey of the Galaxy (ATLASGAL), Galactic Legacy Infrared Mid-Plane Survey Extraordinaire (GLIMPSE)/*Spitzer*, and MIPS/*Spitzer* Survey of the Galactic Plane (MIPSGAL), as well as the source sample and classification. Section 3 presents the calculated physical and chemical parameters, e.g. global averaged integrated intensities, column densities, abundances, and kinematic distances. Section 4 explores and discusses global averaged integrated intensity ratios and abundance ratios of high-mass star forming clumps at different stages for the whole sample and subsamples of each spiral arm of the Galaxy. Section 5 summarizes the outcomes.

2 Archival data

2.1 ATLASGAL survey

ATLASGAL (Schuller et al. 2009) is the first systematic survey of the inner Galactic plane in the sub-mm band.¹ This survey was performed with the Large APEX Bolometer Camera (Siringo et al. 2009), an array of 295 bolometers observing at 870 μm (345 GHz). At this wavelength the APEX Telescope has a full width at half maximum (FWHM) beam size of 19.2 arcsec. The survey region covered a Galactic longitude region of $|\ell| < 60^\circ$ and $280^\circ < \ell < 300^\circ$, and a Galactic latitude $|b| < 1.5^\circ$ and $-2^\circ < b < 1^\circ$. Urquhart et al. (2014) provided a compact source catalog of this survey, which consists of ~ 10163 massive dense clumps.

2.2 MALT90 survey

The MALT90 survey is a large international project that exploited the fast-mapping capability of the ATNF Mopra 22 m telescope and obtained 16 molecular line maps near 90 GHz for 2012 sources to characterize physical and chemical conditions of high-mass star formation regions over a wide range of evolutionary states (from Pre-stellar cores, to Proto-stellar cores, and H II regions). The sample of this survey is a subsample of the ATLASGAL catalog, with angular and spectral resolution approximately 36'' and 0.11 km s^{-1} (Jackson et al. 2013). The MALT90 data were obtained from the online archive.² We plotted the molecular maps using the

¹<http://www3.mpifr-bonn.mpg.de/div/atlasgal/>.

²<http://atoa.atnf.csiro.au/MALT90/>.

GILDAS³ package (Grenoble Image and Line Data Analysis Software).

2.3 GLIMPSE and MIPS surveys

The GLIMPSE survey⁴ is a mid-infrared survey (3.6, 4.5, 5.8, and 8.0 μm) of the inner Galaxy (Benjamin et al. 2003; Carey et al. 2009) performed with the *Spitzer* Space Telescope. The angular resolution is better than 2'' at all wavelengths. GLIMPSE covers $5^\circ \leq |\ell| \leq 65^\circ$ with $|b| \leq 1^\circ$, $2^\circ \leq |\ell| < 5^\circ$ with $|b| \leq 1.5^\circ$, and $|\ell| < 2^\circ$ with $|b| \leq 2^\circ$. The MIPS/*Spitzer* Survey⁵ of the Galactic Plane (MIPSGAL) is a survey of the same region as GLIMPSE at 24 and 70 μm, using the multiband imaging photometer aboard the *Spitzer* Space Telescope (MIPS). The angular resolution at 24 and 70 μm is 6'' and 18'' (Carey et al. 2009). Gutermuth and Heyer (2015) provided the point source catalog of the MIPS survey at 24 μm.

2.4 Source selection and classification

The MALT90 survey simultaneously mapped 16 molecular lines near 90 GHz. Miettinen (2014) provides a list of the observed lines (see Table 2 therein), and discusses the chemical properties of the molecules in detail. The present paper focuses on the N₂H⁺ (1–0), HCO⁺ (1–0), HCN (1–0), and HNC (1–0) lines, as these lines are good tracers for dense gas, and are commonly used to study chemical evolution of high-mass star-forming regions.

Due to its resistance to depletion at low temperatures and high densities, N₂H⁺ is an excellent tracer of cold and dense molecular clouds. Altogether 197 isolated clumps with a S/N ratio of > 3 in the integrated N₂H⁺ (1–0) emission were detected. Then, we obtained the integrated intensity maps of N₂H⁺ (1–0), HCO⁺ (1–0), HCN (1–0), and HNC (1–0) for each source (see Fig. 21).

Following Hoq et al. (2013), we classified the 197 clumps into prestellar, protostellar, and HII/PDR stages. Prestellar clumps show no obvious signs of embedded stars or protostars, and appear dark in the 3.6, 4.5, 8, and 24 μm bands. Eighteen out of 197 sources were classified into the prestellar stage (stage A). The remaining 179 sources showed signs of star forming activities, 74 which had unresolved emission in the MIPS 24 μm band or associated with extended 4.5 μm emission, extended green objects or green fuzzies (Cyganowski et al. 2008), were classified as protostellar (stage B). The remaining 105 sources were classified into HII/PDR stage (stage C). HII regions and photodissociation regions (PDRs) showed extended emission at 8 μm,

due to fluorescently excited polycyclic aromatic hydrocarbon (PAH) emission contained in the 8 μm band. The coordinates and evolutionary classification of the 197 sources are listed in Table 1.

3 Results

3.1 Global averaged integrated intensities and ratios

All detected N₂H⁺ (1–0), HCO⁺ (1–0), HCN (1–0), and HNC (1–0) for each clump were averaged, the global average molecular spectra of these lines obtained (see Fig. 1), and the global averaged integrated intensities for $I(N_2H^+ (1-0))$, $I(HCO^+ (1-0))$, $I(HCN (1-0))$, and $I(HNC (1-0))$, and the ratios between them were derived, as shown in Table 2. The median values of the integrated intensity and integrated intensity ratios of the clumps in each evolutionary stage were shown in Table 6.

3.2 Global averaged column densities and abundances

Following Sanhueza et al. (2012), the optical depth was derived using

$$T_{\text{mb}} = f [J(T_{\text{ex}}) - J(T_{\text{bg}})](1 - e^{-\tau_v}), \quad (1)$$

where T_{mb} is the main beam brightness temperature, f is the filling factor, τ_v is the optical depth of the line, T_{bg} is the background temperature, and $J(T) = \frac{hv}{k} \frac{1}{e^{hv/kT}-1}$, h is the Planck constant, k is the Boltzmann constant. To determine the optical depth of the line, the excitation temperature (T_{ex}), of the line was assumed to be equal to the dust temperature (T_{D}). Because our classification follows that of (Hoq et al. 2013), we use the median values of the dust temperatures (T_{D}) found by Hoq et al. (2013), for each evolutionary stage: 13.9 K, 17.9 K, and 26.0 K for stage A, B and C, respectively. The resulting optical depths of N₂H⁺ (1–0), HCO⁺ (1–0), HCN (1–0), and HNC (1–0) for all clumps are listed in Table 5. The global averaged column densities were calculated based on the global averaged molecular spectra of N₂H⁺ (1–0), HCO⁺ (1–0), HCN (1–0), and HNC (1–0) of each clump by assuming local thermodynamic equilibrium (LTE), using the following formula from Garden et al. (1991)

$$N = \frac{3k}{8\pi^3 B \mu^2 R} \frac{(T_{\text{ex}} + hB/3k)}{(J+1)} \frac{\exp(E_J/kT_{\text{ex}})}{[1 - \exp(-hv/kT_{\text{ex}})]} \times \int \tau_v dv, \quad (2)$$

where v is the transition frequency and the filling factor is assumed as 1, τ_v is the optical depth of the line, μ is the permanent dipole moment of the molecule, and R is the relative intensity of the brightest hyperfine transition with

³<http://iram.fr/IRAMFR/GILDAS/>.

⁴<http://irsa.ipac.caltech.edu/data/SPITZER/GLIMPSE/>.

⁵<http://irsa.ipac.caltech.edu/data/SPITZER/MIPSGAL/>.

Table 1 Source information

Source name (1)	<i>l</i> (°) (2)	<i>b</i> (°) (3)	Stage (4)	Δv (N ₂ H ⁺) (km s ⁻¹) (5)	<i>V</i> _{LSR} (km s ⁻¹) (6)
G000.006+00.156	000.006	+00.156	C	-6.42 (0.03)	1.13 (0.06)
G000.053-00.209	000.053	-00.209	C	14.17 (0.03)	2.02 (0.07)
G000.208-00.518	000.208	-00.518	B	-1.43 (0.06)	2.76 (0.14)
G000.410-00.504	000.410	-00.504	C	20.29 (0.06)	2.50 (0.13)
G000.633+00.601	000.633	+00.601	C	-1.10 (0.04)	1.51 (0.11)
G000.766-00.248	000.766	-00.248	B	-47.97 (0.02)	2.94 (0.04)
G000.836+00.183	000.836	+00.183	C	5.84 (0.12)	2.47 (0.25)
G002.534+00.200	002.534	+00.200	B	9.71 (0.03)	2.13 (0.08)
G002.615+00.135	002.615	+00.135	C	96.75 (0.12)	3.59 (0.19)
G002.623+00.237	002.623	+00.237	B	6.51 (0.03)	1.96 (0.06)
G003.274+00.582	003.274	+00.582	B	45.46 (0.48)	17.98 (0.95)
G003.309+00.333	003.309	+00.333	B	83.49 (0.35)	10.98 (0.72)
G003.309-00.399	003.309	-00.399	B	6.36 (0.06)	2.97 (0.10)
G003.350-00.077	003.350	-00.077	C	8.43 (0.21)	5.29 (0.28)
G003.415-00.354	003.415	-00.354	B	-24.88 (0.05)	3.62 (0.08)
G003.436-00.572	003.436	-00.572	A	2.67 (0.04)	1.54 (0.10)
G004.627-00.665	004.627	-00.665	B	9.70 (0.04)	2.00 (0.08)
G004.827+00.231	004.827	+00.231	B	13.62 (0.03)	1.95 (0.07)
G004.895-00.127	004.895	-00.127	A	9.14 (0.02)	1.57 (0.06)
G005.505-00.245	005.505	-00.245	A	21.66 (0.06)	2.54 (0.12)
G005.615-00.092	005.615	-00.092	B	-26.13 (0.04)	3.01 (0.10)
G005.637+00.238	005.637	+00.238	C	8.21 (0.02)	1.76 (0.04)
G005.831-00.512	005.831	-00.512	C	16.36 (0.03)	1.89 (0.06)
G005.893-00.320	005.893	-00.320	C	10.23 (0.03)	1.83 (0.06)
G006.119-00.636	006.119	-00.636	C	16.39 (0.10)	3.22 (0.16)
G006.188-00.358	006.188	-00.358	C	-32.68 (0.04)	2.70 (0.07)
G006.216-00.609	006.216	-00.609	B	18.60 (0.02)	2.03 (0.05)
G006.551-00.097	006.551	-00.097	C	14.95 (0.16)	5.21 (0.23)
G006.796-00.256	006.796	-00.256	C	21.48 (0.02)	2.62 (0.04)
G007.333-00.567	007.333	-00.567	B	20.48 (0.05)	1.96 (0.19)
G007.632-00.109	007.632	-00.109	A	153.90 (0.05)	2.44 (0.11)
G007.993-00.269	007.993	-00.269	B	39.80 (0.04)	2.39 (0.07)
G008.049-00.244	008.049	-00.244	C	39.83 (0.07)	1.53 (0.17)
G008.206+00.190	008.206	+00.190	B	18.89 (0.05)	1.94 (0.11)
G008.350-00.317	008.350	-00.317	C	38.72 (0.04)	2.07 (0.09)
G008.458-00.224	008.458	-00.224	B	37.54 (0.03)	1.97 (0.07)
G008.955-00.535	008.955	-00.535	A	20.54 (0.12)	3.90 (0.20)
G009.037-00.521	009.037	-00.521	B	37.07 (0.04)	2.13 (0.12)
G009.212-00.202	009.212	-00.202	C	42.44 (0.02)	2.37 (0.04)
G009.283-00.149	009.283	-00.149	B	41.29 (0.02)	2.00 (0.05)
G009.422-00.704	009.422	-00.704	B	19.45 (0.05)	2.72 (0.10)
G009.620+00.195	009.620	+00.195	C	4.21 (0.04)	3.22 (0.07)
G009.877-00.748	009.877	-00.748	C	28.18 (0.02)	2.56 (0.03)
G010.473+00.028	010.473	+00.028	C	66.98 (0.06)	5.72 (0.10)
G010.624-00.383	010.624	-00.383	C	-2.58 (0.03)	2.95 (0.06)
G010.630-00.510	010.630	-00.510	C	-2.94 (0.05)	2.39 (0.12)
G010.661+00.080	010.661	+00.080	A	20.95 (0.11)	3.18 (0.21)
G010.680-00.027	010.680	-00.027	C	50.97 (0.09)	2.70 (0.16)
G010.724-00.332	010.724	-00.332	C	-1.45 (0.03)	1.94 (0.08)

Table 1 (Continued)

Source name (1)	<i>l</i> (°) (2)	<i>b</i> (°) (3)	Stage (4)	Δv (N ₂ H ⁺) (km s ⁻¹) (5)	<i>V</i> _{LSR} (km s ⁻¹) (6)
G010.746+00.015	010.746	+00.015	A	32.14 (0.04)	2.16 (0.06)
G011.033+00.061	011.033	+00.061	C	15.32 (0.29)	6.17 (0.53)
G011.112-00.399	011.112	-00.399	C	-0.23 (0.03)	3.05 (0.05)
G011.903-00.140	011.903	-00.140	B	37.80 (0.07)	3.52 (0.12)
G011.942-00.156	011.942	-00.156	C	42.72 (0.08)	3.74 (0.14)
G012.200-00.033	012.200	-00.033	B	51.11 (0.05)	2.72 (0.10)
G012.418+00.506	012.418	+00.506	C	18.05 (0.03)	2.64 (0.06)
G012.497-00.222	012.497	-00.222	B	35.70 (0.03)	1.89 (0.07)
G012.625-00.017	012.625	-00.017	B	21.69 (0.03)	2.49 (0.06)
G012.680-00.180	012.680	-00.180	C	55.47 (0.04)	3.72 (0.10)
G012.774+00.337	012.774	+00.337	C	18.26 (0.04)	1.54 (0.08)
G012.805-00.318	012.805	-00.318	B	13.73 (0.03)	1.89 (0.06)
G012.905-00.030	012.905	-00.030	B	56.58 (0.02)	2.09 (0.05)
G012.999-00.357	012.999	-00.357	C	15.05 (0.05)	3.40 (0.09)
G013.131-00.150	013.131	-00.150	C	45.09 (0.03)	1.72 (0.06)
G013.209-00.141	013.209	-00.141	C	51.43 (0.03)	3.08 (0.06)
G013.657-00.599	013.657	-00.599	C	47.91 (0.03)	2.75 (0.06)
G013.904-00.512	013.904	-00.512	B	23.01 (0.05)	1.58 (0.16)
G014.101+00.086	014.101	+00.086	C	8.65 (0.10)	3.79 (0.16)
G014.226-00.511	014.226	-00.511	C	19.85 (0.03)	1.97 (0.06)
G014.245-00.071	014.245	-00.071	C	60.75 (0.12)	4.18 (0.19)
G014.606+00.014	014.606	+00.014	C	25.44 (0.08)	4.05 (0.12)
G014.632+00.308	014.632	+00.308	C	26.19 (0.04)	1.71 (0.10)
G014.777-00.486	014.777	-00.486	B	21.96 (0.04)	1.35 (0.09)
G340.054-00.244	340.054	-00.244	C	-53.10 (0.03)	2.98 (0.05)
G340.104-00.313	340.104	-00.313	C	-53.41 (0.04)	1.57 (0.10)
G340.229-00.144	340.229	-00.144	A	-50.99 (0.09)	3.18 (0.15)
G340.261+00.532	340.261	+00.532	C	-57.06 (0.06)	2.09 (0.12)
G340.311-00.436	340.311	-00.436	B	-47.96 (0.06)	2.11 (0.14)
G340.632-00.648	340.632	-00.648	B	-87.39 (0.06)	2.21 (0.13)
G340.764-00.132	340.764	-00.132	B	-39.69 (0.04)	1.93 (0.09)
G340.776-00.119	340.776	-00.119	B	-39.74 (0.03)	1.82 (0.06)
G340.785-00.097	340.785	-00.097	B	-101.3 (0.04)	2.22 (0.10)
G340.878-00.374	340.878	-00.374	C	-43.47 (0.05)	3.14 (0.08)
G340.934-00.233	340.934	-00.233	B	-45.49 (0.05)	2.89 (0.09)
G341.034-00.114	341.034	-00.114	A	-42.82 (0.03)	1.40 (0.07)
G341.038-00.113	341.038	-00.113	A	-42.93 (0.04)	1.76 (0.08)
G341.127-00.350	341.127	-00.350	C	-41.77 (0.07)	2.77 (0.11)
G342.484+00.183	342.484	+00.183	C	-41.71 (0.03)	1.88 (0.07)
G342.706+00.125	342.706	+00.125	C	-41.39 (0.02)	3.07 (0.04)
G342.822+00.382	342.822	+00.382	B	-81.80 (0.04)	2.41 (0.08)
G342.824+00.381	342.824	+00.381	B	-81.79 (0.03)	2.41 (0.07)
G343.127-00.063	343.127	-00.063	B	-30.51 (0.03)	3.24 (0.04)
G343.134-00.484	343.134	-00.484	B	-35.85 (0.05)	2.73 (0.08)
G343.353-00.071	343.353	-00.071	B	-121.1 (0.04)	2.73 (0.07)
G343.478-00.023	343.478	-00.023	C	-27.97 (0.03)	2.73 (0.05)
G343.492-00.068	343.492	-00.068	C	-28.30 (0.03)	1.61 (0.07)
G343.520-00.519	343.520	-00.519	B	-35.04 (0.02)	2.60 (0.04)
G343.689-00.018	343.689	-00.018	C	-34.68 (0.05)	2.14 (0.12)

Table 1 (Continued)

Source name (1)	<i>l</i> (°) (2)	<i>b</i> (°) (3)	Stage (4)	Δv (N ₂ H ⁺) (km s ⁻¹) (5)	<i>V</i> _{LSR} (km s ⁻¹) (6)
G343.720-00.223	343.720	-00.223	C	-27.22 (0.03)	1.92 (0.06)
G343.738-00.112	343.738	-00.112	B	-27.26 (0.04)	2.35 (0.10)
G343.780-00.235	343.780	-00.235	B	-27.62 (0.02)	1.87 (0.03)
G344.915-00.229	344.915	-00.229	B	-85.55 (0.06)	1.99 (0.17)
G345.259-00.035	345.259	-00.035	B	-18.25 (0.04)	2.12 (0.09)
G345.261-00.418	345.261	-00.418	C	-26.08 (0.06)	2.06 (0.13)
G346.078-00.056	346.078	-00.056	C	-84.05 (0.05)	2.78 (0.09)
G346.307+00.114	346.307	+00.114	C	-27.95 (0.04)	1.74 (0.09)
G346.369-00.648	346.369	-00.648	B	5.80 (0.01)	0.41 (0.02)
G346.484+00.220	346.484	+00.220	A	-16.43 (0.05)	2.53 (0.12)
G347.294+00.132	347.294	+00.132	B	-88.88 (0.07)	3.77 (0.11)
G347.627+00.149	347.627	+00.149	C	-94.51 (0.06)	4.68 (0.09)
G347.645+00.143	347.645	+00.143	C	-94.29 (0.13)	4.07 (0.15)
G347.682+00.207	347.682	+00.207	C	-73.09 (0.14)	4.96 (0.24)
G347.871+00.014	347.871	+00.014	C	-31.28 (0.10)	4.32 (0.15)
G347.967-00.434	347.967	-00.434	C	-96.05 (0.03)	2.72 (0.05)
G348.228+00.413	348.228	+00.413	C	-7.00 (0.02)	1.60 (0.05)
G348.290+00.643	348.290	+00.643	B	-7.31 (0.04)	1.36 (0.12)
G348.777+00.149	348.777	+00.149	B	-66.40 (0.13)	3.77 (0.21)
G348.892-00.179	348.892	-00.179	C	8.05 (0.08)	2.93 (0.14)
G349.137+00.024	349.137	+00.024	C	17.38 (0.10)	4.03 (0.16)
G350.014+00.434	350.014	+00.434	C	-31.04 (0.08)	2.60 (0.15)
G350.111+00.092	350.111	+00.092	C	-69.79 (0.11)	4.65 (0.19)
G350.183+00.003	350.183	+00.003	C	-67.28 (0.07)	4.97 (0.12)
G350.271-00.500	350.271	-00.500	A	-22.75 (0.03)	1.43 (0.08)
G350.412-00.062	350.412	-00.062	A	-27.03 (0.03)	1.91 (0.08)
G350.506+00.958	350.506	+00.958	C	-11.13 (0.02)	1.60 (0.05)
G350.522-00.349	350.522	-00.349	C	-22.76 (0.03)	1.92 (0.07)
G350.687-00.491	350.687	-00.491	C	-17.87 (0.02)	2.16 (0.05)
G350.688-00.489	350.688	-00.489	C	-17.83 (0.03)	2.04 (0.05)
G350.710+01.027	350.710	+01.027	C	-3.81 (0.03)	1.45 (0.06)
G350.763+00.793	350.763	+00.793	C	-4.75 (0.03)	1.11 (0.07)
G351.040-00.336	351.040	-00.336	C	-17.97 (0.02)	2.46 (0.04)
G351.532-00.557	351.532	-00.557	B	-22.41 (0.02)	2.02 (0.05)
G351.582-00.352	351.582	-00.352	C	-95.47 (0.06)	4.19 (0.13)
G352.060+00.603	352.060	+00.603	A	1.19 (0.05)	1.57 (0.12)
G352.072+00.679	352.072	+00.679	B	1.93 (0.03)	2.07 (0.06)
G352.142-01.016	352.142	-01.016	B	-12.16 (0.04)	2.43 (0.08)
G352.233-00.162	352.233	-00.162	C	-91.32 (0.07)	3.12 (0.13)
G352.315-00.443	352.315	-00.443	C	-10.39 (0.04)	2.86 (0.08)
G352.492+00.796	352.492	+00.796	C	-1.80 (0.02)	2.17 (0.04)
G352.518-00.155	352.518	-00.155	C	-51.39 (0.27)	5.82 (0.37)
G352.684-00.120	352.684	-00.120	C	-81.20 (0.05)	1.43 (0.15)
G352.857-00.203	352.857	-00.203	C	-56.55 (0.04)	3.14 (0.07)
G352.972+00.925	352.972	+00.925	C	-4.40 (0.03)	1.40 (0.08)
G353.010+00.983	353.010	+00.983	C	-3.73 (0.06)	2.23 (0.13)
G353.115+00.366	353.115	+00.366	C	-2.06 (0.02)	1.79 (0.06)
G353.146+00.663	353.146	+00.663	C	-4.26 (0.11)	2.93 (0.21)
G353.147+00.851	353.147	+00.851	C	-8.84 (0.03)	1.90 (0.08)

Table 1 (Continued)

Source name (1)	<i>l</i> (°) (2)	<i>b</i> (°) (3)	Stage (4)	Δv (N ₂ H ⁺) (km s ⁻¹) (5)	<i>V</i> _{LSR} (km s ⁻¹) (6)
G353.198+00.927	353.198	+00.927	C	-4.31 (0.04)	1.43 (0.08)
G353.215-00.247	353.215	-00.247	C	-16.72 (0.08)	1.98 (0.20)
G353.271+00.641	353.271	+00.641	C	-4.11 (0.03)	1.76 (0.06)
G353.462+00.563	353.462	+00.563	B	-46.21 (0.02)	2.08 (0.05)
G353.547-00.019	353.547	-00.019	C	-58.02 (0.15)	3.65 (0.30)
G353.577+00.661	353.577	+00.661	B	-0.96 (0.04)	1.80 (0.08)
G353.975+00.256	353.975	+00.256	B	2.69 (0.02)	0.94 (0.07)
G354.206-00.038	354.206	-00.038	C	-29.43 (0.06)	2.46 (0.13)
G354.207-00.036	354.207	-00.036	C	-29.41 (0.06)	2.83 (0.10)
G354.628-00.610	354.628	-00.610	A	-21.81 (0.05)	2.16 (0.10)
G354.813+00.976	354.813	+00.976	B	-21.81 (0.05)	2.16 (0.10)
G354.945-00.539	354.945	-00.539	C	-5.93 (0.03)	1.86 (0.07)
G355.182-00.419	355.182	-00.419	B	-2.84 (0.02)	2.69 (0.04)
G355.249+00.363	355.249	+00.363	B	69.04 (0.27)	6.46 (0.59)
G355.265-00.269	355.265	-00.269	B	-2.57 (0.04)	3.00 (0.07)
G355.344+00.148	355.344	+00.148	C	14.32 (0.30)	4.76 (0.59)
G355.412+00.103	355.412	+00.103	B	4.89 (0.04)	1.95 (0.08)
G355.589-00.035	355.589	-00.035	B	-18.73 (0.13)	3.42 (0.24)
G355.740+00.655	355.740	+00.655	B	-33.81 (0.03)	1.59 (0.06)
G355.829-00.501	355.829	-00.501	C	-2.83 (0.08)	2.64 (0.14)
G355.935-00.346	355.935	-00.346	B	-7.29 (0.05)	1.59 (0.15)
G356.008-00.424	356.008	-00.424	B	-0.46 (0.08)	2.35 (0.21)
G356.008-00.758	356.008	-00.758	C	-3.60 (0.05)	1.58 (0.11)
G356.255-00.056	356.255	-00.056	C	-5.07 (0.07)	2.12 (0.19)
G356.305-00.204	356.305	-00.204	C	-8.49 (0.07)	2.28 (0.17)
G356.344-00.068	356.344	-00.068	B	-55.24 (0.06)	2.91 (0.10)
G356.372+00.567	356.372	+00.567	B	-4.37 (0.06)	1.80 (0.13)
G356.482+00.190	356.482	+00.190	B	-5.20 (0.03)	1.73 (0.07)
G356.517+00.664	356.517	+00.664	B	-0.67 (0.04)	1.66 (0.10)
G356.662-00.265	356.662	-00.265	B	-52.60 (0.04)	2.40 (0.08)
G356.858+00.327	356.858	+00.327	B	-14.00 (0.07)	1.93 (0.14)
G357.462-00.339	357.462	-00.339	A	3.99 (0.04)	1.66 (0.12)
G357.554-00.550	357.554	-00.550	C	1.12 (0.03)	2.52 (0.06)
G357.558-00.323	357.558	-00.323	B	2.26 (0.19)	5.79 (0.28)
G357.786-00.311	357.786	-00.311	B	4.68 (0.04)	1.76 (0.08)
G357.921-00.337	357.921	-00.337	C	-1.26 (0.15)	3.73 (0.26)
G357.967-00.163	357.967	-00.163	C	-3.45 (0.08)	3.71 (0.14)
G357.998-00.154	357.998	-00.154	C	-3.89 (0.17)	4.67 (0.33)
G358.388-00.484	358.388	-00.484	C	-2.64 (0.04)	2.59 (0.09)
G358.460-00.393	358.460	-00.393	B	-3.60 (0.03)	2.63 (0.05)
G358.807-00.087	358.807	-00.087	B	-54.10 (0.08)	2.19 (0.22)
G358.980+00.083	358.980	+00.083	B	-2.15 (0.04)	1.62 (0.09)
G359.210-00.076	359.210	-00.076	C	31.91 (0.56)	18.74 (1.13)
G359.469-00.035	359.469	-00.035	A	-1.63 (0.02)	1.58 (0.08)
G359.716-00.375	359.716	-00.375	C	17.24 (0.03)	1.76 (0.07)
G359.733+00.005	359.733	+00.005	C	70.78 (0.17)	11.50 (0.35)
G359.742+00.027	359.742	+00.027	A	-83.67 (0.51)	24.35 (0.89)
G359.911-00.305	359.911	-00.305	B	16.62 (0.04)	1.69 (0.09)
G359.941+00.173	359.941	+00.173	C	15.08 (0.08)	2.46 (0.17)
G359.944+00.152	359.944	+00.152	C	15.00 (0.11)	3.02 (0.23)

This table lists the information of the all 197 sources. Column 1 is the source name; Columns 2 and 3 are the Galactic longitude and the Galactic latitude; Column 4 lists the evolutionary classifications of the 197 sources; Column 5 lists the full line widths at half maximum (FWHM) of N₂H⁺ (1–0); Column 6 lists the local standard of rest (LSR) velocities of N₂H⁺ (1–0).

Table 2 Integrated intensities and integrated intensity ratio

Source name (1)	Integrated intensities				Integrated intensity ratio					
	$I(N_2H^+)$ (K km s $^{-1}$) (2)	$I(HCO^+)$ (K km s $^{-1}$) (3)	$I(HCN)$ (K km s $^{-1}$) (4)	$I(HNC)$ (K km s $^{-1}$) (5)	$I(N_2H^+)/I(HCO^+)$ (6)	$I(N_2H^+)/I(HCN)$ (7)	$I(N_2H^+)/I(HNC)$ (8)	$I(HCO^+)/I(HCN)$ (9)	$I(HCO^+)/I(HNC)$ (10)	$I(HCN)/I(HNC)$ (11)
G000.006+00.156	1.98	2.23	2.94	1.74	0.27	0.21	0.59	0.77	2.13	2.77
G000.053-00.209	1.86	1.90	1.87	1.48	0.31	0.31	0.52	1.00	1.70	1.70
G000.208-00.518	2.88	2.82	1.88	2.41	3.53	2.82	1.41	0.80	0.40	0.50
G000.410-00.504	1.83	2.50	2.46	2.20	0.40	0.28	0.59	0.71	1.49	2.09
G000.633+00.601	1.47	1.49	1.59	1.05	0.22	0.19	0.88	0.85	3.99	4.71
G000.766-00.248	3.22	1.63	1.69	1.86	5.18	12.00	1.46	2.32	0.28	0.12
G000.836+00.183	1.44	1.16	1.38	1.25	2.39	0.92	0.68	0.38	0.29	0.74
G002.534+00.200	2.78	2.42	1.59	1.72	0.71	1.99	1.57	2.81	2.21	0.79
G002.615+00.135	1.73	1.68	1.72	1.58	0.90	1.16	1.75	1.29	1.95	1.51
G002.623+00.237	2.22	1.68	1.63	1.84	0.83	2.16	1.00	2.60	1.21	0.47
G003.274+00.582	1.86	3.42	4.05	1.89	0.21	0.18	0.86	0.87	4.02	4.65
G003.309+00.333	2.00	1.84	3.55	2.10	0.39	0.20	0.68	0.51	1.73	3.38
G003.309-00.399	3.06	2.07	2.01	2.13	1.84	1.59	2.32	0.86	1.26	1.46
G003.350-00.077	1.93	1.56	1.71	2.16	3.60	1.93	0.64	0.54	0.18	0.33
G003.415-00.354	3.43	2.82	2.01	2.60	0.98	2.52	1.11	2.58	1.14	0.44
G003.436-00.572	2.06	1.38	1.50	1.59	2.98	1.74	1.80	0.59	0.60	1.03
G004.627-00.665	2.00	1.53	1.46	1.59	0.85	2.94	1.22	3.44	1.43	0.42
G004.827+00.231	1.78	1.61	1.47	1.36	0.80	0.96	1.16	1.19	1.45	1.21
G004.895-00.127	2.24	2.27	1.41	1.88	0.45	2.34	0.94	5.17	2.07	0.40
G005.505-00.245	1.57	1.20	1.11	1.26	9.37	11.04	1.88	1.18	0.20	0.17
G005.615-00.092	2.20	2.00	1.57	1.39	0.58	1.13	1.91	1.96	3.30	1.68
G005.637+00.238	2.92	2.76	2.39	2.20	0.80	0.91	0.90	1.14	1.12	0.99
G005.831-00.512	3.24	4.16	2.69	2.46	0.32	0.60	0.78	1.87	2.44	1.30
G005.893-00.320	2.18	2.53	2.15	1.73	0.46	0.57	0.97	1.23	2.10	1.71
G006.119-00.636	1.77	2.69	3.17	1.94	0.20	0.16	0.51	0.80	2.50	3.14
G006.188-00.358	3.34	3.14	2.99	2.50	0.79	0.62	1.27	0.79	1.60	2.03
G006.216-00.609	2.85	2.55	3.04	2.02	0.41	0.32	0.68	0.79	1.66	2.11
G006.551-00.097	1.77	1.25	1.40	1.30	0.93	0.65	1.11	0.70	1.19	1.70
G006.796-00.256	3.07	1.89	2.32	2.21	1.19	0.87	1.05	0.73	0.89	1.21
G007.333-00.567	2.01	1.85	2.23	1.69	0.48	0.18	0.68	0.37	1.41	3.79
G007.632-00.109	2.56	1.52	1.49	1.79	1.21	18.95	0.38	15.68	0.31	0.02
G007.993-00.269	3.32	3.00	3.28	2.27	0.37	0.26	0.56	0.70	1.49	2.11
G008.049-00.244	1.39	2.17	1.98	1.48	0.25	0.42	0.74	1.67	2.90	1.74
G008.206+00.190	1.54	1.34	1.64	1.19	0.37	0.18	0.62	0.48	1.66	3.47
G008.350-00.317	1.74	3.00	3.19	1.93	0.19	0.18	0.38	0.96	1.99	2.08
G008.458-00.224	1.91	2.82	1.93	1.57	0.30	0.48	0.75	1.61	2.53	1.57
G008.955-00.535	1.66	1.20	1.51	1.28	16.82	0.59	1.47	0.04	0.09	2.50
G009.037-00.521	1.75	1.60	1.43	1.44	0.42	1.18	2.09	2.82	5.00	1.77
G009.212-00.202	2.81	3.48	1.93	1.84	0.53	1.03	1.52	1.96	2.88	1.47
G009.283-00.149	2.18	2.46	1.64	1.58	0.54	1.08	1.59	1.99	2.92	1.47
G009.422-00.704	1.05	1.16	0.96	1.06	0.35	0.65	0.54	1.86	1.53	0.83
G009.620+00.195	3.04	3.15	3.30	2.71	0.51	0.52	0.63	1.02	1.23	1.20
G009.877-00.748	3.95	2.93	2.83	2.06	0.77	0.76	1.57	0.99	2.03	2.05
G010.473+00.028	4.78	5.61	4.50	3.66	0.50	0.64	0.98	1.28	1.98	1.55
G010.624-00.383	3.71	8.24	9.86	5.03	0.25	0.22	0.46	0.88	1.82	2.07
G010.630-00.510	1.94	2.38	1.97	1.65	0.31	0.46	1.11	1.48	3.61	2.44
G010.661+00.080	1.99	1.96	1.56	1.93	0.42	2.64	0.61	6.38	1.48	0.23
G010.680-00.027	1.86	1.54	1.48	1.42	1.29	1.65	0.79	1.28	0.61	0.48
G010.724-00.332	2.17	2.33	2.03	1.73	0.25	0.32	0.95	1.30	3.84	2.95
G010.746+00.015	1.71	1.52	1.37	1.54	0.42	1.03	0.77	2.44	1.83	0.75

Table 2 (Continued)

Source name (1)	Integrated intensities				Integrated intensity ratio					
	$I(N_2H^+)$ (K km s $^{-1}$) (2)	$I(HCO^+)$ (K km s $^{-1}$) (3)	$I(HCN)$ (K km s $^{-1}$) (4)	$I(HNC)$ (K km s $^{-1}$) (5)	$\frac{I(N_2H^+)}{I(HCO^+)}$ (6)	$\frac{I(N_2H^+)}{I(HCN)}$ (7)	$\frac{I(N_2H^+)}{I(HNC)}$ (8)	$\frac{I(HCO^+)}{I(HCN)}$ (9)	$\frac{I(HCO^+)}{I(HNC)}$ (10)	$\frac{I(HCN)}{I(HNC)}$ (11)
G011.033+00.061	1.81	1.32	1.25	1.24	0.77	3.74	4.29	4.85	5.56	1.15
G011.112-00.399	3.38	2.54	1.89	1.92	1.12	1.93	2.14	1.73	1.92	1.11
G011.903-00.140	2.09	1.45	1.34	1.53	0.77	1.23	0.79	1.61	1.03	0.64
G011.942-00.156	2.05	2.13	1.87	1.82	0.43	0.51	0.57	1.18	1.33	1.12
G012.200-00.033	1.83	1.99	1.62	1.46	0.47	0.48	1.01	1.03	2.16	2.10
G012.418+00.506	2.73	3.43	4.21	2.78	0.27	0.24	0.56	0.89	2.13	2.39
G012.497-00.222	1.91	2.20	2.13	1.63	0.20	0.22	0.50	1.08	2.50	2.32
G012.625-00.017	3.36	2.65	2.32	2.81	1.28	2.06	1.33	1.61	1.04	0.65
G012.680-00.180	2.82	1.77	1.36	1.55	1.19	4.79	2.90	4.02	2.44	0.61
G012.774+00.337	1.79	1.96	2.57	1.75	0.34	0.23	0.55	0.68	1.62	2.37
G012.805-00.318	2.58	1.23	1.21	1.20	4.31	3.38	3.05	0.78	0.71	0.90
G012.905-00.030	2.61	1.55	1.53	1.61	0.67	1.23	1.02	1.83	1.52	0.83
G012.999-00.357	3.18	1.33	1.37	1.19	1.95	28.04	13.83	14.36	7.08	0.49
G013.131-00.150	2.18	1.70	1.50	1.59	0.30	0.39	0.39	1.31	1.30	0.99
G013.209-00.141	2.45	1.56	1.23	1.43	1.08	2.90	1.28	2.69	1.19	0.44
G013.657-00.599	2.75	2.35	2.35	6.50	0.60	1.14	4.83	1.89	8.01	4.25
G013.904-00.512	1.86	2.00	2.34	1.90	0.55	0.25	0.57	0.46	1.04	2.26
G014.101+00.086	1.81	1.66	1.62	1.40	0.25	0.54	0.50	2.19	2.03	0.92
G014.226-00.511	2.38	2.54	2.70	2.01	0.44	0.40	0.69	0.90	1.55	1.72
G014.245-00.071	1.66	1.48	1.27	1.29	0.62	3.08	0.96	4.96	1.54	0.31
G014.606+00.014	2.96	1.50	1.66	1.58	2.15	1.87	1.42	0.87	0.66	0.76
G014.632+00.308	2.67	1.83	1.77	1.78	0.58	0.86	1.03	1.49	1.79	1.20
G014.777-00.486	1.46	2.10	1.60	1.28	0.12	0.20	0.99	1.67	8.43	5.04
G340.054-00.244	2.93	4.37	3.83	2.98	0.35	0.41	0.72	1.19	2.08	1.74
G340.104-00.313	1.45	1.76	1.62	1.28	0.24	0.31	0.77	1.28	3.21	2.51
G340.229-00.144	1.76	2.83	1.80	2.36	0.18	0.37	0.25	2.11	1.41	0.67
G340.261+00.532	1.66	2.55	2.75	1.67	0.16	0.14	0.34	0.84	2.06	2.44
G340.311-00.436	1.65	1.95	1.83	1.45	0.17	0.22	0.61	1.33	3.67	2.76
G340.632-00.648	1.54	1.34	1.38	1.43	0.79	0.87	0.95	1.09	1.20	1.10
G340.764-00.132	2.32	1.56	1.42	1.41	11.88	6.27	1.40	0.53	0.12	0.22
G340.776-00.119	2.31	1.47	1.44	1.40	3.98	34.63	7.12	8.71	1.79	0.21
G340.785-00.097	2.79	2.47	2.74	2.29	0.38	0.37	0.86	0.97	2.24	2.30
G340.878-00.374	3.91	1.96	1.94	2.13	2.10	1.59	1.23	0.76	0.59	0.77
G340.934-00.233	1.94	1.80	1.33	1.41	0.49	1.40	1.48	2.86	3.03	1.06
G341.034-00.114	1.79	1.43	1.57	1.34	1.21	0.54	0.99	0.44	0.82	1.84
G341.038-00.113	1.61	1.29	1.17	1.24	1.08	2.48	1.27	2.30	1.18	0.51
G341.127-00.350	2.45	2.78	3.04	2.42	0.27	0.27	0.52	1.00	1.93	1.93
G342.484+00.183	2.92	1.94	2.09	1.61	0.47	0.44	1.00	0.93	2.13	2.30
G342.706+00.125	4.35	3.99	2.73	3.13	0.71	1.35	1.37	1.90	1.93	1.02
G342.822+00.382	2.11	2.08	1.79	1.95	0.38	1.45	0.82	3.78	2.15	0.57
G342.824+00.381	2.43	2.35	1.69	2.07	0.50	1.12	0.82	2.22	1.63	0.74
G343.127-00.063	4.43	4.22	3.80	3.26	0.62	0.95	1.10	1.53	1.79	1.16
G343.134-00.484	2.63	1.80	1.74	1.99	2.01	1.24	0.95	0.62	0.47	0.76
G343.353-00.071	2.75	2.26	2.34	1.97	0.53	1.02	0.95	1.95	1.80	0.92
G343.478-00.023	4.14	3.33	5.54	3.13	0.83	0.47	0.97	0.56	1.17	2.09
G343.492-00.068	2.97	2.08	2.82	2.29	0.70	0.47	0.98	0.67	1.40	2.07
G343.520-00.519	2.84	1.66	1.60	1.73	1.53	1.42	1.21	0.93	0.79	0.86
G343.689-00.018	2.14	1.79	2.04	1.53	1.01	0.43	0.77	0.43	0.76	1.78
G343.720-00.223	1.93	1.34	1.62	1.32	0.60	0.47	0.75	0.79	1.26	1.60
G343.738-00.112	1.87	1.69	1.69	1.74	0.42	0.39	0.35	0.93	0.84	0.90

Table 2 (Continued)

Source name (1)	Integrated intensities				Integrated intensity ratio					
	$I(\text{N}_2\text{H}^+)$ (K km s $^{-1}$) (2)	$I(\text{HCO}^+)$ (K km s $^{-1}$) (3)	$I(\text{HCN})$ (K km s $^{-1}$) (4)	$I(\text{HNC})$ (K km s $^{-1}$) (5)	$\frac{I(\text{N}_2\text{H}^+)}{I(\text{HCO}^+)}$ (6)	$\frac{I(\text{N}_2\text{H}^+)}{I(\text{HCN})}$ (7)	$\frac{I(\text{N}_2\text{H}^+)}{I(\text{HNC})}$ (8)	$\frac{I(\text{HCO}^+)}{I(\text{HCN})}$ (9)	$\frac{I(\text{HCO}^+)}{I(\text{HNC})}$ (10)	$\frac{I(\text{HCN})}{I(\text{HNC})}$ (11)
G343.780-00.235	2.71	1.98	1.70	1.93	0.94	1.82	1.27	1.94	1.35	0.70
G344.915-00.229	1.88	2.25	1.94	1.73	0.46	0.32	0.41	0.69	0.89	1.29
G345.259-00.035	2.02	1.34	1.39	1.52	11.37	2.74	0.81	0.24	0.07	0.30
G345.261-00.418	1.70	1.71	1.65	1.43	0.71	0.46	0.61	0.64	0.86	1.34
G346.078-00.056	2.74	2.05	2.00	1.88	0.57	0.61	1.36	1.07	2.37	2.22
G346.307+00.114	1.74	1.88	2.04	1.48	0.31	0.34	0.82	1.10	2.62	2.39
G346.369-00.648	2.13	1.90	1.93	1.76	1.04	2.02	1.82	1.94	1.74	0.90
G346.484+00.220	2.61	1.93	2.13	2.12	1.20	1.33	1.15	1.11	0.96	0.86
G347.294+00.132	2.60	1.81	1.61	1.70	0.66	0.69	1.07	1.04	1.62	1.56
G347.627+00.149	4.74	4.88	6.22	4.05	0.48	0.36	0.69	0.75	1.43	1.92
G347.645+00.143	3.45	4.80	5.35	3.75	0.30	0.26	0.70	0.87	2.31	2.67
G347.682+00.207	2.11	2.45	1.74	2.00	0.36	0.99	1.11	2.76	3.08	1.12
G347.871+00.014	2.59	3.03	2.58	2.39	0.33	0.50	0.81	1.54	2.48	1.61
G347.967-00.434	2.66	2.44	2.31	1.85	0.60	0.59	1.34	0.98	2.25	2.29
G348.228+00.413	3.07	3.49	4.16	2.84	0.44	0.28	0.69	0.63	1.56	2.48
G348.290+00.643	1.83	1.99	1.59	1.58	0.23	0.38	0.76	1.65	3.34	2.03
G348.777+00.149	1.77	1.32	1.19	1.29	0.37	1.41	0.93	3.83	2.53	0.66
G348.892-00.179	1.79	2.56	2.76	1.97	0.27	0.39	0.62	1.44	2.29	1.59
G349.137+00.024	3.62	5.57	4.43	3.40	0.21	0.41	1.06	1.97	5.07	2.58
G350.014+00.434	2.01	2.75	3.06	2.23	0.25	0.21	0.43	0.82	1.71	2.09
G350.111+00.092	8.61	8.63	7.22	7.22	0.43	1.16	0.84	2.71	1.97	0.73
G350.183+00.003	3.02	2.44	1.71	2.70	0.87	1.90	0.82	2.19	0.95	0.43
G350.271-00.500	2.05	1.51	1.79	1.69	0.83	0.64	0.67	0.77	0.80	1.04
G350.412-00.062	2.57	1.97	1.59	1.85	0.37	1.15	1.52	3.08	4.07	1.32
G350.506+00.958	3.66	6.50	7.77	3.00	0.12	0.09	0.33	0.77	2.75	3.58
G350.522-00.349	3.01	1.86	1.82	2.18	0.80	1.37	0.87	1.72	1.10	0.64
G350.687-00.491	2.35	2.29	1.73	1.69	0.61	1.10	2.31	1.81	3.79	2.10
G350.688-00.489	3.35	2.86	2.44	2.31	0.63	1.15	1.21	1.83	1.92	1.05
G350.710+01.027	2.30	2.05	1.98	1.66	0.37	0.33	1.23	0.88	3.29	3.75
G350.763+00.793	1.70	1.58	2.23	1.54	0.25	0.17	0.37	0.68	1.49	2.21
G351.040-00.336	3.41	2.36	2.54	2.39	1.05	1.14	1.21	1.09	1.15	1.06
G351.532-00.557	2.36	1.62	1.37	1.56	1.38	7.86	1.87	5.69	1.35	0.24
G351.582-00.352	2.65	2.98	1.71	1.94	0.93	1.78	1.67	1.92	1.80	0.94
G352.060+00.603	1.73	1.38	1.51	1.55	0.47	0.38	0.38	0.80	0.81	1.02
G352.072+00.679	2.14	2.88	1.94	1.76	0.47	0.72	0.99	1.52	2.10	1.38
G352.142-01.016	1.76	2.98	1.56	1.65	1.01	0.68	0.83	0.68	0.82	1.21
G352.233-00.162	1.98	1.69	1.61	1.55	0.45	0.58	0.69	1.29	1.53	1.19
G352.315-00.443	2.76	3.10	2.98	2.10	0.32	0.31	0.94	0.98	2.92	2.99
G352.492+00.796	3.29	2.57	2.90	2.39	0.90	0.94	1.06	1.04	1.17	1.13
G352.518-00.155	1.66	1.97	2.36	1.78	0.28	0.20	0.85	0.72	3.09	4.30
G352.684-00.120	1.67	1.79	1.98	1.72	0.35	0.24	0.48	0.69	1.36	1.98
G352.857-00.203	2.12	2.26	2.59	1.91	0.51	0.45	0.67	0.88	1.31	1.48
G352.972+00.925	2.75	3.81	4.90	2.16	0.19	0.19	0.63	1.02	3.35	3.29
G353.010+00.983	1.76	3.51	3.93	1.82	0.09	0.08	0.33	0.92	3.73	4.05
G353.115+00.366	2.49	3.11	3.54	2.18	0.27	0.24	0.61	0.91	2.30	2.52
G353.146+00.663	1.60	7.58	9.68	3.47	0.03	0.03	0.09	0.80	2.56	3.20
G353.147+00.851	2.55	3.41	4.28	2.44	0.37	0.30	0.76	0.82	2.07	2.54
G353.198+00.927	2.11	5.96	8.59	2.86	0.05	0.03	0.12	0.69	2.62	3.80
G353.215-00.247	1.80	1.78	1.67	1.31	0.17	0.32	2.50	1.82	14.47	7.95
G353.271+00.641	2.48	4.85	5.51	2.47	0.12	0.12	0.36	0.98	3.00	3.07

Table 2 (Continued)

Source name (1)	Integrated intensities				Integrated intensity ratio					
	$I(\text{N}_2\text{H}^+)$ (K km s $^{-1}$) (2)	$I(\text{HCO}^+)$ (K km s $^{-1}$) (3)	$I(\text{HCN})$ (K km s $^{-1}$) (4)	$I(\text{HNC})$ (K km s $^{-1}$) (5)	$\frac{I(\text{N}_2\text{H}^+)}{I(\text{HCO}^+)}$ (6)	$\frac{I(\text{N}_2\text{H}^+)}{I(\text{HCN})}$ (7)	$\frac{I(\text{N}_2\text{H}^+)}{I(\text{HNC})}$ (8)	$\frac{I(\text{HCO}^+)}{I(\text{HCN})}$ (9)	$\frac{I(\text{HCO}^+)}{I(\text{HNC})}$ (10)	$\frac{I(\text{HCN})}{I(\text{HNC})}$ (11)
G353.462+00.563	2.59	2.82	2.36	2.00	0.49	1.05	1.07	2.17	2.21	1.02
G353.547-00.019	1.56	2.22	2.87	1.82	0.20	0.14	0.42	0.70	2.10	3.01
G353.577+00.661	2.37	2.37	2.24	1.62	0.30	0.27	0.61	0.88	2.02	2.28
G353.975+00.256	1.98	2.05	1.88	1.80	0.77	0.75	1.11	0.98	1.44	1.48
G354.206-00.038	1.92	1.51	1.54	1.58	1.07	0.66	0.47	0.62	0.44	0.72
G354.207-00.036	2.06	1.83	1.60	1.80	0.59	0.80	1.89	1.36	3.21	2.37
G354.628-00.610	1.58	2.06	1.63	1.64	0.29	0.41	0.51	1.42	1.76	1.25
G354.813+00.976	1.75	1.33	1.30	1.20	1.84	1.04	1.39	0.57	0.76	1.34
G354.945-00.539	2.38	1.93	2.55	1.63	0.42	0.22	0.65	0.52	1.56	3.01
G355.182-00.419	3.52	3.04	2.32	2.31	0.62	0.87	1.27	1.41	2.04	1.45
G355.249+00.363	1.67	1.86	1.64	1.74	0.64	0.65	1.19	1.02	1.87	1.85
G355.265-00.269	2.34	1.83	1.49	1.48	0.52	1.04	1.50	2.00	2.88	1.44
G355.344+00.148	1.42	2.44	1.76	1.57	0.22	0.36	0.77	1.63	3.48	2.14
G355.412+00.103	2.77	1.36	1.82	1.65	2.39	1.52	1.25	0.64	0.52	0.82
G355.589-00.035	1.56	1.20	1.26	1.32	1.50	1.19	0.86	0.79	0.57	0.72
G355.740+00.655	1.72	1.61	1.58	1.73	0.79	0.87	0.71	1.10	0.90	0.82
G355.829-00.501	2.85	2.90	2.68	2.66	0.68	0.70	1.08	1.02	1.58	1.55
G355.935-00.346	1.54	1.62	1.49	1.25	0.29	0.40	0.80	1.39	2.80	2.01
G356.008-00.424	1.36	1.72	1.80	1.18	0.38	0.25	1.88	0.67	5.00	7.46
G356.008-00.758	1.71	1.99	1.70	1.74	0.37	0.52	0.77	1.40	2.06	1.47
G356.255-00.056	1.53	1.70	1.47	1.27	0.23	0.42	1.90	1.86	8.43	4.53
G356.305-00.204	1.54	1.87	1.88	1.48	0.58	0.24	1.08	0.42	1.87	4.47
G356.344-00.068	1.99	1.75	1.51	1.49	0.52	0.83	1.94	1.59	3.74	2.35
G356.372+00.567	3.42	2.66	2.60	2.52	0.64	0.52	0.55	0.81	0.87	1.07
G356.482+00.190	2.02	1.95	1.69	1.82	0.36	0.89	0.81	2.49	2.29	0.92
G356.517+00.664	1.70	1.66	1.68	1.70	0.52	0.49	0.78	0.94	1.52	1.61
G356.662-00.265	2.26	2.74	2.68	2.19	0.31	0.59	1.02	1.88	3.28	1.74
G356.858+00.327	1.29	1.48	1.50	1.26	0.38	0.45	1.16	1.20	3.05	2.55
G357.462-00.339	2.18	1.31	1.31	1.25	12.41	3.43	1.68	0.28	0.14	0.49
G357.554-00.550	3.92	4.00	3.92	3.03	0.44	0.38	0.76	0.86	1.73	2.00
G357.558-00.323	2.22	1.73	1.39	1.77	2.25	1.69	0.94	0.75	0.42	0.55
G357.786-00.311	1.76	1.54	1.23	1.34	0.66	2.55	1.56	3.88	2.37	0.61
G357.921-00.337	2.00	1.38	1.08	1.52	2.00	9.31	0.63	4.66	0.32	0.07
G357.967-00.163	2.29	1.16	1.30	1.57	19.96	2.01	2.96	0.10	0.15	1.48
G357.998-00.154	2.36	1.40	1.31	1.37	3.34	4.36	8.73	1.31	2.61	2.00
G358.388-00.484	3.32	3.08	3.54	2.46	0.59	0.53	1.07	0.89	1.80	2.02
G358.460-00.393	5.44	4.18	3.28	3.36	1.14	1.14	1.73	1.01	1.52	1.51
G358.807-00.087	1.70	1.47	1.55	1.57	0.56	6.76	1.71	12.17	3.07	0.25
G358.980+00.083	2.08	1.70	1.62	1.49	0.84	0.75	1.90	0.90	2.28	2.54
G359.210-00.076	1.88	3.18	4.23	1.86	0.21	0.15	1.04	0.73	4.93	6.79
G359.469-00.035	2.08	1.68	1.28	1.40	3.67	52.99	1.38	14.45	0.38	0.03
G359.716-00.375	2.63	3.96	5.25	2.56	0.21	0.12	0.31	0.59	1.51	2.56
G359.733+00.005	3.51	4.81	4.94	3.82	0.45	0.42	0.69	0.94	1.53	1.63
G359.742+00.027	1.98	3.62	4.38	2.54	0.23	0.12	0.53	0.53	2.32	4.40
G359.911-00.305	2.22	1.98	1.96	1.42	0.20	0.19	0.67	0.91	3.29	3.63
G359.941+00.173	2.54	2.88	2.21	1.95	0.74	0.46	1.19	0.62	1.62	2.62
G359.944+00.152	3.19	2.81	2.58	2.20	0.73	0.59	1.46	0.82	2.00	2.45

This table lists the integrated intensities of N_2H^+ (1–0), HCO^+ (1–0), HCN (1–0), HNC (1–0) and their integrated intensity ratios. Column 1 is the source name; Columns 2 to 5 list the integrated intensities of N_2H^+ (1–0), HCO^+ (1–0), HCN (1–0), HNC (1–0); Columns 6 to 11 list the integrated intensities ratios.

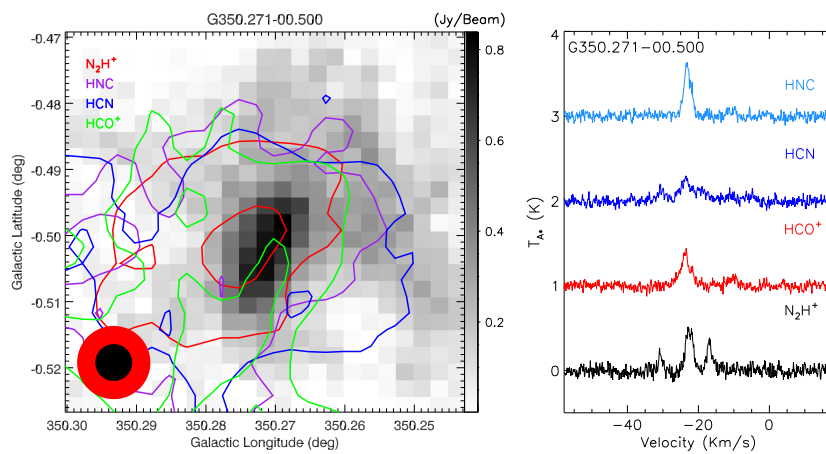


Fig. 1 This is an example of high-mass star-forming clump, G350.271-00.500. The left panel shows the contour maps for the integrated intensities of N_2H^+ (1–0), HCO^+ (1–0), HCN (1–0) and HNC (1–0) overlaid on 870 μm emission (in gray scale). The red circle in the bottom left corner represents the FWHM beam size for molecu-

lar lines, the enclosed black circle indicates the FWHM beam size of 870 μm emission observations. The right panel displays the global averaged spectra of N_2H^+ (1–0), HCO^+ (1–0), HCN (1–0) and HNC (1–0). Levels 1 and 2 of N_2H^+ (1–0), HCO^+ (1–0), HCN (1–0) and HNC (1–0) correspond to 3σ and 9σ , respectively

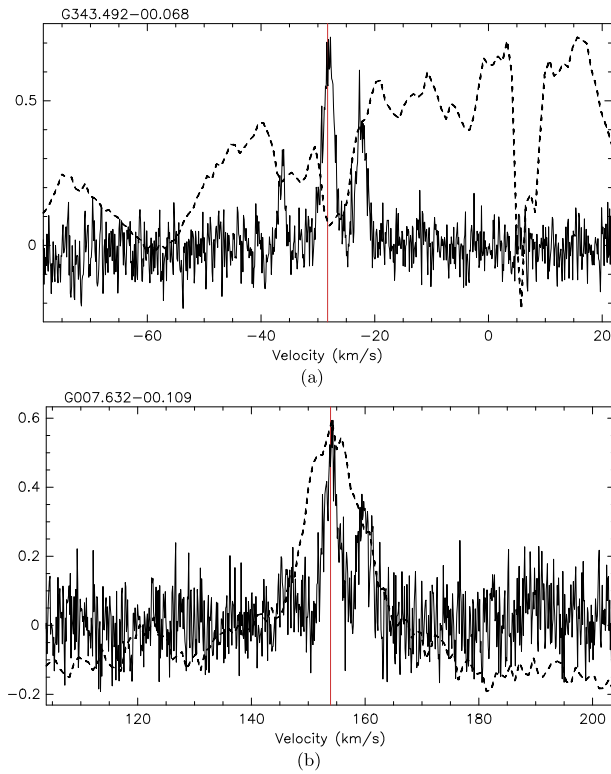


Fig. 2 Two sources located at the near (G343.492-00.068) and far (007.632-00.109) distances, their kinematic distances ambiguity was resolved by HI self-absorption. The N_2H^+ (1–0) spectra (solid black line) overlaid with the HI 21 cm spectra (bold dashed line), with the HI data scaled to the peak of N_2H^+ (1–0). The vertical solid red line indicates the velocity of the clump. HI spectra were extracted from the Southern Galactic Plane Survey (McClure-Griffiths et al. 2005) archive

respect to the others. R is only relevant for hyperfine transitions because it considers the satellite lines corrected by

their relative opacities. $R = 5/9$ for N_2H^+ , 1 for HCO^+ and HNC , and $3/5$ for HCN . J is the rotational quantum number of the lower state, $E_J = hBJ(J + 1)$ is the energy in level J , and B is the rotational constant of the linear molecule. The dipole moment and rotational constant of these four molecules are shown in Table 3. The global averaged column densities of N_2H^+ , HCO^+ , HCN , and HNC are shown in Table 4. The median column densities of the four molecules in each evolutionary stage are shown in Table 6.

The average H_2 column densities of the sources were derived using the LABOCA 870 micron flux densities over the projected area where the molecular line emission was detected via the formula, $N_{\text{H}_2} = \frac{S_{\nu} R}{B_{\nu}(T_D)\Omega_{\kappa_{\nu}}\mu m_H}$, where S_{ν} is

Table 3 Parameters used for N_2H^+ , HCO^+ , HCN and HNC column density calculation

Molecule (1)	Dipole moment μ (D) (2)	Rotational constant B (GHz) (3)	References (4)
N_2H^+	3.40	46.586871	1, 2, 3, 10
HCO^+	3.89	44.594423	4, 5, 6, 10
HCN	2.985	44.315976	9
HNC	3.05	45.331980	7, 8, 10

The values of the parameters used for N_2H^+ , HCO^+ , HCN and HNC column density calculation are listed in this table. Column 1 is the molecule; Column 2 is the dipole moment; Column 3 is the rotational constant; Column 4 lists the references

References: (1) Botschwina (1984); (2) Havenith et al. (1990); (3) Paganini et al. (2009); (4) Botschwina et al. (1993); (5) Yamaguchi et al. (1994); (6) Lattanzi et al. (2007); (7) Blackman et al. (1976); (8) van der Tak et al. (2009); (9) Ahrens et al. (2002); (10) Sanhueza et al. (2012)

Table 4 Optical depths and column densities

Source name	Optical depth	Column density						H ₂ column density					
		$\tau_{\text{N}_2\text{H}^+}$ (2)	τ_{HCO^+} (3)	τ_{HNC} (4)	$\text{N}_{\text{N}_2\text{H}^+}$ (10^{13} cm^{-2}) (6)	N_{HCO^+} (10^{13} cm^{-2}) (7)	N_{HNC} (10^{13} cm^{-2}) (8)	$\text{N}_{\text{H}_2\text{HCO}^+}$ (10^{22} cm^{-2}) (9)	$\text{N}(\text{H}_2)\text{N}_2\text{H}^+$ (10^{22} cm^{-2}) (10)	$\text{N}(\text{H}_2)\text{HCO}^+$ (10^{22} cm^{-2}) (11)	$\text{N}(\text{H}_2)\text{HNC}$ (10^{22} cm^{-2}) (12)	$\text{N}(\text{H}_2)\text{Mean}$ (10^{22} cm^{-2}) (13)	$\text{N}(\text{H}_2)\text{Mean}$ (10^{22} cm^{-2}) (14)
G000.006+00.156	1.9	2.3	1.4	1.9	0.9	3.3	1.1	6.5	3.7	3.8	4.9	4.7	4.7
G000.053-00.209	1.7	1.4	1.6	1.0	1.7	0.7	2.3	4.9	2.3	2.3	2.9	3.1	3.1
G000.208-00.518	4.3	3.4	4.7	0.6	2.2	0.8	3.3	0.2	13.3	9.5	10.3	7.7	10.2
G000.410-00.504	1.6	1.6	1.9	1.5	1.7	0.8	2.7	1.1	4.0	2.7	1.9	3.3	3.0
G000.633+00.601	1.2	1.0	1.2	0.6	1.3	0.5	1.7	0.5	4.5	1.8	1.7	2.4	2.6
G000.766-00.248	4.9	2.4	2.2	2.5	2.5	0.6	1.5	1.0	10.6	17.7	23.8	10.0	15.5
G000.836+00.183	1.1	0.9	0.9	0.6	1.1	0.4	1.3	0.4	3.1	1.1	3.1	2.0	2.4
G002.534+00.200	4.2	2.4	1.6	1.1	2.1	0.6	1.1	0.4	5.7	3.6	5.6	5.4	5.1
G002.615+00.135	1.5	1.2	1.6	1.2	1.5	0.6	2.2	0.9	4.8	4.5	5.4	6.3	5.3
G002.623+00.237	3.1	1.3	2.1	1.7	1.6	0.3	1.5	0.7	3.9	2.5	4.8	3.3	3.6
G003.274+00.582	3.8	11.2	9.7	3.0	1.9	2.7	6.9	1.1	5.7	3.8	3.7	5.3	4.6
G003.309+00.333	3.4	6.8	7.9	2.6	1.7	1.7	5.6	1.0	2.5	1.1	1.1	1.9	1.7
G003.309-00.399	4.4	1.7	2.8	2.6	2.3	0.4	2.0	1.0	7.7	7.3	6.6	9.5	7.8
G003.350-00.077	1.6	0.7	1.3	0.9	1.6	0.3	1.8	0.7	3.7	2.0	5.2	3.5	3.6
G003.415-00.354	5.6	3.0	3.4	3.2	2.9	0.7	2.4	1.2	10.4	8.7	12.8	9.1	10.3
G003.436-00.572	3.7	1.4	2.1	2.7	1.2	0.2	0.9	0.6	3.7	3.3	2.9	4.2	3.5
G004.627-00.665	2.6	1.4	1.5	1.7	1.4	0.3	1.0	0.7	2.3	1.5	2.6	2.1	2.1
G004.827+00.231	2.6	1.2	1.9	1.5	1.3	0.3	1.3	0.6	3.1	2.4	2.6	2.7	2.7
G004.895-00.127	3.9	2.8	2.1	3.1	1.3	0.4	0.9	0.7	3.2	1.5	3.4	2.7	2.7
G005.505-00.245	2.4	1.0	1.1	1.5	0.8	0.2	0.5	0.4	10.9	13.9	14.3	10.6	12.4
G005.615-00.092	3.4	2.3	2.0	1.8	1.7	0.6	1.4	0.7	3.8	2.2	3.1	4.3	3.4
G005.637+00.238	2.9	2.1	2.2	1.7	3.0	1.1	3.1	1.3	5.3	4.4	4.3	4.0	4.5
G005.831-00.512	3.1	3.1	2.2	1.7	3.2	1.5	3.1	1.3	5.7	3.0	3.4	3.9	4.0
G005.893-00.320	2.0	1.8	1.9	1.3	2.1	0.9	2.7	1.0	3.3	2.0	2.0	2.5	2.5
G006.119-00.636	1.4	2.3	2.7	1.5	1.4	1.1	3.8	1.1	4.8	2.9	2.8	4.4	3.7
G006.188-00.358	3.1	2.6	2.6	2.0	3.2	1.3	3.7	1.6	5.7	4.5	3.5	5.3	4.8
G006.216-00.609	4.3	3.3	4.1	2.7	2.2	0.8	2.9	1.0	7.7	4.5	3.9	5.1	5.3
G006.551-00.097	1.8	0.8	1.2	0.9	1.8	0.4	1.7	0.7	6.7	4.3	4.0	6.0	5.3
G006.796-00.256	3.0	1.5	2.2	1.8	3.0	0.7	3.1	1.4	4.4	3.5	3.1	3.5	3.6
G007.333-00.567	2.7	2.1	2.8	1.7	1.4	0.5	2.0	0.7	5.5	3.5	2.0	3.9	3.7
G007.632-00.109	5.0	3.4	3.5	2.7	1.6	0.5	1.6	0.6	14.5	12.4	1.8	7.2	9.0
G007.993-00.269	4.9	3.4	4.3	2.4	2.5	0.8	3.0	0.9	11.9	5.3	4.3	5.9	6.8
G008.049-00.244	1.1	1.5	1.4	0.9	1.1	0.7	2.1	0.7	1.2	0.6	1.0	1.1	1.0
G008.206+00.190	2.0	1.4	2.2	1.1	1.0	0.3	1.5	0.4	2.3	1.0	0.8	0.9	1.2

Table 4 (Continued)

Source name (1)	Optical depth $\tau_{\text{N}_2\text{H}^+}$ (2)	Column density						H ₂ column density				
		τ_{HNC} (4)	τ_{HCO^+} (3)	$\text{N}_{\text{N}_2\text{H}^+}$ (10^{13} cm $^{-2}$) (6)	N_{HCO^+} (10^{13} cm $^{-2}$) (7)	N_{HNC} (10^{13} cm $^{-2}$) (8)	$\text{N}_{\text{H}_2\text{HNC}}$ (10^{22} cm $^{-2}$) (9)	$\text{N}(\text{H}_2)\text{N}_2\text{H}^+$ (10^{22} cm $^{-2}$) (10)	$\text{N}(\text{H}_2)\text{HCO}^+$ (10^{22} cm $^{-2}$) (11)	$\text{N}(\text{H}_2)\text{HNC}$ (10^{22} cm $^{-2}$) (12)	$\text{N}(\text{H}_2)\text{Mean}$ (10^{22} cm $^{-2}$) (13)	
G008.350-00.317	1.6	2.6	2.7	1.4	1.6	1.3	3.8	1.1	2.5	1.2	1.2	1.6
G008.458-00.224	2.9	3.6	2.5	1.9	1.5	0.9	1.8	0.7	1.6	0.7	0.7	1.0
G008.955-00.535	3.3	1.2	3.7	1.5	1.1	0.2	1.7	0.4	6.8	9.5	1.7	3.5
G009.037-00.521	2.5	1.8	1.7	1.7	1.3	0.4	1.2	0.7	4.4	1.9	3.4	5.4
G009.212-00.202	2.7	2.6	1.6	1.5	2.8	1.3	2.3	1.1	2.9	2.0	2.2	2.5
G009.283-00.149	2.8	3.0	1.9	1.8	1.4	0.7	1.4	0.7	2.0	1.2	1.6	1.8
G009.422-00.704	1.4	1.4	1.3	1.2	0.7	0.3	0.9	0.5	1.3	0.4	0.7	0.8
G009.620+00.195	3.0	2.4	3.0	2.2	3.1	1.2	4.3	1.7	9.8	5.8	6.2	7.0
G009.877-00.748	4.0	2.3	2.5	1.8	4.1	1.1	3.6	1.4	5.9	3.7	3.5	4.5
G010.473+00.028	5.4	4.6	4.5	3.2	5.5	2.3	6.4	2.5	14.3	8.8	9.1	10.8
G010.624-00.383	3.5	6.9	9.3	4.3	3.6	3.4	13.3	3.3	19.3	12.1	12.6	14.3
G010.630-00.510	1.7	1.7	1.6	1.2	1.7	0.9	2.2	0.9	2.9	1.5	1.6	2.1
G010.661+00.080	3.7	2.3	2.1	2.5	1.2	0.3	0.9	0.6	4.9	2.5	1.7	3.5
G010.680-00.027	1.6	0.9	1.5	0.8	1.6	0.5	2.1	0.6	4.1	3.8	2.6	3.2
G010.724-00.332	1.8	1.7	1.7	1.4	1.8	0.8	2.4	1.1	2.9	1.4	1.5	2.1
G010.746+00.015	3.2	1.7	2.3	2.1	1.0	0.3	1.0	0.5	5.1	2.6	4.3	4.0
G011.033+00.061	1.7	0.6	0.8	0.7	1.7	0.3	1.1	0.5	2.9	1.3	1.0	4.6
G011.112-00.399	3.3	1.9	1.8	1.5	3.4	0.9	2.5	1.1	4.9	4.2	5.0	5.4
G011.903-00.140	3.3	1.9	2.2	1.9	1.7	0.5	1.5	0.7	10.1	5.9	7.8	6.6
G011.942-00.156	2.0	1.8	1.6	1.4	2.1	0.9	2.3	1.1	2.9	1.5	1.6	1.9
G012.200-00.033	2.4	2.3	2.0	1.7	1.2	0.6	1.4	0.6	5.5	3.1	2.6	4.6
G012.418+00.506	2.7	2.8	3.7	2.3	2.8	1.4	5.2	1.8	9.3	3.9	4.2	6.1
G012.497-00.222	2.9	2.8	2.7	2.1	1.5	0.7	1.9	0.8	4.8	1.1	1.2	2.3
G012.625-00.017	5.0	3.6	3.1	3.6	2.6	0.9	2.2	1.4	9.8	9.5	11.8	10.5
G012.680-00.180	3.0	1.3	2.1	1.0	3.1	0.7	3.0	0.8	8.2	6.6	8.7	9.0
G012.774+00.337	1.4	1.5	2.1	1.2	1.4	0.7	2.9	0.9	7.5	4.2	4.2	5.1
G012.805-00.318	3.6	2.4	2.2	0.8	1.8	0.6	1.6	0.3	5.6	2.8	3.8	4.5
G012.905-00.030	3.7	1.2	1.9	1.3	1.9	0.3	1.4	0.5	7.3	3.3	5.3	5.2
G012.999-00.357	3.3	1.0	0.6	0.9	3.3	0.5	0.9	0.7	4.0	1.4	0.4	4.2
G013.131-00.150	2.1	1.0	1.8	0.9	2.1	0.5	2.6	0.7	4.2	1.6	1.8	2.4
G013.209-00.141	2.5	1.1	0.8	1.1	2.6	0.5	1.1	0.9	6.1	4.5	6.6	5.5
G013.657-00.599	2.8	1.6	2.1	5.4	2.8	0.8	2.9	4.1	4.2	2.5	4.2	7.4
G013.904-00.512	2.5	2.0	3.2	2.0	1.3	0.5	2.2	0.7	5.7	4.0	2.7	4.1

Table 4 (Continued)

Source name	Optical depth	Column density						H ₂ column density					
		$\tau_{\text{N}_2\text{H}^+}$	τ_{HCO^+}	τ_{HCN}	$\text{N}_{\text{N}_2\text{H}^+}$ (10^{13} cm^{-2})	N_{HCO^+} (10^{13} cm^{-2})	N_{HCN} (10^{13} cm^{-2})	$\text{N}(\text{H}_2)_{\text{N}_2\text{H}^+}$ (10^{22} cm^{-2})	$\text{N}(\text{H}_2)_{\text{HCO}^+}$ (10^{22} cm^{-2})	$\text{N}(\text{H}_2)_{\text{HCN}}$ (10^{22} cm^{-2})	$\text{N}(\text{H}_2)_{\text{HNC}}$ (10^{22} cm^{-2})	$\text{N}(\text{H}_2)_{\text{Mean}}$ (10^{22} cm^{-2})	
(1)	(2)	(3)	(4)	(5)	(6)	(7)	(8)	(9)	(10)	(11)	(12)	(13)	(14)
G014.101+00.086	1.3	1.3	1.1	1.4	0.7	1.9	0.9	5.0	1.5	2.9	2.3	2.9	2.9
G014.226-00.511	2.3	1.9	2.2	1.5	2.4	0.9	3.2	1.2	7.7	4.4	4.2	5.2	5.4
G014.245-00.071	1.4	1.1	0.8	1.0	1.5	0.5	1.2	0.7	5.1	3.3	5.0	4.0	4.4
G014.606+00.014	2.9	0.5	1.8	1.1	2.9	0.3	2.5	0.8	5.6	4.4	3.0	3.9	4.2
G014.632+00.308	2.3	1.0	1.4	1.0	2.4	0.5	1.9	0.8	4.6	2.3	3.0	3.7	3.4
G014.777-00.486	2.0	2.2	2.0	1.2	1.0	0.5	1.4	0.5	2.9	0.9	1.2	3.1	2.0
G340.054-00.244	2.8	3.5	3.6	2.4	2.9	1.7	5.1	1.9	10.3	5.8	6.1	7.9	7.5
G340.104-00.313	1.1	1.1	1.2	0.8	1.1	0.6	1.7	0.6	2.5	1.2	1.3	1.8	1.7
G340.229-00.144	3.3	4.7	3.6	4.2	1.1	0.7	1.6	1.0	6.9	3.7	3.9	3.7	4.5
G340.261+00.532	1.3	2.0	2.3	1.2	1.3	1.0	3.2	1.0	3.0	1.8	1.6	2.2	2.1
G340.311-00.436	2.3	2.3	2.3	1.6	1.2	0.6	1.6	0.6	2.4	1.1	1.4	1.9	1.7
G340.632-00.648	2.0	1.4	1.7	1.6	1.0	0.4	1.2	0.6	3.9	2.7	2.4	3.1	3.0
G340.764-00.132	3.2	0.7	1.1	1.2	1.6	0.2	0.8	0.5	5.2	0.5	2.1	3.1	2.7
G340.776-00.119	3.2	0.5	2.2	1.2	1.6	0.1	1.5	0.5	4.5	3.2	4.3	5.3	4.3
G340.785-00.097	3.8	2.6	3.6	2.8	2.0	0.6	2.5	1.1	11.1	5.1	5.4	8.9	7.6
G340.878-00.374	4.0	1.6	1.6	1.6	4.1	0.8	2.3	1.2	7.2	6.6	5.5	4.9	6.0
G340.934-00.233	2.8	1.7	1.5	1.4	0.4	1.1	0.5	5.5	2.9	3.7	5.3	4.4	4.4
G341.034-00.114	3.1	1.9	2.8	1.9	1.0	0.3	1.2	0.5	6.4	4.6	3.6	4.6	4.8
G341.038-00.113	3.0	1.9	1.8	1.7	1.0	0.3	0.8	0.4	5.5	4.0	4.3	4.9	4.7
G341.127-00.350	2.1	1.7	2.6	1.6	2.2	0.8	3.7	1.3	4.7	2.0	2.2	3.0	3.0
G342.484+00.183	2.8	1.4	1.6	1.1	2.9	0.7	2.3	0.9	8.4	3.6	3.6	5.6	5.3
G342.706+00.125	4.5	3.4	2.4	2.7	4.6	1.7	3.4	2.1	6.6	4.5	5.6	6.5	5.8
G342.822+00.382	2.8	2.4	2.1	2.3	1.4	0.6	1.5	0.9	2.6	1.0	2.8	2.0	2.1
G342.824+00.381	3.4	2.8	2.2	2.4	1.8	0.7	1.6	0.9	2.4	1.3	1.7	1.8	1.8
G343.127-00.063	7.3	5.2	5.3	4.5	3.7	1.3	3.8	1.7	22.0	13.8	18.4	18.4	18.2
G343.134-00.484	4.1	2.0	2.3	2.1	0.5	1.6	0.8	5.7	6.1	4.6	4.2	5.2	5.2
G343.353-00.071	4.1	2.7	3.0	2.4	2.1	0.7	2.1	0.9	14.7	8.5	13.1	11.2	11.9
G343.478-00.023	4.2	2.8	4.8	2.6	4.3	1.4	6.9	2.0	10.5	7.7	7.1	8.3	8.4
G343.492-00.068	2.5	1.3	2.3	1.8	2.6	0.6	3.3	1.4	4.9	3.7	3.6	4.6	4.2
G343.520-00.519	4.0	1.8	2.1	2.1	0.4	1.5	0.8	6.6	5.7	5.3	5.0	5.6	5.6
G343.689-00.018	1.9	1.2	1.6	1.1	2.0	0.6	2.3	0.8	3.6	3.1	2.1	2.5	2.8
G343.720-00.223	1.9	0.9	1.4	1.0	2.0	0.5	2.0	0.7	4.3	2.1	2.3	2.7	2.8
G343.738-00.112	2.6	1.9	0.2	1.6	1.3	0.5	0.1	0.6	4.8	2.4	2.2	2.1	2.9

Table 4 (Continued)

Source name (1)	Optical depth $\tau_{\text{N}_2\text{H}^+}$ (2)	Column density						H ₂ column density				
		τ_{HCN} (3)	τ_{HCO^+} (4)	$\text{N}_{\text{N}_2\text{H}^+}$ (10^{13} cm $^{-2}$) (5)	N_{HCO^+} (10^{13} cm $^{-2}$) (6)	N_{HCN} (10^{13} cm $^{-2}$) (7)	N_{HCO^+} (10^{13} cm $^{-2}$) (8)	$\text{N}(\text{H}_2)_{\text{N}_2\text{H}^+}$ (10^{22} cm $^{-2}$) (9)	$\text{N}(\text{H}_2)_{\text{HCN}}$ (10^{22} cm $^{-2}$) (10)	$\text{N}(\text{H}_2)_{\text{HCO}^+}$ (10^{22} cm $^{-2}$) (11)	$\text{N}(\text{H}_2)_{\text{HNC}}$ (10^{22} cm $^{-2}$) (12)	
G343.780-00.235	4.2	2.3	2.2	2.1	0.6	1.6	0.8	2.3	1.5	2.3	2.0	2.0
G344.915-00.229	2.0	2.4	2.1	1.5	1.0	0.6	1.5	0.6	3.6	2.4	2.0	2.4
G345.259-00.035	2.7	0.5	1.2	0.7	1.4	0.1	0.8	0.3	3.7	1.0	2.7	2.5
G345.261-00.418	1.4	1.1	1.2	0.6	1.5	0.6	1.7	0.4	3.0	2.3	1.5	2.1
G346.078-00.056	2.3	1.3	1.8	1.3	2.4	0.6	2.5	1.0	4.8	2.4	2.0	3.3
G346.307+00.114	1.3	1.3	1.6	1.0	1.3	0.7	2.3	0.8	3.6	2.0	2.4	3.3
G346.369-00.648	2.9	1.3	1.8	1.2	1.5	0.3	1.3	0.5	1.9	0.9	1.8	2.8
G346.484+00.220	5.0	2.6	3.4	3.1	1.6	0.4	1.5	0.7	12.8	11.2	13.4	12.5
G347.294+00.132	3.6	2.1	2.2	2.2	1.9	0.5	1.6	0.8	10.1	5.7	5.4	7.7
G347.627+00.149	4.8	4.0	5.6	3.3	4.9	2.0	8.0	2.5	8.6	5.7	5.5	6.5
G347.645+00.143	3.2	4.0	4.8	3.2	3.3	2.0	6.8	2.4	10.3	5.7	5.5	8.6
G347.682+00.207	1.9	1.8	2.5	1.5	1.9	0.9	3.6	1.2	1.8	1.5	1.5	1.7
G347.871+00.014	2.4	2.6	2.4	2.0	2.5	1.3	3.5	1.5	6.0	3.1	3.7	4.4
G347.967-00.434	2.8	1.9	2.1	1.6	2.8	0.9	3.0	1.2	7.2	4.6	4.3	6.8
G348.228+00.413	2.8	2.7	3.4	2.0	2.9	1.3	4.8	1.6	5.0	3.4	2.5	3.7
G348.290+00.643	2.5	2.3	1.6	1.4	1.3	0.6	1.2	0.5	6.2	2.2	2.5	4.1
G348.777+00.149	2.6	1.4	1.1	1.4	1.3	0.3	0.7	0.5	5.4	2.2	2.1	3.7
G348.892-00.179	1.6	2.2	2.4	1.6	1.6	1.1	3.4	1.2	5.1	2.3	3.3	3.6
G349.137+00.024	3.4	4.7	3.9	2.6	3.5	2.3	5.5	2.0	7.3	3.9	5.3	6.0
G350.014+00.434	2.0	2.1	2.6	1.7	2.0	1.0	3.7	1.3	7.8	3.9	3.6	4.9
G350.111+00.092	8.6	6.7	7.4	5.7	8.8	3.3	10.6	4.4	22.5	12.7	20.8	18.1
G350.183+00.003	3.2	2.1	1.9	2.3	3.3	1.0	2.7	1.8	4.9	3.9	4.8	4.1
G350.271-00.500	4.0	2.3	3.1	2.8	1.3	0.4	1.4	0.7	6.1	3.9	4.6	4.5
G350.412-00.062	4.9	3.0	2.2	2.8	1.6	0.5	1.0	0.7	10.5	5.8	8.4	10.7
G350.506+00.958	3.8	5.8	6.8	2.6	3.9	2.9	9.6	2.0	21.0	8.2	7.7	10.0
G350.522-00.349	2.7	0.9	1.3	1.6	2.8	0.5	1.8	1.2	3.7	2.5	2.9	3.0
G350.687-00.491	2.4	1.7	1.4	1.4	2.4	0.8	2.0	1.1	2.5	1.6	2.1	2.5
G350.688-00.489	3.1	2.0	1.9	1.7	3.2	1.0	2.7	1.3	4.1	2.4	3.5	3.4
G350.710+01.027	2.1	1.5	1.6	1.2	2.2	0.7	2.2	0.9	3.9	1.6	1.3	3.4
G351.040-00.336	3.2	1.8	2.2	1.8	3.3	0.9	3.1	1.4	5.0	3.5	4.1	4.2
G351.532-00.557	3.7	1.1	1.2	1.3	1.9	0.3	0.8	0.5	3.9	3.0	4.2	4.1
G351.582-00.352	3.0	3.2	2.1	1.6	3.1	1.6	3.0	1.2	10.5	10.5	11.3	11.2

Table 4 (Continued)

Source name	Optical depth	Column density						H ₂ column density					
		$\tau_{\text{N}_2\text{H}^+}$	τ_{HCO^+}	τ_{HCN}	$\text{N}_{\text{N}_2\text{H}^+}$ (10^{13} cm^{-2})	N_{HCO^+} (10^{13} cm^{-2})	N_{HCN} (10^{13} cm^{-2})	$\text{N}(\text{H}_2)_{\text{N}_2\text{H}^+}$ (10^{22} cm^{-2})	$\text{N}(\text{H}_2)_{\text{HCO}^+}$ (10^{22} cm^{-2})	$\text{N}(\text{H}_2)_{\text{HCN}}$ (10^{22} cm^{-2})	$\text{N}(\text{H}_2)_{\text{HNC}}$ (10^{22} cm^{-2})	$\text{N}(\text{H}_2)_{\text{Mean}}$ (10^{22} cm^{-2})	
(1)	(2)	(3)	(4)	(5)	(6)	(7)	(8)	(9)	(10)	(11)	(12)	(13)	(14)
G352.060+00.603	3.3	2.2	2.3	2.0	1.1	0.3	1.0	0.5	5.2	2.1	1.7	2.2	2.8
G352.072+00.679	3.0	3.8	2.5	1.5	0.9	1.7	0.6	4.8	3.3	3.4	4.1	3.9	3.9
G352.142-01.016	2.5	2.9	1.8	2.1	1.3	0.7	1.3	0.8	3.4	3.0	2.1	2.8	2.8
G352.233-00.162	1.8	1.0	1.3	1.1	1.9	0.5	1.8	0.9	3.7	1.9	2.3	2.2	2.5
G352.315-00.443	2.5	2.4	2.6	1.8	2.6	1.2	3.7	1.4	6.5	3.1	3.0	5.1	4.4
G352.492+00.796	3.2	1.6	2.4	2.0	3.3	0.8	3.3	1.5	6.4	4.9	5.6	5.2	5.5
G352.518-00.155	1.4	1.6	2.1	1.4	1.4	0.8	2.9	1.1	4.8	2.3	2.1	4.6	3.5
G352.684-00.120	1.3	1.2	1.6	1.2	1.3	0.6	2.3	0.9	3.5	2.0	1.5	2.2	2.3
G352.857-00.203	2.1	1.9	2.3	1.6	2.1	0.9	3.3	1.2	5.8	3.6	3.6	3.9	4.2
G352.972+00.925	2.7	3.0	4.2	1.8	2.7	1.5	5.9	1.4	2.6	1.5	1.7	1.8	1.9
G353.010+00.983	1.5	2.9	3.5	1.4	1.6	1.4	4.9	1.1	2.9	1.0	1.0	1.7	1.7
G353.115+00.366	2.3	2.1	2.8	1.9	2.4	1.1	4.0	1.4	5.8	3.0	3.1	4.1	4.0
G353.146+00.663	1.2	6.4	8.1	2.9	1.2	3.1	11.5	2.2	14.5	8.8	8.9	9.6	10.4
G353.147+00.851	2.4	3.1	3.9	2.0	2.5	1.5	5.5	1.5	6.4	3.8	3.5	5.0	4.7
G353.198+00.927	1.9	4.9	7.6	2.3	2.0	2.4	10.7	1.8	14.3	10.1	10.0	10.8	11.3
G353.215-00.247	1.7	1.1	1.2	0.7	1.7	0.6	1.7	0.5	3.6	1.2	1.6	3.5	2.5
G353.271+00.641	2.1	3.8	4.7	2.0	2.2	1.9	6.7	1.5	10.7	4.6	5.0	6.4	6.7
G353.462+00.563	3.9	3.3	3.1	2.5	2.0	0.8	2.2	1.0	4.8	2.7	4.5	4.1	4.0
G353.547-00.019	1.2	1.7	2.8	1.4	1.2	0.9	4.0	1.0	4.1	2.9	2.8	3.8	3.4
G353.577+00.661	3.3	3.2	2.7	1.9	1.7	0.8	1.9	0.7	6.1	3.0	2.6	3.8	3.9
G353.975+00.256	2.6	1.7	2.2	1.9	1.3	0.4	1.5	0.7	4.4	3.9	3.6	4.6	4.1
G354.206-00.038	1.5	0.9	1.0	0.8	1.6	0.4	1.4	0.6	3.9	3.3	2.2	2.4	2.9
G354.207-00.036	1.9	1.1	1.1	1.2	2.0	0.5	1.6	0.9	2.8	1.6	1.9	3.9	2.5
G354.628-00.610	3.0	3.6	2.7	2.9	1.0	0.6	1.2	0.7	4.6	2.6	2.7	3.5	3.4
G354.813+00.976	2.6	1.4	1.4	1.0	1.3	0.3	1.0	0.4	4.5	4.6	2.2	2.6	3.5
G354.945-00.539	2.4	1.6	2.3	1.2	2.4	0.8	3.2	0.9	3.6	1.5	1.1	1.8	2.0
G355.182-00.419	5.4	3.8	3.2	3.1	2.8	0.9	2.3	1.2	6.5	3.5	3.7	5.5	4.8
G355.249+00.363	2.6	2.0	2.1	2.0	1.3	0.5	1.5	0.8	3.6	2.9	2.6	4.0	3.3
G355.265-00.269	3.3	2.1	1.8	1.8	1.7	0.5	1.3	0.7	5.5	2.5	3.7	5.0	4.2
G355.344+00.148	1.2	2.2	1.5	1.4	1.3	1.1	2.1	1.1	5.2	3.3	3.6	4.6	4.2
G355.412+00.103	4.1	1.0	2.2	1.7	2.1	0.2	1.6	0.6	6.6	5.5	6.1	5.2	5.8
G355.589-00.035	2.1	1.1	1.4	0.1	1.1	0.3	1.0	0.05	3.8	3.0	2.1	2.9	2.9
G355.740+00.655	2.4	1.7	1.8	2.0	1.2	0.4	1.3	0.8	4.1	3.2	3.5	3.4	3.6

Table 4 (Continued)

Source name (1)	Optical depth $\tau_{\text{N}_2\text{H}^+}$ (2)	Column density					H ₂ column density					
		τ_{HCO^+} (3)	τ_{HCN} (4)	$\text{N}_{\text{N}_2\text{H}^+}$ (10^{13} cm ⁻²) (5)	N_{HCO^+} (10^{13} cm ⁻²) (6)	N_{HCN} (10^{13} cm ⁻²) (7)	N_{HNC} (10^{13} cm ⁻²) (8)	$\text{N}(\text{H}_2)\text{N}_2\text{H}^+$ (10^{22} cm ⁻²) (9)	$\text{N}(\text{H}_2)\text{HCO}^+$ (10^{22} cm ⁻²) (10)	$\text{N}(\text{H}_2)\text{HCN}$ (10^{22} cm ⁻²) (11)	$\text{N}(\text{H}_2)\text{HNC}$ (10^{22} cm ⁻²) (12)	$\text{N}(\text{H}_2)\text{Mean}$ (10^{22} cm ⁻²) (14)
G355.829-00.501	2.4	1.8	2.0	1.7	2.4	0.9	2.9	1.3	3.6	2.5	2.8	3.5
G355.935-00.346	2.3	1.3	1.7	0.9	1.2	0.3	1.2	0.4	5.2	2.8	2.8	4.0
G356.008-00.424	1.9	2.0	2.3	1.4	1.0	0.5	1.6	0.5	3.9	2.8	2.0	5.5
G356.008-00.758	1.4	1.4	1.2	1.3	1.4	0.7	1.7	1.0	3.3	2.1	2.2	2.6
G356.255-00.056	1.3	0.9	1.0	0.9	1.4	0.5	1.4	0.7	2.1	0.7	1.1	1.6
G356.305-00.204	1.0	0.9	1.5	0.7	1.0	0.4	2.1	0.5	3.4	2.4	1.7	3.5
G356.344-00.068	2.9	2.0	1.9	2.0	1.5	0.5	1.4	0.8	4.8	2.9	3.5	5.7
G356.372+00.567	5.1	2.6	3.2	1.9	2.6	0.6	2.2	0.7	6.7	3.7	3.0	3.4
G356.482+00.190	2.8	2.4	2.3	2.2	1.5	0.6	1.6	0.9	4.9	2.4	3.6	3.7
G356.517+00.664	2.6	1.7	2.2	1.8	1.3	0.4	1.5	0.7	3.9	2.8	2.6	3.7
G356.662-00.265	3.5	3.5	3.4	2.7	1.8	0.9	2.4	1.0	7.3	3.5	5.4	7.0
G356.858+00.327	1.6	1.6	1.9	1.5	0.8	0.4	1.3	0.6	2.2	1.2	1.5	2.6
G357.462-00.339	4.1	2.7	1.6	1.5	1.3	0.4	0.7	0.4	10.7	5.1	3.0	4.6
G357.554-00.550	3.8	3.4	3.3	2.5	3.9	1.7	4.7	1.9	6.7	3.8	3.3	4.6
G357.558-00.323	3.4	2.1	2.1	2.2	1.8	0.5	1.5	0.8	11.0	15.5	9.5	9.3
G357.786-00.311	2.5	1.3	1.1	1.2	1.3	0.3	0.8	0.5	3.8	2.8	3.4	3.9
G357.921-00.337	1.8	0.7	1.2	1.1	1.8	0.3	1.7	0.8	4.3	5.2	9.4	2.7
G357.967-00.163	2.3	1.1	1.8	1.1	2.3	0.6	2.5	0.8	10.4	4.6	5.1	17.0
G357.998-00.154	2.6	0.6	1.0	0.4	2.7	0.3	1.5	0.3	4.3	4.6	3.5	6.4
G358.388-00.484	3.7	2.2	3.6	0.9	3.8	1.1	5.1	0.7	6.9	5.2	5.3	6.0
G358.460-00.393	8.8	3.9	4.6	4.1	4.5	1.0	3.2	1.6	10.7	7.8	7.4	10.6
G358.807-00.087	2.4	3.1	4.9	1.5	1.2	0.8	3.4	0.6	7.6	4.5	7.2	8.9
G358.980+00.083	2.9	1.7	2.1	1.5	1.5	0.4	1.5	0.6	2.8	1.7	1.5	3.3
G359.210-00.076	2.3	5.8	5.2	1.6	2.4	2.9	7.4	1.2	6.4	5.3	5.2	6.0
G359.469-00.035	4.0	4.1	40.5	2.8	1.3	0.6	18.0	0.7	26.8	32.1	29.4	23.2
G359.716-00.375	2.4	3.3	4.5	2.0	2.4	1.6	6.3	1.5	7.5	3.7	3.1	4.5
G359.733+00.005	4.0	4.9	6.2	4.2	4.1	2.4	8.8	3.2	8.6	8.1	8.2	8.4
G359.742+00.027	5.2	13.5	10.4	4.1	1.7	2.1	4.7	1.0	28.8	24.5	22.7	27.0
G359.911-00.305	3.3	2.1	2.5	1.5	1.7	0.5	1.7	0.6	8.8	2.3	2.2	4.6
G359.941+00.173	3.3	2.4	2.0	1.6	3.4	1.2	2.9	1.2	11.9	10.9	10.5	11.3
G359.944+00.152	4.2	2.3	2.2	1.7	4.3	1.1	3.1	1.3	11.6	9.2	10.4	11.7

This table lists the optical depth, column density and H₂ column density for N₂H⁺ (1–0), HCO⁺ (1–0) and HNC (1–0), Column 1 is the source name; Columns 2 to 5 list the optical depth for N₂H⁺ (1–0), HCO⁺ (1–0), HCN (1–0); Columns 6 to 9 list the column density; Columns 10 to 13 list the H₂ column density for each molecule; Column 14 lists the averaged H₂ column density for the four molecular lines

Table 5 Molecular abundances and abundance ratio

Source name (1)	Molecular abundances				Abundance ratios					
	$X(N_2H^+)$ (10^{-9}) (2)	$X(HCO^+)$ (10^{-9}) (3)	$X(HCN)$ (10^{-9}) (4)	$X(HNC)$ (10^{-9}) (5)	$\frac{X(N_2H^+)}{X(HCO^+)}$ (6)	$\frac{X(N_2H^+)}{X(HCN)}$ (7)	$\frac{X(N_2H^+)}{X(HNC)}$ (8)	$\frac{X(HCO^+)}{X(HCN)}$ (9)	$\frac{X(HCO^+)}{X(HNC)}$ (10)	$\frac{X(HCN)}{X(HNC)}$ (11)
G000.006+00.156	0.30	0.25	0.89	0.22	1.19	0.33	1.36	0.28	1.14	4.08
G000.053-00.209	0.35	0.29	1.00	0.27	1.18	0.35	1.30	0.29	1.10	3.76
G000.208-00.518	0.16	0.09	0.32	0.03	1.88	0.51	5.85	0.27	3.11	11.54
G000.410-00.504	0.41	0.30	1.44	0.34	1.38	0.29	1.22	0.21	0.88	4.27
G000.633+00.601	0.28	0.29	1.02	0.19	0.99	0.28	1.52	0.28	1.54	5.44
G000.766-00.248	0.24	0.03	0.07	0.10	7.21	3.62	2.42	0.50	0.34	0.67
G000.836+00.183	0.35	0.39	0.41	0.22	0.91	0.85	1.61	0.94	1.78	1.89
G002.534+00.200	0.37	0.16	0.21	0.08	2.28	1.82	4.86	0.80	2.14	2.67
G002.615+00.135	0.32	0.13	0.41	0.14	2.47	0.78	2.20	0.32	0.89	2.82
G002.623+00.237	0.41	0.13	0.31	0.20	3.10	1.34	2.06	0.43	0.67	1.54
G003.274+00.582	0.34	0.72	1.87	0.21	0.47	0.18	1.61	0.39	3.42	8.86
G003.309+00.333	0.69	1.49	4.95	0.53	0.46	0.14	1.31	0.30	2.82	9.39
G003.309-00.399	0.29	0.06	0.30	0.10	5.04	0.99	2.83	0.20	0.56	2.87
G003.350-00.077	0.44	0.17	0.35	0.19	2.63	1.25	2.31	0.48	0.88	1.85
G003.415-00.354	0.28	0.09	0.19	0.14	3.23	1.49	2.04	0.46	0.63	1.37
G003.436-00.572	0.32	0.07	0.32	0.15	4.90	0.99	2.08	0.20	0.42	2.10
G004.627-00.665	0.60	0.22	0.40	0.32	2.67	1.49	1.89	0.56	0.71	1.26
G004.827+00.231	0.43	0.12	0.51	0.22	3.53	0.84	1.97	0.24	0.56	2.34
G004.895-00.127	0.40	0.28	0.28	0.28	1.41	1.43	1.44	1.01	1.02	1.01
G005.505-00.245	0.07	0.01	0.04	0.03	6.14	2.03	2.11	0.33	0.34	1.04
G005.615-00.092	0.45	0.26	0.46	0.16	1.74	0.99	2.90	0.57	1.67	2.95
G005.637+00.238	0.57	0.24	0.72	0.32	2.35	0.79	1.78	0.34	0.76	2.25
G005.831-00.512	0.55	0.51	0.91	0.35	1.08	0.61	1.61	0.56	1.49	2.65
G005.893-00.320	0.63	0.45	1.35	0.38	1.39	0.47	1.66	0.34	1.19	3.54
G006.119-00.636	0.29	0.39	1.38	0.26	0.76	0.21	1.11	0.28	1.46	5.25
G006.188-00.358	0.56	0.28	1.05	0.29	2.00	0.53	1.89	0.26	0.95	3.58
G006.216-00.609	0.29	0.18	0.74	0.20	1.56	0.39	1.45	0.25	0.93	3.75
G006.551-00.097	0.27	0.09	0.43	0.11	2.87	0.62	2.42	0.22	0.84	3.90
G006.796-00.256	0.68	0.22	1.01	0.40	3.18	0.68	1.73	0.21	0.55	2.55
G007.333-00.567	0.25	0.15	0.99	0.17	1.67	0.25	1.46	0.15	0.87	5.88
G007.632-00.109	0.11	0.04	0.89	0.09	2.62	0.13	1.24	0.05	0.47	9.90
G007.993-00.269	0.21	0.16	0.70	0.16	1.36	0.30	1.34	0.22	0.99	4.42
G008.049-00.244	0.91	1.24	2.02	0.64	0.74	0.45	1.41	0.61	1.92	3.13
G008.206+00.190	0.45	0.33	2.06	0.46	1.37	0.22	0.98	0.16	0.71	4.48
G008.350-00.317	0.65	1.10	3.31	0.74	0.59	0.20	0.88	0.33	1.49	4.49
G008.458-00.224	0.91	1.23	2.61	0.73	0.74	0.35	1.24	0.47	1.68	3.57
G008.955-00.535	0.16	0.02	1.00	0.10	7.84	0.16	1.56	0.02	0.20	9.92
G009.037-00.521	0.30	0.23	0.36	0.11	1.29	0.83	2.68	0.64	2.08	3.23
G009.212-00.202	0.95	0.64	1.07	0.41	1.49	0.89	2.33	0.60	1.57	2.61
G009.283-00.149	0.70	0.59	0.84	0.33	1.18	0.83	2.13	0.70	1.81	2.57
G009.422-00.704	0.55	0.76	1.30	0.64	0.73	0.43	0.87	0.58	1.19	2.04
G009.620+00.195	0.31	0.21	0.70	0.28	1.52	0.45	1.14	0.29	0.75	2.54
G009.877-00.748	0.71	0.30	1.01	0.27	2.32	0.70	2.58	0.30	1.11	3.67
G010.473+00.028	0.39	0.26	0.71	0.22	1.49	0.54	1.73	0.37	1.17	3.19
G010.624-00.383	0.19	0.28	1.06	0.25	0.67	0.18	0.75	0.27	1.12	4.20
G010.630-00.510	0.59	0.58	1.41	0.35	1.03	0.42	1.69	0.41	1.64	4.02
G010.661+00.080	0.25	0.14	0.53	0.13	1.73	0.46	1.97	0.27	1.14	4.25
G010.680-00.027	0.39	0.12	0.83	0.29	3.19	0.48	1.35	0.15	0.43	2.85
G010.724-00.332	0.62	0.57	1.56	0.39	1.09	0.40	1.57	0.37	1.45	3.95
G010.746+00.015	0.20	0.11	0.24	0.12	1.92	0.84	1.67	0.44	0.87	1.98

Table 5 (Continued)

Source name (1)	Molecular abundances				Abundance ratios					
	$X(\text{N}_2\text{H}^+)$ (10^{-9}) (2)	$X(\text{HCO}^+)$ (10^{-9}) (3)	$X(\text{HCN})$ (10^{-9}) (4)	$X(\text{HNC})$ (10^{-9}) (5)	$\frac{X(\text{N}_2\text{H}^+)}{X(\text{HCO}^+)}$ (6)	$\frac{X(\text{N}_2\text{H}^+)}{X(\text{HCN})}$ (7)	$\frac{X(\text{N}_2\text{H}^+)}{X(\text{HNC})}$ (8)	$\frac{X(\text{HCO}^+)}{X(\text{HCN})}$ (9)	$\frac{X(\text{HCO}^+)}{X(\text{HNC})}$ (10)	$\frac{X(\text{HCO}^+)}{X(\text{HNC})}$ (11)
G011.033+00.061	0.59	0.22	1.16	0.11	2.66	0.51	5.40	0.19	2.03	10.56
G011.112-00.399	0.69	0.22	0.50	0.21	3.19	1.39	3.28	0.44	1.03	2.36
G011.903-00.140	0.17	0.08	0.20	0.11	2.14	0.87	1.57	0.40	0.73	1.81
G011.942-00.156	0.72	0.60	1.51	0.61	1.19	0.47	1.18	0.40	0.99	2.49
G012.200-00.033	0.23	0.19	0.53	0.14	1.24	0.43	1.65	0.35	1.34	3.84
G012.418+00.506	0.30	0.36	1.25	0.29	0.84	0.24	1.03	0.28	1.22	4.30
G012.497-00.222	0.31	0.61	1.58	0.35	0.51	0.20	0.89	0.39	1.74	4.51
G012.625-00.017	0.26	0.09	0.18	0.13	2.85	1.43	2.00	0.50	0.70	1.39
G012.680-00.180	0.37	0.10	0.34	0.08	3.73	1.10	4.47	0.29	1.20	4.08
G012.774+00.337	0.19	0.17	0.69	0.18	1.09	0.28	1.04	0.25	0.96	3.77
G012.805-00.318	0.32	0.20	0.42	0.05	1.60	0.78	6.17	0.49	3.85	7.90
G012.905-00.030	0.26	0.09	0.26	0.10	2.89	1.00	2.73	0.35	0.94	2.73
G012.999-00.357	0.84	0.37	2.05	0.16	2.29	0.41	5.38	0.18	2.35	13.15
G013.131-00.150	0.50	0.31	1.46	0.38	1.61	0.34	1.31	0.21	0.81	3.81
G013.209-00.141	0.43	0.12	0.17	0.18	3.56	2.53	2.38	0.71	0.67	0.94
G013.657-00.599	0.67	0.31	0.70	0.22	2.13	0.95	3.05	0.45	1.43	3.21
G013.904-00.512	0.23	0.12	0.84	0.19	1.89	0.27	1.22	0.14	0.65	4.50
G014.101+00.086	0.27	0.45	0.64	0.37	0.60	0.42	0.73	0.70	1.22	1.75
G014.226-00.511	0.31	0.21	0.75	0.23	1.46	0.41	1.35	0.28	0.93	3.30
G014.245-00.071	0.29	0.16	0.23	0.19	1.81	1.23	1.55	0.68	0.85	1.26
G014.606+00.014	0.53	0.06	0.84	0.22	9.14	0.63	2.45	0.07	0.27	3.89
G014.632+00.308	0.52	0.21	0.65	0.22	2.46	0.80	2.39	0.33	0.97	3.00
G014.777-00.486	0.34	0.58	1.22	0.15	0.58	0.28	2.31	0.48	3.95	8.22
G340.054-00.244	0.28	0.30	0.84	0.24	0.95	0.34	1.20	0.36	1.27	3.54
G340.104-00.313	0.43	0.46	1.30	0.34	0.92	0.33	1.27	0.35	1.38	3.89
G340.229-00.144	0.16	0.20	0.41	0.27	0.80	0.38	0.57	0.48	0.71	1.50
G340.261+00.532	0.44	0.54	1.99	0.44	0.80	0.22	0.99	0.27	1.23	4.48
G340.311-00.436	0.48	0.54	1.16	0.31	0.90	0.42	1.55	0.46	1.73	3.73
G340.632-00.648	0.26	0.13	0.52	0.20	2.02	0.51	1.29	0.25	0.64	2.54
G340.764-00.132	0.31	0.32	0.37	0.15	0.95	0.84	2.00	0.89	2.11	2.38
G340.776-00.119	0.36	0.04	0.35	0.09	10.11	1.03	4.05	0.10	0.40	3.95
G340.785-00.097	0.18	0.13	0.47	0.12	1.38	0.38	1.46	0.27	1.05	3.87
G340.878-00.374	0.57	0.12	0.41	0.26	4.80	1.38	2.23	0.29	0.46	1.62
G340.934-00.233	0.26	0.14	0.29	0.10	1.82	0.90	2.63	0.49	1.44	2.92
G341.034-00.114	0.16	0.06	0.34	0.10	2.45	0.46	1.55	0.19	0.63	3.36
G341.038-00.113	0.17	0.07	0.18	0.09	2.41	0.95	2.03	0.40	0.84	2.14
G341.127-00.350	0.46	0.41	1.70	0.42	1.12	0.27	1.11	0.24	0.99	4.08
G342.484+00.183	0.34	0.20	0.62	0.16	1.77	0.55	2.21	0.31	1.25	4.00
G342.706+00.125	0.70	0.37	0.61	0.32	1.90	1.14	2.19	0.60	1.16	1.92
G342.822+00.382	0.55	0.59	0.54	0.44	0.94	1.03	1.25	1.09	1.33	1.22
G342.824+00.381	0.74	0.54	0.89	0.52	1.38	0.83	1.43	0.60	1.04	1.72
G343.127-00.063	0.17	0.09	0.21	0.09	1.83	0.82	1.82	0.45	0.99	2.21
G343.134-00.484	0.36	0.08	0.35	0.19	4.62	1.05	1.94	0.23	0.42	1.85
G343.353-00.071	0.14	0.08	0.16	0.08	1.81	0.86	1.71	0.48	0.94	1.98
G343.478-00.023	0.41	0.18	0.96	0.24	2.26	0.42	1.69	0.19	0.75	4.01
G343.492-00.068	0.53	0.17	0.91	0.31	3.05	0.59	1.73	0.19	0.57	2.94
G343.520-00.519	0.31	0.08	0.29	0.16	3.98	1.07	1.95	0.27	0.49	1.82
G343.689-00.018	0.55	0.20	1.07	0.33	2.74	0.51	1.68	0.19	0.61	3.28
G343.720-00.223	0.46	0.22	0.88	0.27	2.09	0.52	1.68	0.25	0.80	3.24
G343.738-00.112	0.28	0.19	0.06	0.29	1.43	4.29	0.95	2.99	0.67	0.22

Table 5 (Continued)

Source name (1)	Molecular abundances				Abundance ratios					
	$X(\text{N}_2\text{H}^+)$ (10^{-9}) (2)	$X(\text{HCO}^+)$ (10^{-9}) (3)	$X(\text{HCN})$ (10^{-9}) (4)	$X(\text{HNC})$ (10^{-9}) (5)	$X(\text{N}_2\text{H}^+)$ $X(\text{HCO}^+)$ (6)	$X(\text{N}_2\text{H}^+)$ $X(\text{HCN})$ (7)	$X(\text{N}_2\text{H}^+)$ $X(\text{HNC})$ (8)	$X(\text{HCO}^+)$ $X(\text{HCN})$ (9)	$X(\text{HCO}^+)$ $X(\text{HNC})$ (10)	$X(\text{HCN})$ $X(\text{HNC})$ (11)
G343.780-00.235	0.94	0.38	0.69	0.41	2.47	1.37	2.29	0.56	0.93	1.68
G344.915-00.229	0.29	0.25	0.88	0.28	1.17	0.32	1.02	0.28	0.88	3.16
G345.259-00.035	0.37	0.13	0.31	0.11	2.83	1.22	3.31	0.43	1.17	2.71
G345.261-00.418	0.50	0.24	1.10	0.25	2.09	0.45	1.96	0.22	0.94	4.33
G346.078-00.056	0.49	0.26	1.26	0.25	1.88	0.39	2.00	0.21	1.07	5.12
G346.307+00.114	0.37	0.33	0.97	0.23	1.12	0.38	1.59	0.34	1.42	4.18
G346.369-00.648	0.77	0.35	0.70	0.30	2.17	1.10	2.57	0.50	1.18	2.35
G346.484+00.220	0.13	0.04	0.11	0.06	3.48	1.12	2.16	0.32	0.62	1.93
G347.294+00.132	0.18	0.09	0.29	0.11	2.03	0.64	1.73	0.32	0.85	2.70
G347.627+00.149	0.58	0.35	1.47	0.39	1.67	0.39	1.49	0.24	0.89	3.78
G347.645+00.143	0.32	0.35	1.24	0.28	0.91	0.25	1.11	0.28	1.22	4.37
G347.682+00.207	1.07	0.62	2.35	0.63	1.74	0.46	1.71	0.26	0.98	3.74
G347.871+00.014	0.42	0.40	0.93	0.31	1.04	0.45	1.34	0.44	1.29	2.96
G347.967-00.434	0.39	0.21	0.69	0.18	1.92	0.57	2.23	0.30	1.16	3.91
G348.228+00.413	0.58	0.39	1.91	0.42	1.46	0.30	1.36	0.21	0.93	4.51
G348.290+00.643	0.21	0.26	0.46	0.13	0.79	0.44	1.58	0.56	1.99	3.57
G348.777+00.149	0.25	0.16	0.36	0.13	1.58	0.69	1.89	0.44	1.20	2.75
G348.892-00.179	0.32	0.47	1.02	0.33	0.67	0.31	0.96	0.47	1.44	3.08
G349.137+00.024	0.48	0.59	1.04	0.26	0.80	0.46	1.85	0.57	2.31	4.04
G350.014+00.434	0.26	0.27	1.01	0.27	0.96	0.25	0.97	0.26	1.01	3.82
G350.111+00.092	0.39	0.26	0.51	0.24	1.52	0.77	1.61	0.51	1.06	2.08
G350.183+00.003	0.66	0.27	0.56	0.44	2.46	1.18	1.52	0.48	0.62	1.29
G350.271-00.500	0.21	0.09	0.29	0.15	2.32	0.72	1.41	0.31	0.61	1.98
G350.412-00.062	0.15	0.08	0.11	0.06	1.86	1.33	2.36	0.71	1.27	1.78
G350.506+00.958	0.18	0.35	1.25	0.20	0.53	0.15	0.91	0.28	1.72	6.16
G350.522-00.349	0.75	0.19	0.62	0.44	4.03	1.20	1.69	0.30	0.42	1.41
G350.687-00.491	0.96	0.52	0.94	0.29	1.84	1.02	3.30	0.56	1.80	3.23
G350.688-00.489	0.78	0.41	0.78	0.37	1.89	1.00	2.13	0.53	1.13	2.13
G350.710+01.027	0.56	0.44	1.70	0.27	1.26	0.33	2.07	0.26	1.65	6.30
G350.763+00.793	0.41	0.49	2.04	0.48	0.84	0.20	0.86	0.24	1.02	4.27
G351.040-00.336	0.66	0.25	0.75	0.33	2.64	0.88	1.98	0.33	0.75	2.25
G351.532-00.557	0.48	0.09	0.20	0.13	5.23	2.43	3.86	0.47	0.74	1.59
G351.582-00.352	0.30	0.15	0.27	0.10	1.97	1.11	3.02	0.57	1.53	2.71
G352.060+00.603	0.20	0.16	0.60	0.22	1.25	0.34	0.94	0.27	0.75	2.80
G352.072+00.679	0.32	0.28	0.50	0.14	1.15	0.64	2.35	0.56	2.04	3.65
G352.142-01.016	0.37	0.24	0.61	0.29	1.55	0.61	1.26	0.39	0.81	2.06
G352.233-00.162	0.50	0.26	0.79	0.39	1.92	0.64	1.28	0.33	0.67	2.01
G352.315-00.443	0.40	0.39	1.24	0.27	1.04	0.33	1.49	0.31	1.43	4.58
G352.492+00.796	0.51	0.16	0.60	0.29	3.13	0.84	1.76	0.27	0.56	2.08
G352.518-00.155	0.29	0.34	1.36	0.24	0.86	0.22	1.25	0.25	1.45	5.79
G352.684-00.120	0.38	0.31	1.49	0.39	1.23	0.26	0.97	0.21	0.79	3.77
G352.857-00.203	0.37	0.26	0.93	0.31	1.40	0.39	1.17	0.28	0.84	2.96
G352.972+00.925	1.05	0.98	3.42	0.75	1.07	0.31	1.40	0.29	1.31	4.56
G353.010+00.983	0.54	1.40	4.72	0.63	0.39	0.12	0.87	0.30	2.24	7.55
G353.115+00.366	0.40	0.36	1.30	0.35	1.13	0.31	1.17	0.28	1.03	3.74
G353.146+00.663	0.08	0.36	1.29	0.23	0.23	0.06	0.35	0.28	1.52	5.53
G353.147+00.851	0.39	0.40	1.57	0.30	0.99	0.25	1.28	0.25	1.30	5.15
G353.198+00.927	0.14	0.24	1.07	0.17	0.58	0.13	0.84	0.22	1.46	6.50
G353.215-00.247	0.48	0.48	1.09	0.16	1.00	0.44	3.05	0.44	3.04	6.98
G353.271+00.641	0.20	0.40	1.32	0.24	0.50	0.15	0.86	0.31	1.71	5.62

Table 5 (Continued)

Source name (1)	Molecular abundances				Abundance ratios					
	$X(\text{N}_2\text{H}^+)$ (10^{-9}) (2)	$X(\text{HCO}^+)$ (10^{-9}) (3)	$X(\text{HCN})$ (10^{-9}) (4)	$X(\text{HNC})$ (10^{-9}) (5)	$X(\text{N}_2\text{H}^+)$ $X(\text{HCO}^+)$ (6)	$X(\text{N}_2\text{H}^+)$ $X(\text{HCN})$ (7)	$X(\text{N}_2\text{H}^+)$ $X(\text{HNC})$ (8)	$X(\text{HCO}^+)$ $X(\text{HCN})$ (9)	$X(\text{HCO}^+)$ $X(\text{HNC})$ (10)	$X(\text{HCN})$ $X(\text{HNC})$ (11)
G353.462+00.563	0.42	0.31	0.48	0.24	1.38	0.89	1.78	0.64	1.29	2.01
G353.547-00.019	0.31	0.30	1.45	0.28	1.02	0.21	1.11	0.21	1.09	5.25
G353.577+00.661	0.27	0.26	0.72	0.19	1.06	0.38	1.45	0.36	1.36	3.81
G353.975+00.256	0.30	0.11	0.43	0.16	2.79	0.69	1.89	0.25	0.68	2.73
G354.206-00.038	0.40	0.13	0.64	0.25	3.10	0.63	1.60	0.20	0.52	2.53
G354.207-00.036	0.72	0.33	0.88	0.23	2.18	0.82	3.08	0.38	1.42	3.76
G354.628-00.610	0.21	0.22	0.44	0.20	0.96	0.47	1.05	0.49	1.09	2.22
G354.813+00.976	0.30	0.07	0.45	0.14	4.01	0.65	2.13	0.16	0.53	3.25
G354.945-00.539	0.68	0.50	2.95	0.51	1.34	0.23	1.32	0.17	0.98	5.77
G355.182-00.419	0.43	0.27	0.61	0.22	1.59	0.70	1.94	0.44	1.22	2.77
G355.249+00.363	0.37	0.17	0.58	0.20	2.22	0.63	1.87	0.29	0.84	2.95
G355.265-00.269	0.30	0.21	0.34	0.13	1.44	0.89	2.29	0.61	1.59	2.59
G355.344+00.148	0.24	0.32	0.57	0.23	0.75	0.42	1.03	0.56	1.38	2.45
G355.412+00.103	0.32	0.04	0.26	0.12	7.27	1.25	2.62	0.17	0.36	2.09
G355.589-00.035	0.29	0.09	0.46	0.02	3.19	0.63	17.45	0.20	5.46	27.64
G355.740+00.655	0.29	0.13	0.38	0.23	2.30	0.78	1.30	0.34	0.57	1.67
G355.829-00.501	0.68	0.36	1.04	0.36	1.89	0.65	1.88	0.35	1.00	2.88
G355.935-00.346	0.22	0.12	0.43	0.09	1.89	0.52	2.54	0.28	1.34	4.86
G356.008-00.424	0.25	0.18	0.82	0.10	1.42	0.31	2.56	0.22	1.80	8.37
G356.008-00.758	0.43	0.34	0.80	0.33	1.27	0.54	1.29	0.42	1.02	2.40
G356.255-00.056	0.65	0.62	1.34	0.40	1.04	0.48	1.62	0.47	1.56	3.35
G356.305-00.204	0.30	0.18	1.27	0.16	1.72	0.24	1.93	0.14	1.12	8.17
G356.344-00.068	0.31	0.17	0.39	0.14	1.82	0.79	2.22	0.43	1.22	2.81
G356.372+00.567	0.39	0.17	0.75	0.22	2.26	0.51	1.79	0.23	0.79	3.51
G356.482+00.190	0.30	0.24	0.44	0.23	1.23	0.67	1.29	0.55	1.06	1.93
G356.517+00.664	0.34	0.15	0.59	0.18	2.28	0.57	1.84	0.25	0.81	3.23
G356.662-00.265	0.25	0.25	0.45	0.15	1.02	0.55	1.72	0.55	1.69	3.10
G356.858+00.327	0.37	0.35	0.90	0.22	1.08	0.42	1.71	0.39	1.58	4.12
G357.462-00.339	0.12	0.08	0.24	0.08	1.51	0.52	1.60	0.35	1.06	3.07
G357.554-00.550	0.58	0.45	1.45	0.41	1.30	0.40	1.40	0.31	1.09	3.52
G357.558-00.323	0.16	0.03	0.16	0.09	4.73	1.04	1.77	0.22	0.38	1.71
G357.786-00.311	0.34	0.12	0.23	0.12	2.88	1.45	2.76	0.50	0.96	1.91
G357.921-00.337	0.43	0.07	0.18	0.31	6.43	2.40	1.37	0.37	0.21	0.57
G357.967-00.163	0.22	0.12	0.49	0.05	1.80	0.45	4.57	0.25	2.54	10.18
G357.998-00.154	0.63	0.07	0.42	0.05	9.66	1.49	12.60	0.15	1.30	8.46
G358.388-00.484	0.56	0.21	0.97	0.12	2.67	0.57	4.78	0.22	1.79	8.34
G358.460-00.393	0.42	0.12	0.44	0.15	3.35	0.95	2.80	0.28	0.84	2.95
G358.807-00.087	0.16	0.17	0.48	0.07	0.94	0.33	2.41	0.35	2.57	7.25
G358.980+00.083	0.53	0.25	1.00	0.17	2.10	0.53	3.10	0.25	1.48	5.89
G359.210-00.076	0.38	0.54	1.42	0.20	0.69	0.27	1.90	0.38	2.74	7.16
G359.469-00.035	0.05	0.02	0.62	0.03	2.44	0.08	1.64	0.03	0.67	20.93
G359.716-00.375	0.32	0.45	2.06	0.42	0.73	0.16	0.77	0.22	1.07	4.92
G359.733+00.005	0.48	0.30	1.07	0.37	1.61	0.45	1.30	0.28	0.81	2.91
G359.742+00.027	0.06	0.09	0.21	0.04	0.69	0.29	1.61	0.42	2.36	5.64
G359.911-00.305	0.19	0.22	0.78	0.12	0.88	0.25	1.58	0.28	1.80	6.48
G359.941+00.173	0.28	0.11	0.27	0.11	2.60	1.03	2.66	0.40	1.03	2.59
G359.944+00.152	0.37	0.12	0.30	0.11	3.08	1.25	3.39	0.41	1.10	2.72

This table lists the molecular abundances of N_2H^+ (1–0), HCO^+ (1–0), HCN (1–0), HNC (1–0) and their abundance ratios. Column 1 is the source name; Columns 2 to 5 list the molecular abundances of N_2H^+ (1–0), HCO^+ (1–0), HCN (1–0), HNC (1–0); Columns 6 to 11 list the abundance ratios

Table 6 Median values of derived clump properties for each evolutionary stage

Property (1)	Stage A (Median) (2)	Stage B (Median) (3)	Stage C (Median) (4)
Integrated intensity (K km s ⁻¹)			
<i>I</i> (N ₂ H ⁺)	1.99	2.10	2.38
<i>I</i> (HCO ⁺)	1.52	1.86	2.38
<i>I</i> (HCN)	1.51	1.66	2.32
<i>I</i> (HNC)	1.61	1.67	1.91
Integrated intensity ratios			
<i>I</i> (N ₂ H ⁺)/ <i>I</i> (HCO ⁺)	0.96	0.57	0.45
<i>I</i> (HCO ⁺)/ <i>I</i> (HNC)	0.89	1.66	1.95
<i>I</i> (HCO ⁺)/ <i>I</i> (HCN)	1.30	1.20	0.98
<i>I</i> (N ₂ H ⁺)/ <i>I</i> (HNC)	0.96	1.02	0.82
<i>I</i> (N ₂ H ⁺)/ <i>I</i> (HCN)	1.24	0.95	0.46
<i>I</i> (HCN)/ <i>I</i> (HNC)	0.81	1.21	1.98
Column densities (10 ¹³ cm ⁻²)			
N _{N₂H⁺}	1.2	1.5	2.4
N _{HCO⁺}	0.4	0.5	0.9
N _{HCN}	1.1	1.5	2.9
N _{HNC}	0.6	0.7	1.1
Molecular abundance (10 ⁻⁹)			
<i>X</i> (N ₂ H ⁺)	0.16	0.31	0.43
<i>X</i> (HCO ⁺)	0.08	0.17	0.30
<i>X</i> (HCN)	0.31	0.46	1.01
<i>X</i> (HNC)	0.10	0.16	0.27
Abundance ratios			
<i>X</i> (N ₂ H ⁺)/ <i>X</i> (HCO ⁺)	2.12	1.82	1.49
<i>X</i> (N ₂ H ⁺)/ <i>X</i> (HCN)	0.50	0.70	0.45
<i>X</i> (N ₂ H ⁺)/ <i>X</i> (HNC)	1.61	1.89	1.60
<i>X</i> (HCO ⁺)/ <i>X</i> (HCN)	0.33	0.39	0.29
<i>X</i> (HCO ⁺)/ <i>X</i> (HNC)	0.73	1.05	1.11
<i>X</i> (HCN)/ <i>X</i> (HNC)	2.18	2.84	3.76

This table lists the summary median values of derived clump properties for each evolutionary stage. Column 1 lists the properties of the sources; Columns 2 to 4 list the median values of each evolutionary stages

the total 870 micron flux density over the line-emitting area; R is the gas-to-dust mass ratio, assumed = 100; Ω is the solid angle; μ is the mean molecular weight of the interstellar medium, assumed = 2.8; m_H is the mass of a hydrogen atom; B_ν is the Planck function for dust temperature T_D ; and κ_ν is the dust-absorption coefficient, taken as 1.85 cm² g⁻¹ (Ossenkopf and Henning 1994). Global averaged H₂ column densities corresponding to four molecules of each clump are shown in Table 4. Finally, the abundances X (N₂H⁺), X (HCO⁺), X (HCN), X (HNC), and abundance ratios between them were derived for each clump, as shown in Table 5. The median abundance and abundance ratios of the clumps in each evolutionary stage are shown in Table 6.

Table 7 Distance information

Source name (1)	Stage (2)	D _k (kpc) (3)	D _{GC} (kpc) (4)	Spiral arm (5)
G000.208-00.518	B	18.5	10.00	2
G000.633+00.601	C	25.23	16.73	1
G003.350-00.077	C	12.33	3.88	1
G003.415-00.354	B	21.05	12.58	2
G004.627-00.665	B	2.8	5.71	2
G004.827+00.231	B	3.43	5.09	2
G004.895-00.127	A	2.6	5.91	2
G005.505-00.245	A	12.5	4.12	1
G005.637+00.238	C	2.5	6.02	1
G005.831-00.512	C	13.27	4.89	3
G005.893-00.320	C	14.18	5.79	3
G006.119-00.636	C	3.35	5.18	2
G006.188-00.358	C	5.1	3.47	4
G006.216-00.609	B	3.5	5.04	2
G006.551-00.097	C	13.58	5.23	3
G006.796-00.256	C	3.7	4.85	2
G007.333-00.567	B	3.46	5.09	2
G007.993-00.269	B	4.7	3.90	4
G008.049-00.244	C	11.94	3.72	1
G008.206+00.190	B	3.09	5.46	2
G008.350-00.317	C	4.56	4.04	2
G008.458-00.224	B	4.47	4.13	2
G008.955-00.535	A	3.09	5.47	2
G009.037-00.521	B	12.28	4.11	1
G009.212-00.202	C	4.57	4.06	2
G009.283-00.149	B	4.5	4.12	2
G009.422-00.704	B	13.67	5.47	3
G009.620+00.195	C	5.2	3.48	4
G009.877-00.748	C	13	4.85	1
G010.473+00.028	C	5.63	3.14	3
G010.624-00.383	C	17.7	9.48	4
G010.630-00.510	C	16.98	8.77	4
G010.661+00.080	A	13.68	5.55	3
G010.680-00.027	C	11.81	3.80	1
G010.724-00.332	C	5.2	3.53	4
G010.746+00.015	A	12.83	4.75	1
G011.033+00.061	C	2.87	5.71	2
G011.112-00.399	C	16.4	8.22	4
G011.903-00.140	B	4.1	4.57	2
G011.942-00.156	C	4.1	4.57	2
G012.200-00.033	B	12	4.11	1
G012.418+00.506	C	2.33	6.24	1
G012.497-00.222	B	12.78	4.84	1
G012.625-00.017	B	12.9	4.97	1
G012.680-00.180	C	4.59	4.15	2
G012.774+00.337	C	14.4	6.39	3
G012.805-00.318	B	14.51	6.50	3
G012.905-00.030	B	11.77	3.97	1
G012.999-00.357	C	1.9	6.66	1
G013.131-00.150	C	12.5	4.64	1
G013.209-00.141	C	4.6	4.16	2
G013.657-00.599	C	4.3	4.44	2
G013.904-00.512	B	2.59	6.02	1
G014.101+00.086	C	5.67	3.30	4
G014.226-00.511	C	2.29	6.31	1
G014.245-00.071	C	11.6	3.96	1

Table 7 (Continued)

Source name (1)	Stage (2)	D _k (kpc) (3)	D _{GC} (kpc) (4)	Spiral arm (5)
G014.606+00.014	C	2.74	5.89	1
G014.632+00.308	C	13.52	5.71	3
G014.777-00.486	B	13.84	6.03	3
G340.054-00.244	C	4	4.93	2
G340.104-00.313	C	12	4.94	3
G340.229-00.144	A	12.11	5.02	3
G340.261+00.532	C	11.84	4.79	1
G340.311-00.436	B	12.26	5.13	4
G340.632-00.648	B	5.12	4.04	4
G340.764-00.132	B	12.68	5.43	4
G340.776-00.119	B	12.68	5.43	4
G340.785-00.097	B	9.9	3.37	3
G340.878-00.374	C	3.4	5.40	2
G340.934-00.233	B	12.39	5.17	4
G341.034-00.114	A	3.36	5.43	2
G341.038-00.113	A	3.37	5.42	2
G341.127-00.350	C	3.4	5.40	2
G342.484+00.183	C	12.6	5.17	3
G342.706+00.125	C	12.64	5.18	3
G342.822+00.382	B	5.08	3.94	4
G342.824+00.381	B	5.08	3.94	4
G343.127-00.063	B	2.8	5.88	2
G343.478-00.023	C	2.71	5.95	2
G343.492-00.068	C	2.74	5.92	2
G343.520-00.519	B	3.2	5.51	2
G343.689-00.018	C	13.08	5.47	3
G343.720-00.223	C	13.59	5.93	4
G343.738-00.112	B	2.67	5.98	2
G343.780-00.235	B	2.72	5.94	2
G344.915-00.229	B	10.84	3.44	3
G345.259-00.035	B	14.09	6.26	4
G345.261-00.418	C	2.8	5.84	2
G346.078-00.056	C	10.7	3.19	3
G346.307+00.114	C	13.32	5.45	3
G346.369-00.648	B	17.05	9.02	2
G346.484+00.220	A	14.2	6.26	4
G347.294+00.132	B	10.67	3.03	3
G347.682+00.207	C	11.11	3.34	3
G347.871+00.014	C	3.4	5.22	2
G347.967-00.434	C	5.53	3.30	4
G348.228+00.413	C	15.2	7.09	4
G348.290+00.643	B	1.29	7.24	1
G348.777+00.149	B	11.25	3.35	3
G348.892-00.179	C	19.7	11.48	2
G349.137+00.024	C	11.3	3.36	3
G350.014+00.434	C	12.83	4.70	3
G350.111+00.092	C	11.4	3.36	3
G350.183+00.003	C	5.49	3.23	4
G350.271-00.500	A	13.37	5.20	3
G350.412-00.062	A	3.4	5.18	2
G350.506+00.958	C	14.55	6.33	4
G350.522-00.349	C	3.1	5.47	2
G350.687-00.491	C	2.7	5.85	2
G350.688-00.489	C	2.7	5.85	2
G350.710+01.027	C	15.62	7.36	4
G350.763+00.793	C	1.12	7.40	1

Table 7 (Continued)

Source name (1)	Stage (2)	D _k (kpc) (3)	D _{GC} (kpc) (4)	Spiral arm (5)
G351.040-00.336	C	2.89	5.66	2
G351.532-00.557	B	13.2	4.95	3
G351.582-00.352	C	5.1	3.53	4
G352.060+00.603	A	16.7	8.37	4
G352.072+00.679	B	16.9	8.56	4
G352.142-01.016	B	14.21	5.91	3
G352.315-00.443	C	2.1	6.43	1
G352.492+00.796	C	0.68	7.83	1
G352.972+00.925	C	15.38	7.02	4
G353.010+00.983	C	15.52	7.16	4
G353.115+00.366	C	15.89	7.52	4
G353.146+00.663	C	16	7.63	4
G353.147+00.851	C	14.53	6.18	4
G353.198+00.927	C	15.37	7.00	4
G353.215-00.247	C	3.74	4.81	2
G353.271+00.641	C	1.19	7.32	1
G353.577+00.661	B	16.17	7.78	4
G353.975+00.256	B	17.4	8.99	2
G354.206-00.038	C	11.99	3.64	1
G354.207-00.036	C	11.99	3.64	1
G354.628-00.610	A	12.47	4.09	3
G354.813+00.976	B	4.32	4.22	4
G354.945-00.539	C	14.71	6.29	4
G355.182-00.419	B	1.2	7.30	1
G355.249+00.363	B	12.16	3.76	1
G355.265-00.269	B	15.55	7.11	4
G355.412+00.103	B	3	5.51	2
G355.589-00.035	B	4.34	4.19	4
G355.829-00.501	C	15.36	6.91	4
G355.935-00.346	B	14.08	5.63	3
G356.008-00.424	B	16.25	7.79	4
G356.008-00.758	C	1.7	6.81	1
G356.255-00.056	C	14.52	6.06	3
G356.305-00.204	C	13.64	5.19	3
G356.372+00.567	B	1.8	6.70	1
G356.482+00.190	B	14.39	5.93	3
G356.517+00.664	B	16.1	7.63	4
G356.662-00.265	B	5.1	3.42	4
G356.858+00.327	B	12.34	3.88	1
G357.462-00.339	A	20.94	12.45	2
G357.554-00.550	C	17.59	9.11	4
G357.558-00.323	B	18.57	10.08	2
G357.786-00.311	B	23.85	15.36	1
G357.921-00.337	C	3.16	5.34	2
G357.967-00.163	C	14.63	6.14	3
G357.998-00.154	C	2.87	5.63	2
G358.388-00.484	C	2.4	6.10	1
G358.460-00.393	B	2.9	5.60	2
G359.941+00.173	C	4.6	3.90	4
G359.944+00.152	C	4.6	3.90	4

This table lists the distance information of the sources. Column 1 is the source name; Column 2 lists the evolutionary classifications of the 197 sources; Column 3 lists the kinematic distance of the sources; Column 4 lists the distance from the Galactic Center of the source; Column 5 lists the classifications of the sources lie in different spiral arms

3.3 Distance

Distance is critical to derive the physical parameters of the clump and determine its position in the Galaxy. The kinematic distance of each clump was derived by using on the Galactic rotation model of Reid et al. (2009) (R_o is the Galactocentric distance of the Sun, and Θ_o is the circular rotation speed of the Sun. $R_o = 8.4 \pm 0.6$ kpc, $\Theta_o = 254 \pm 16 \text{ km s}^{-1}$) with the radial velocity derived from N_2H^+ (1–0). The local standard of rest (LSR) velocities of N_2H^+ (1–0) are listed in Table 1 and HI data from the Southern Galactic Plane Survey (SGPS) (McClure-Griffiths et al. 2005) were used to resolve possible kinematic distance

ambiguity (Fig. 2). Finally, the kinematic distances of 162 clumps (see Table 7) were obtained. The kinematic distances of clumps located within the direction $-3^\circ \leq \ell \leq 3^\circ$ were not derived due to large errors.

4 Discussion

4.1 Global averaged integrated intensities and ratios

Feedback from star formation can change the physical conditions and chemical composition of star forming clumps. It

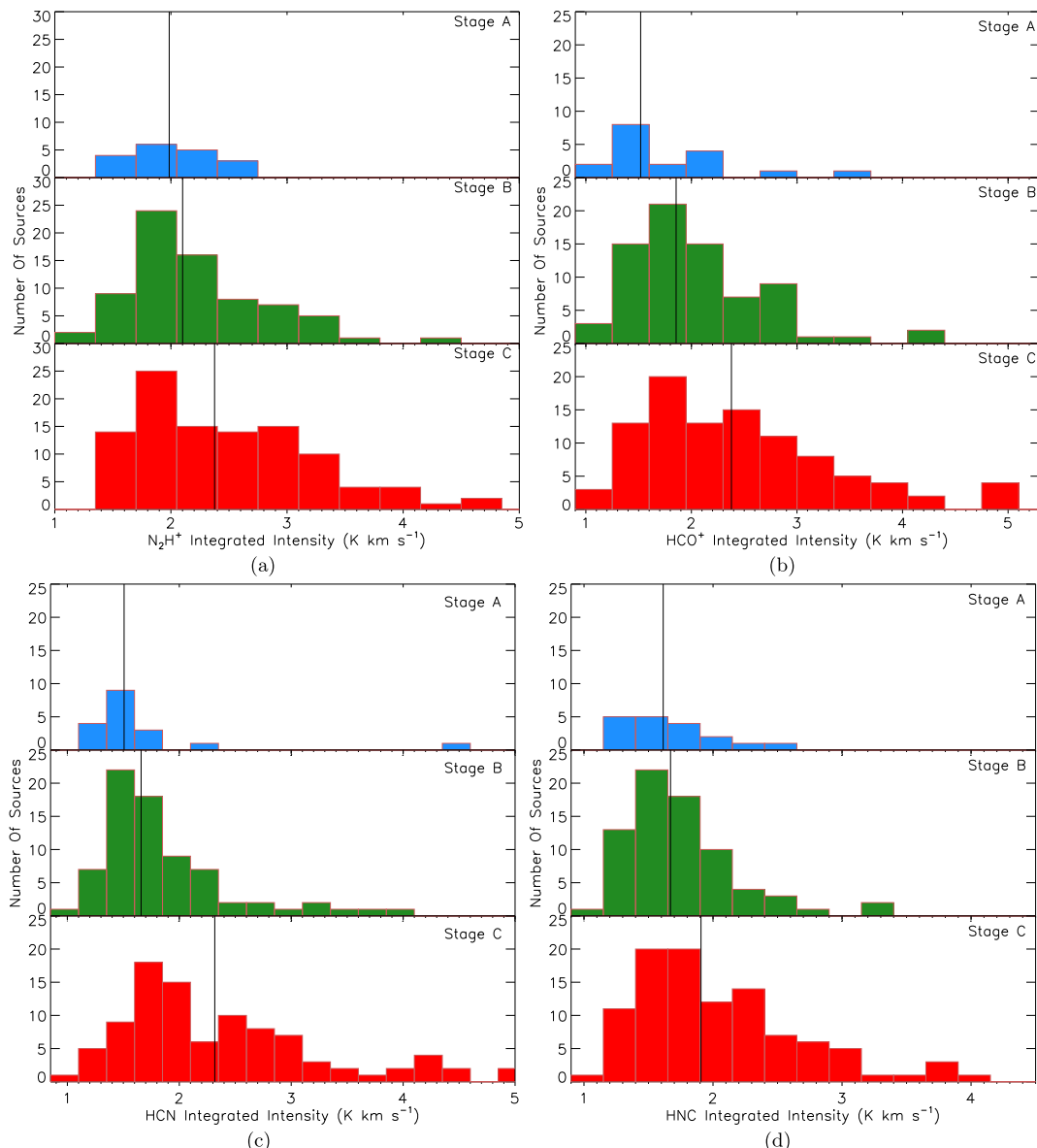


Fig. 3 The histograms of the global averaged integrated intensities of N_2H^+ (1–0), HCO^+ (1–0), HCN (1–0) and HNC (1–0) for the stage A, B and C, respectively. The name of the evolutionary stage is given on

the top right corner of each panel. The vertical solid lines indicate the median values of the integrated intensities for each evolutionary stage. The median values are given in Table 6

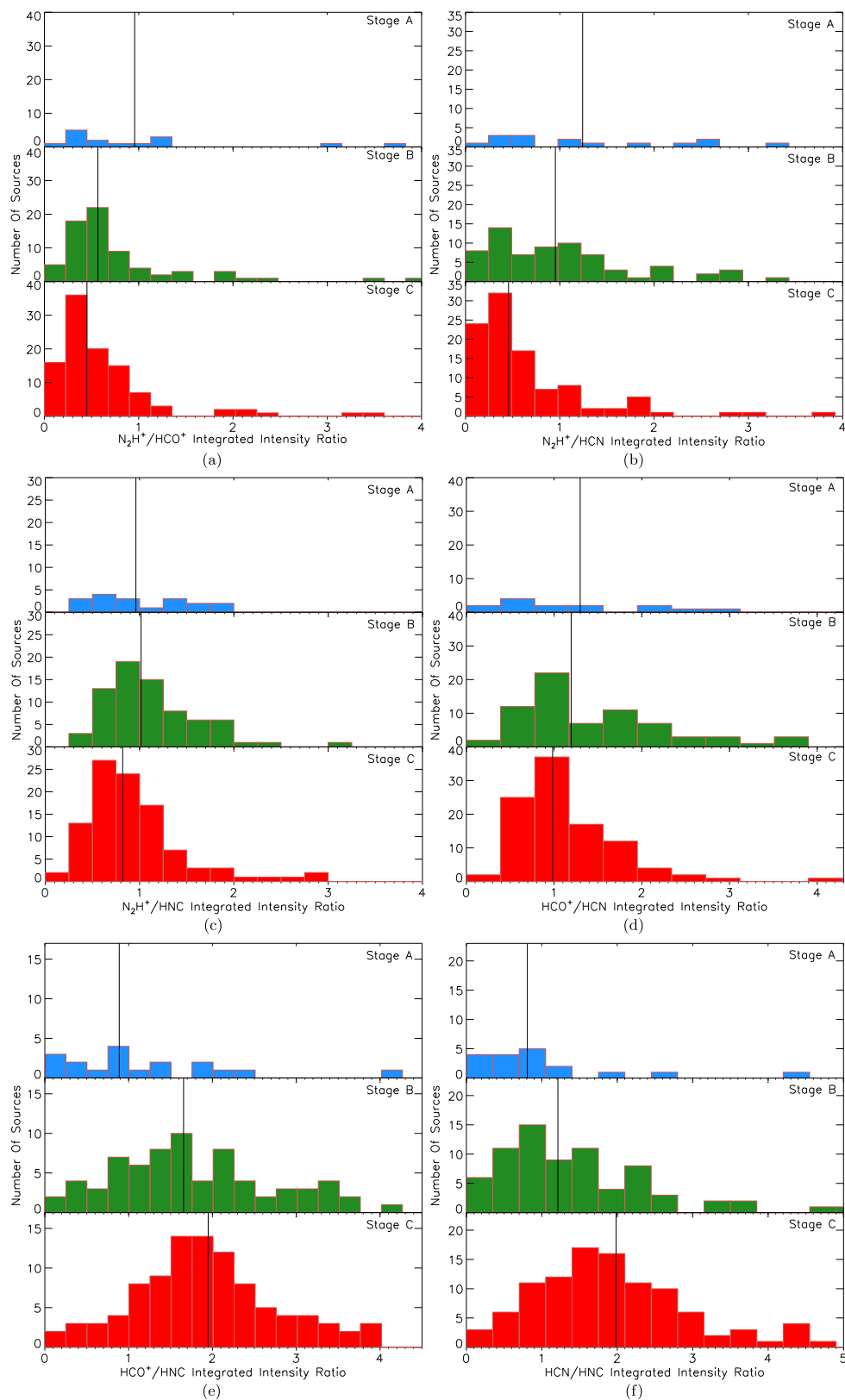


Fig. 4 The histograms of the global averaged integrated intensity ratios of $I(\text{N}_2\text{H}^+ (1-0))/I(\text{HCO}^+ (1-0))$, $I(\text{N}_2\text{H}^+ (1-0))/I(\text{HCN} (1-0))$, $I(\text{N}_2\text{H}^+ (1-0))/I(\text{HNC} (1-0))$, $I(\text{HCO}^+ (1-0))/I(\text{HCN} (1-0))$, $I(\text{HCO}^+ (1-0))/I(\text{HNC} (1-0))$ and $I(\text{HCN} (1-0))/I(\text{HNC} (1-0))$ for the stage A, B and C, respectively. The name of the evo-

lutionary stage is given on the top right corner of each panel. The vertical solid lines indicate the median values of the integrate intensity ratios for each evolutionary stage. The median values are given in Table 6

is reasonable to expect that the global averaged integrated intensities of molecules and the ratios between them will change with clump evolution.

Figure 3 shows global averaged integrated intensities for $I(N_2H^+ (1-0))$, $I(HCO^+ (1-0))$, $I(HCN (1-0))$, and $I(HNC (1-0))$ of all sources in stages A, B and C. Median values of $I(N_2H^+ (1-0))$ increase by $\sim 6\%$ and $\sim 13\%$ from stage A to B and B to C. Median values of $I(HNC (1-0))$ increase by $\sim 4\%$ and $\sim 14\%$ from stage A to B and B to C. Median values of $I(HCO^+ (1-0))$ increase by $\sim 22\%$ and $\sim 28\%$ from stage A to B and B

to C. Median values of $I(HCN (1-0))$ increase by $\sim 10\%$ and $\sim 40\%$ from stage A to B and B to C (see the corresponding median values in Table 6). $I(N_2H^+ (1-0))$ and $I(HNC (1-0))$ increase relatively slowly with evolutionary stage, whereas $I(HCO^+ (1-0))$ and $I(HCN (1-0))$ increase much faster.

From Fig. 4 and Table 6, we can see that median values of $I(N_2H^+ (1-0))/I(HCO^+ (1-0))$ decrease by $\sim 41\%$ and $\sim 21\%$ from stage A to B and B to C. Median values of $I(N_2H^+ (1-0))/I(HCN (1-0))$ decrease by $\sim 23\%$ and $\sim 52\%$ from stage A to B and B to C. Median val-

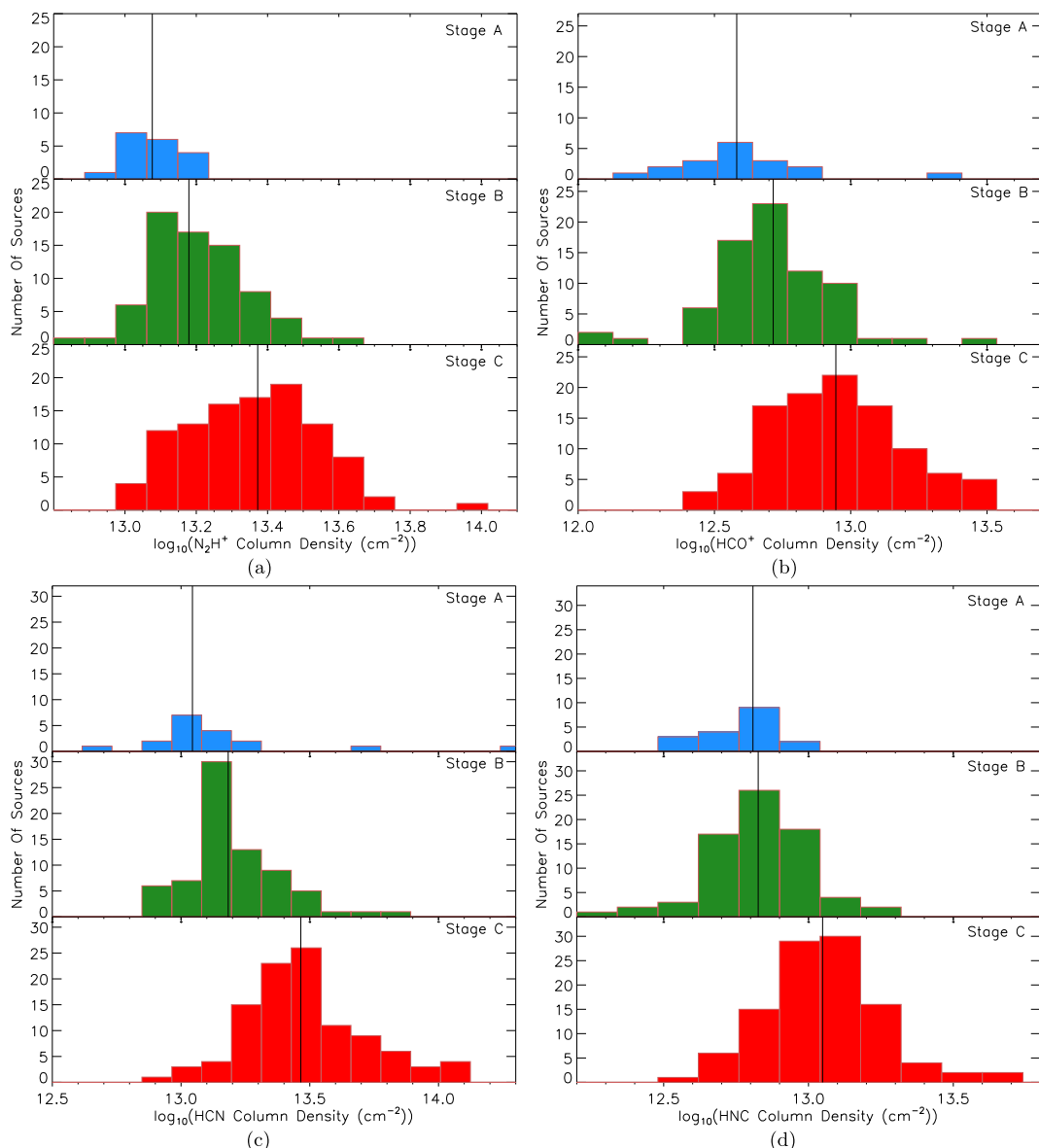


Fig. 5 The histograms of the global averaged column densities of N_2H^+ , HCO^+ , HCN and HNC for the stage A, B and C, respectively. The name of the evolutionary stage is given on the top right corner of

each panel. The vertical solid lines indicate the median values of the column densities for each evolutionary stage. The median values are given in Table 6

ues of $I(\text{HCO}^+)/I(\text{HNC})$ increase by $\sim 86\%$ and $\sim 18\%$ from stage A to B and to C. Median values of $I(\text{HCN}\ (1-0))/I(\text{HNC}\ (1-0))$ increase by $\sim 50\%$ and $\sim 64\%$ from stage A to B and B to C. Thus, these four ratios are promising tracers from stage A to B and B to C.

We note that there is significant overlap in these line ratios between different stages (Fig. 4). One possible reason could be that high-mass star formation is a complex and consecutive process, rather than being separable into completely distinct stages.

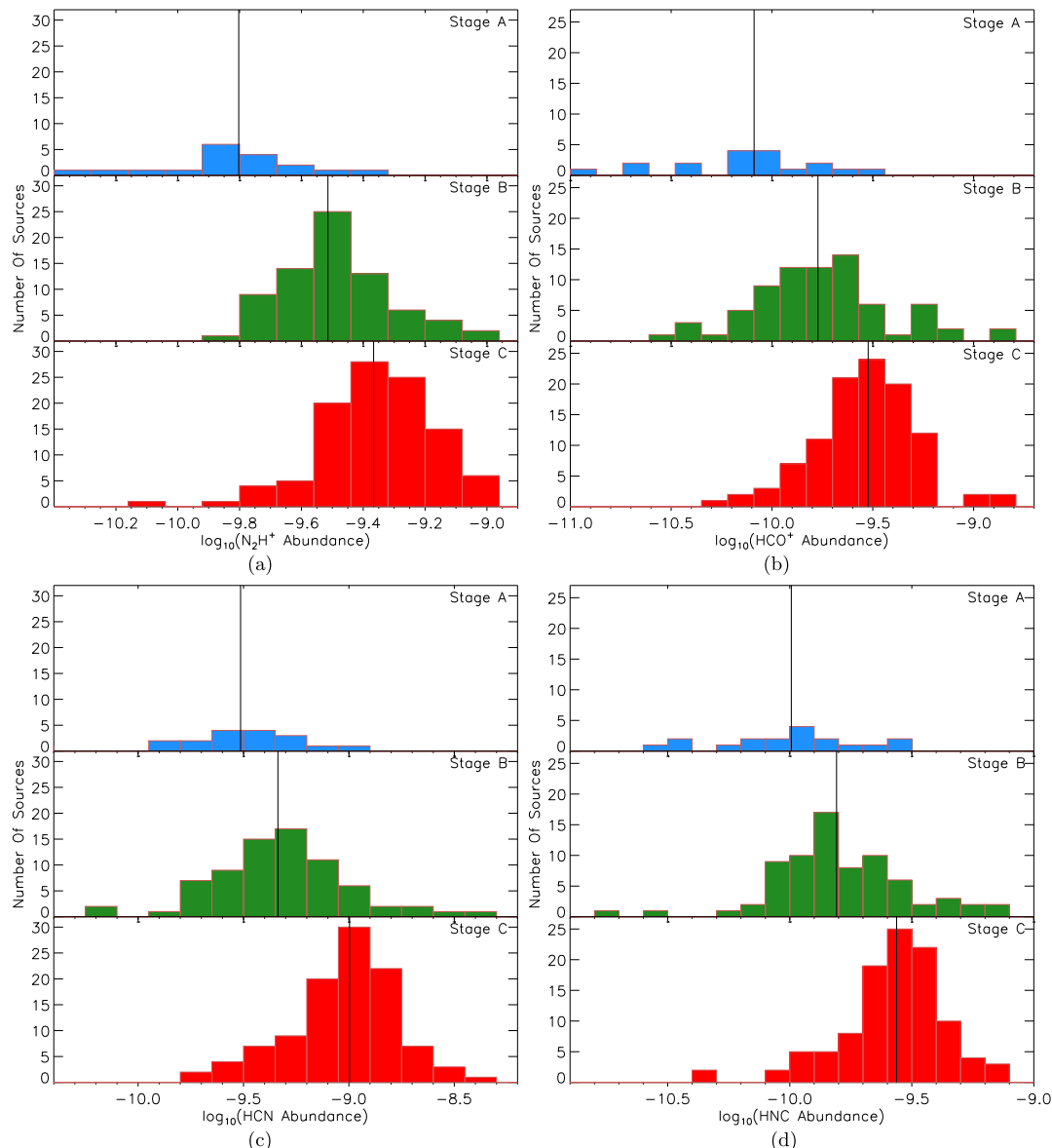


Fig. 6 The histograms of the global averaged abundances of N_2H^+ , HCO^+ , HCN and HNC for the stage A, B and C (in logarithm), respectively. The name of the evolutionary stage is given on the top right corner of each panel. The vertical solid lines indicate the median values of the abundance for each evolutionary stage. The median values are given in Table 6

4.2 The global averaged abundances and ratios between them

Global averaged column density $N(\text{N}_2\text{H}^+)$ and abundance $X(\text{N}_2\text{H}^+)$ increase from stage A to B, and B to C (Figs. 5(a) and 6(a)). The N_2H^+ column densities lie in the range 7.0×10^{12} – $8.8 \times 10^{13} \text{ cm}^{-2}$, with median values for stages A, B, and C of 1.2×10^{13} , 1.5×10^{13} , and $2.4 \times 10^{13} \text{ cm}^{-2}$, respectively. The N_2H^+ abundances lie in the range 5.0×10^{-12} – 1.1×10^{-9} , with median values increasing by 95 % and 41 % from stage A to B and B to C. CO is a major de-

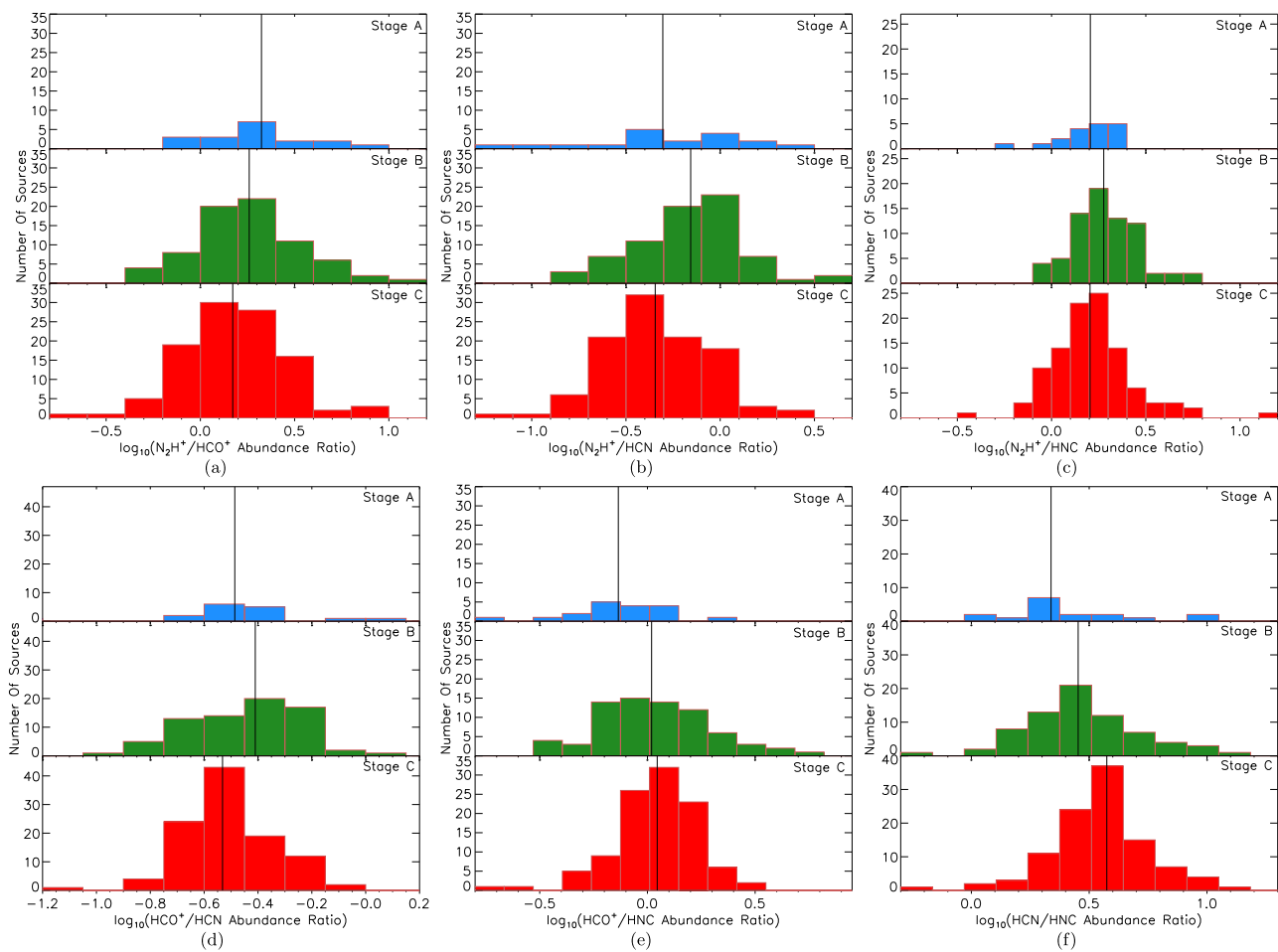


Fig. 7 The histograms of the global averaged abundance ratios (in logarithm) of $X(\text{N}_2\text{H}^+)/X(\text{HCO}^+)$, $X(\text{N}_2\text{H}^+)/X(\text{HCN})$, $X(\text{N}_2\text{H}^+)/X(\text{HNC})$, $X(\text{HCO}^+)/X(\text{HCN})$, $X(\text{HCO}^+)/X(\text{HNC})$ and $X(\text{HCN})/X(\text{HNC})$ for the stage A, B and C, respectively. The name of

the evolutionary stage is given on the top right corner of each panel. The vertical solid lines indicate the median values of the abundance ratios for each evolutionary stage. The median values are given in Table 6

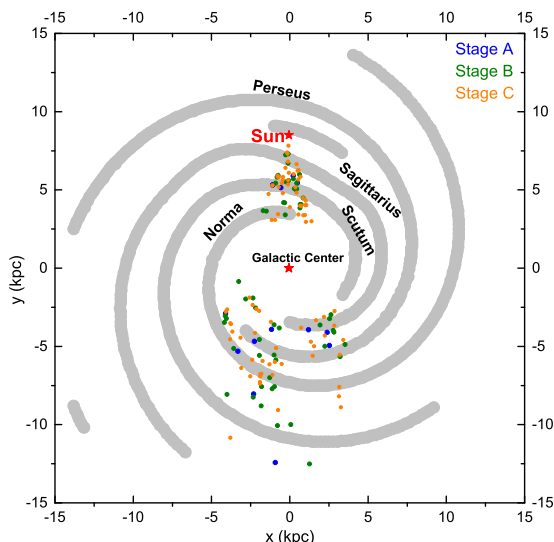


Fig. 8 The distribution of high-mass star-forming clumps in the Galaxy. The positions of the spiral arms are taken from Cordes and Lazio (2002)

destroyer of N_2H^+ , so N_2H^+ abundance should be relatively high in stage A clumps since CO is frozen out onto dust grains at this evolutionary stage, then decrease in stages B and C with CO being released back into the gas phase as the dust temperature increases. However, the observed result is contrary to this prediction, N_2H^+ abundance increase as a function of the evolution stage. And this result was also observed in other samples (Sanhueza et al. 2012; Hoq et al. 2013; Miettinen 2014).

In the case of HCO^+ , as CO is the parent molecule, the HCO^+ abundance should be depleted in the early, prestellar phase and increase in the later, warmer phases when CO is released back into the gas phase (Caselli et al. 1999; Sanhueza et al. 2012; Hoq et al. 2013). This accords well with the observed global averaged column density $N(\text{HCO}^+)$ and abundance $X(\text{HCO}^+)$ which increase as the clumps

evolve (Figs. 5(b) and 6(b)). The HCO^+ column densities lie in the range 1.0×10^{12} – $3.4 \times 10^{13} \text{ cm}^{-2}$, with median values for stages A, B, and C of 4.0×10^{12} , 5.0×10^{12} , and $9.0 \times 10^{12} \text{ cm}^{-2}$, respectively. The HCO^+ abundances lie in the range 1.0×10^{-11} – 1.5×10^{-9} , with median values for stages A, B, and C of 8.0×10^{-11} , 1.7×10^{-10} , and

3.0×10^{-10} , increasing by $\sim 106\%$ and $\sim 77\%$ from stage A to B and B to C. Median values of $X(\text{N}_2\text{H}^+)/X(\text{HCO}^+)$ for stages A, B, and C decrease by $\sim 14\%$ and $\sim 18\%$ from stage A to B and B to C (Fig. 7(a), Table 6). This suggests that production of HCO^+ is very efficient in stages B and C.

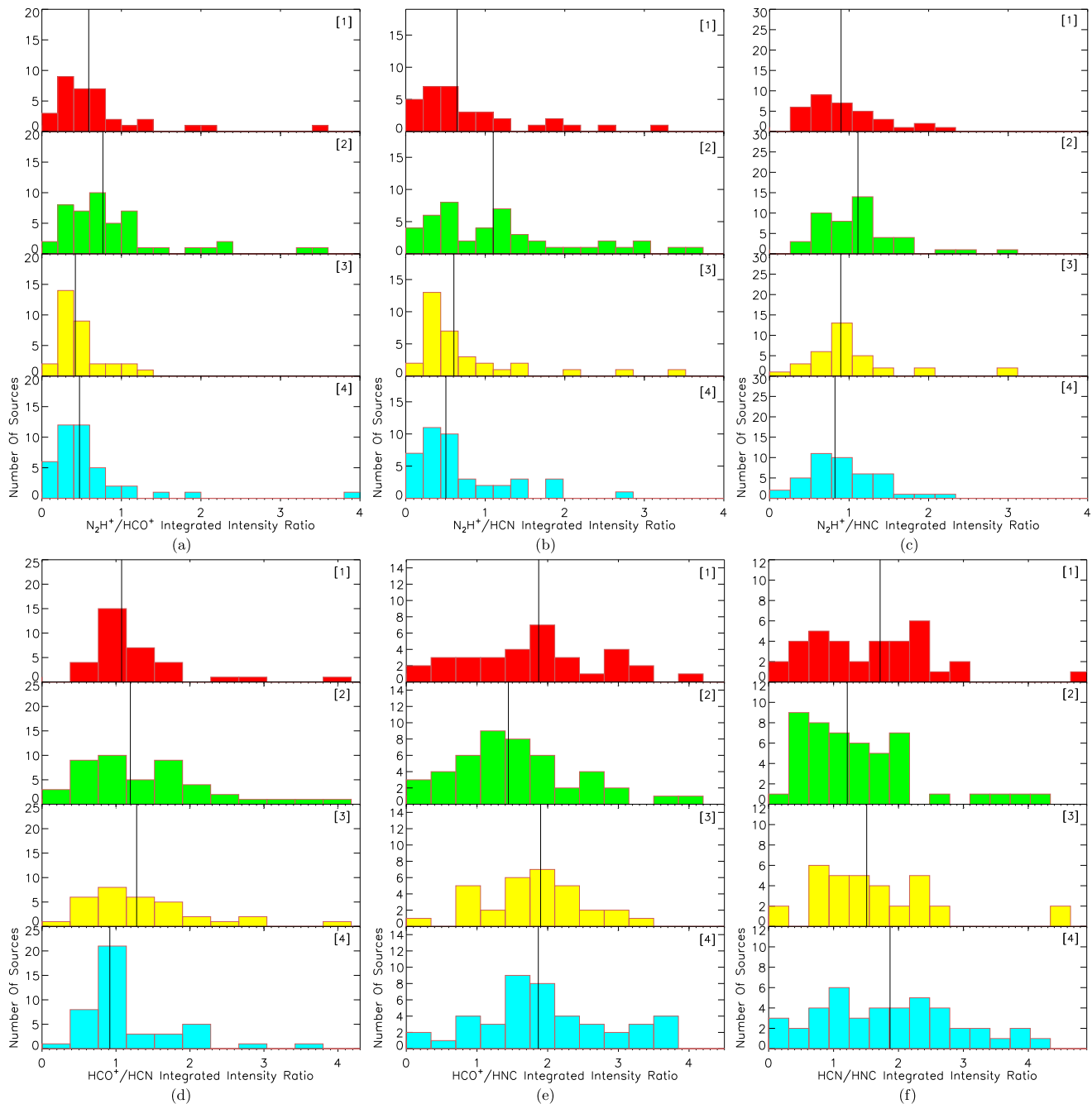


Fig. 9 The histograms of the global averaged integrated intensity ratios of $I(\text{N}_2\text{H}^+ (1-0))/I(\text{HCO}^+ (1-0))$, $I(\text{N}_2\text{H}^+ (1-0))/I(\text{HCN} (1-0))$, $I(\text{N}_2\text{H}^+ (1-0))/I(\text{HNC} (1-0))$, $I(\text{HCO}^+ (1-0))/I(\text{HCN} (1-0))$, $I(\text{HCO}^+ (1-0))/I(\text{HNC} (1-0))$ and $I(\text{HCN} (1-0))/I(\text{HNC} (1-0))$ for the stage A, B and C in each spiral arm of the Galaxy, respectively. The name of the spiral arm is given on the top right corner of each panel. The vertical solid lines indicate the median values for each spiral arm. The median values are given in Table 8

(1-0)) for the stage A, B and C in each spiral arm of the Galaxy, respectively. The name of the spiral arm is given on the top right corner of each panel. The vertical solid lines indicate the median values for each spiral arm. The median values are given in Table 8

Figures 5(d) and 6(d) show that $N(\text{HNC})$ and $X(\text{HNC})$ increase as a function of evolutionary stage. The HNC column densities lie in the range 5.0×10^{11} – $4.4 \times 10^{13} \text{ cm}^{-2}$, with median values for stages A, B, and C of 6.0×10^{12} , 7.0×10^{12} , and $1.1 \times 10^{13} \text{ cm}^{-2}$, respectively. The HNC abundances lie in the range 2.0×10^{-11} – 7.5×10^{-10} , its

median values increase by $\sim 54\%$ and $\sim 75\%$ from stage A to B and B to C. Since HNC transfers to HCN at high temperature (the high temperature limit means 24 K) (Schilke et al. 1992; Hirota et al. 1998; Vasyunina et al. 2011; Han et al. 2015), it is reasonable to expect $N(\text{HNC})$ and $X(\text{HNC})$ to decrease, while $N(\text{HCN})$ and $X(\text{HCN})$ in-

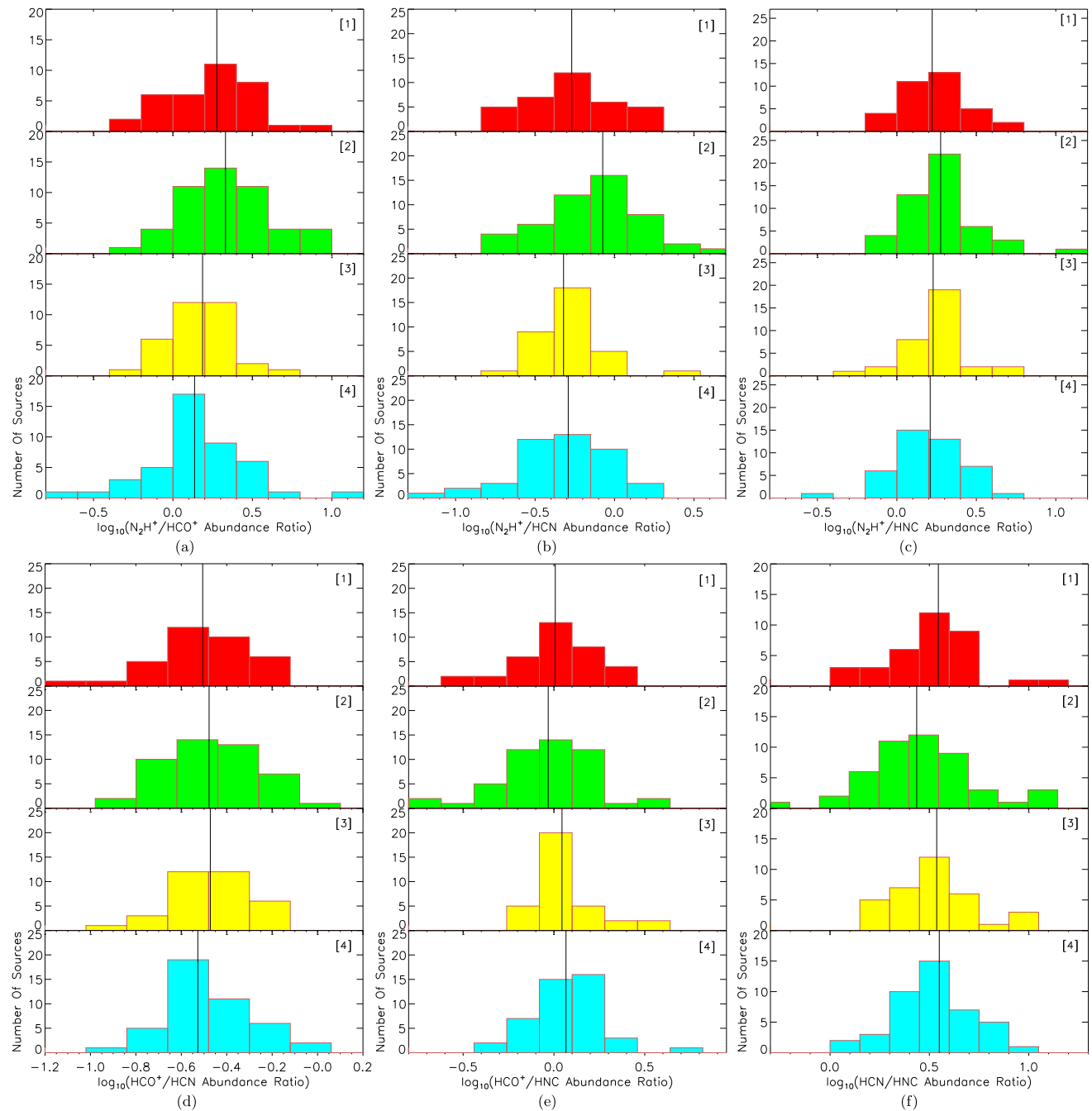


Fig. 10 The histograms of the global averaged abundance ratios (in logarithm) of $X(\text{N}_2\text{H}^+)/X(\text{HCO}^+)$, $X(\text{N}_2\text{H}^+)/X(\text{HCN})$, $X(\text{N}_2\text{H}^+)/X(\text{HNC})$, $X(\text{HCO}^+)/X(\text{HCN})$, $X(\text{HCO}^+)/X(\text{HNC})$ and $X(\text{HCN})/X(\text{HNC})$ for the stage A, B and C in each spiral arm of the Galaxy,

respectively. The name of the spiral arm is given on the top right corner of each panel. The vertical solid lines indicate the median values for each spiral arm. The median values are given in Table 8

crease as clumps evolve. This result was also observed in other samples (Sanhueza et al. 2012; Miettinen 2014). As expected, $N(\text{HCN})$ and $X(\text{HCN})$ increase with clump evolutionary stage (Figs. 5(c) and 6(c)). The HCN column densities lie in the range 1.0×10^{12} – $1.8 \times 10^{14} \text{ cm}^{-2}$, with median values for stages A, B, and C of 1.1×10^{13} , 1.5×10^{13} , and $2.9 \times 10^{13} \text{ cm}^{-2}$, respectively. The HCN abundances lie in the range 4.0×10^{-11} – 4.9×10^{-9} , its median values, increase by $\sim 50\%$ and $\sim 117\%$ from stage A to B and B to C. Median values of $X(\text{HCN})/X(\text{HNC})$ increase by $\sim 30\%$ and $\sim 32\%$ from stage A to B and B to C (Fig. 7(f), Table 6).

Therefore, $X(\text{HCN})/X(\text{HNC})$ could be used to trace evolution from stage A to B and B to C. On the other hand, me-

dian values of $X(\text{HCO}^+)/X(\text{HNC})$ increase by $\sim 43\%$ and $\sim 6\%$ from stage A to B and B to C (Fig. 7(e), Table 6), it is more suitable for distinguishing high-mass star forming clumps in stage A from those in stages B and C.

4.3 Chemical properties of high-mass star forming clumps in spiral arms

4.3.1 Clumps in different spiral arms

The high-mass star forming clumps were identified on the Galactic plane, and the spiral arm positions were taken from Cordes and Lazio (2002) (Fig. 8). The Sagittarius, Scutum-Centaurus, Perseus, and Norma spiral are hereafter called spiral arm 1, 2, 3, and 4, respectively.

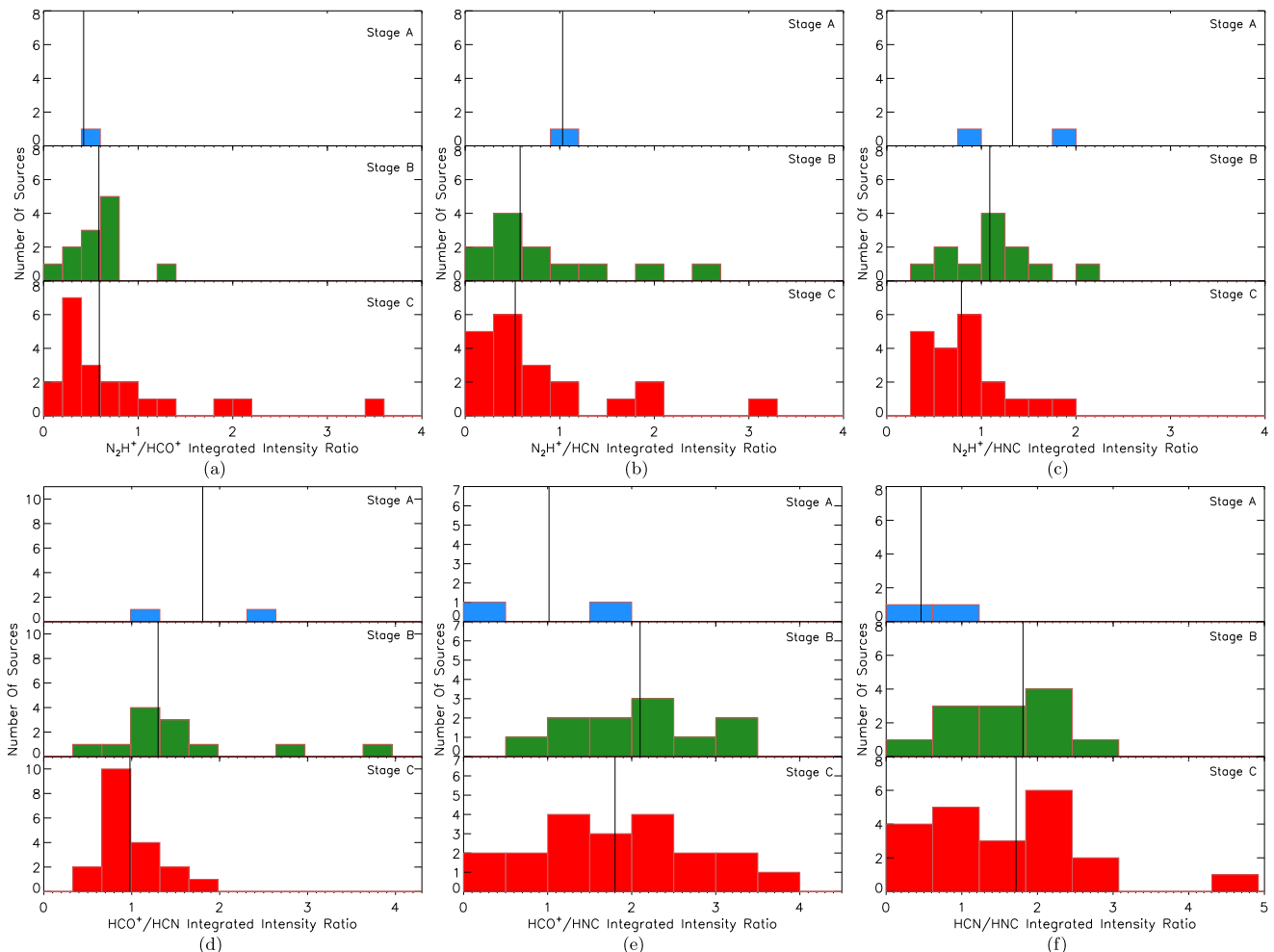


Fig. 11 The histograms of the global averaged integrated intensity ratios of $I(\text{N}_2\text{H}^+ (1-0))/I(\text{HCO}^+ (1-0))$, $I(\text{N}_2\text{H}^+ (1-0))/I(\text{HCN} (1-0))$, $I(\text{HCO}^+ (1-0))/I(\text{HCN} (1-0))$, $I(\text{HCO}^+ (1-0))/I(\text{HNC} (1-0))$ and $I(\text{HCN} (1-0))/I(\text{HNC} (1-0))$ for the stage A, B and C in the spiral arm 1 of the

Galaxy, respectively. The name of the evolutionary stage is given on the top right corner of each panel. The vertical solid lines indicate the median values of the integrate intensity ratios for each evolutionary stage. The median values are given in Table 8

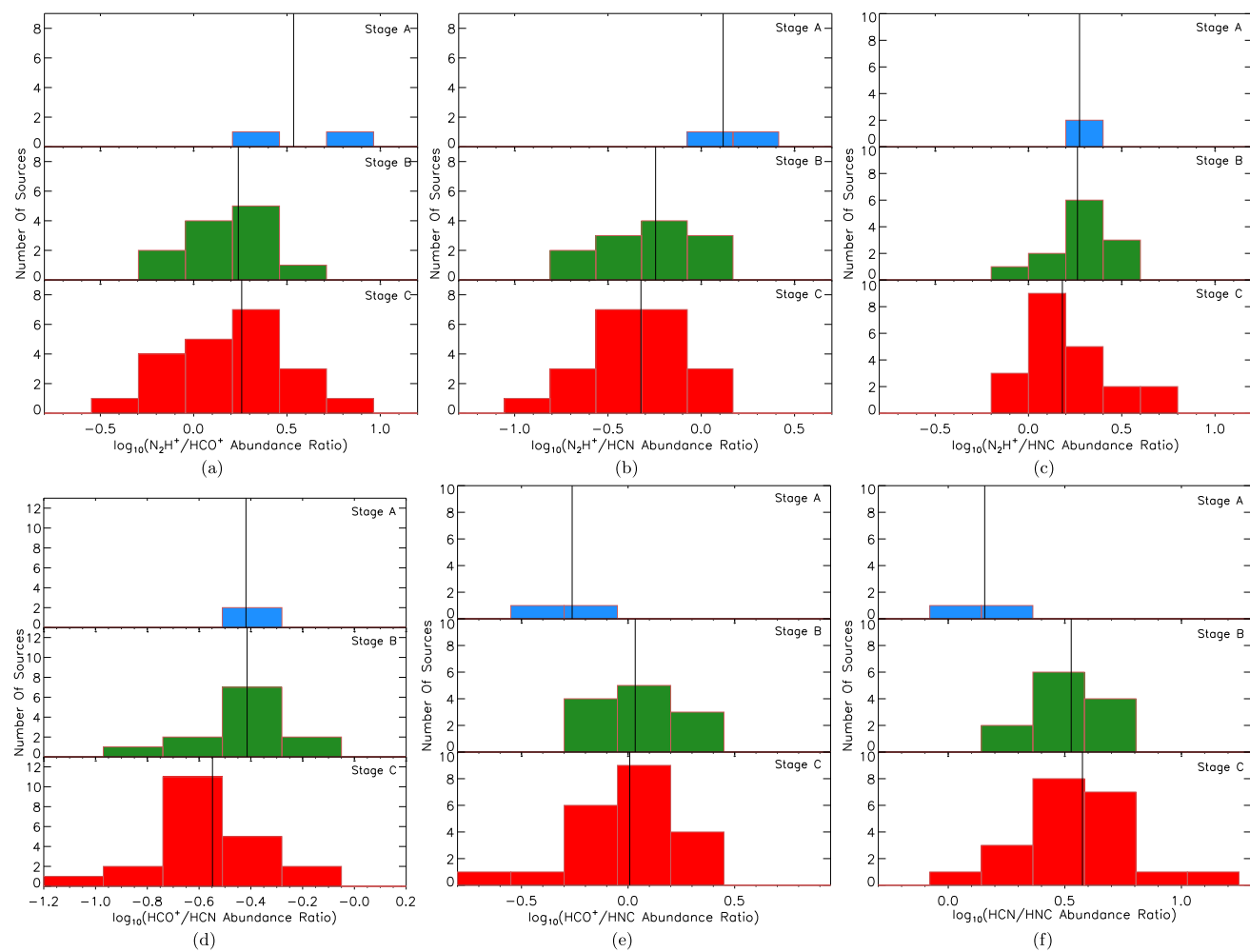


Fig. 12 The histograms of the global averaged abundance ratios (in logarithm) of $X(\text{N}_2\text{H}^+)/X(\text{HCO}^+)$, $X(\text{N}_2\text{H}^+)/X(\text{HCN})$, $X(\text{N}_2\text{H}^+)/X(\text{HNC})$, $X(\text{HCO}^+)/X(\text{HCN})$, $X(\text{HCO}^+)/X(\text{HNC})$ and $X(\text{HCN})/X(\text{HNC})$ for the stage A, B and C in the spiral arm 1 of the Galaxy, respectively. The name of the evolutionary stage is given on the top right corner of each panel. The vertical solid lines indicate the median values of the abundance ratios for each evolutionary stage. The median values are given in Table 8

Galaxy, respectively. The name of the evolutionary stage is given on the top right corner of each panel. The vertical solid lines indicate the median values of the abundance ratios for each evolutionary stage. The median values are given in Table 8

Figures 9 and 10 show the global averaged integrated intensity ratios and abundance ratios of high-mass star forming clumps located in spiral arms 1–4 separately. There are no significant regular changes among the spiral arms.

Figures 11 and 12 show global averaged integrated intensity and abundances ratios for the high-mass star forming clumps at different evolutionary stages located in spiral arm 1, and their median values are shown in Table 8. Median values of $I(\text{N}_2\text{H}^+ (1-0))/I(\text{HCO}^+ (1-0))$ increase by ~38 % from stage A to B, with no significant variation from stage B to C. Median values of $I(\text{N}_2\text{H}^+ (1-0))/I(\text{HCN} (1-0))$ decrease by ~44 % and ~9 % from stage A to B and B to C. Median values of $I(\text{HCN} (1-0))/I(\text{HNC} (1-0))$ increase by ~292 % from stage A to B, with no significant variation from stage

B to C. They are suitable for distinguishing clumps in stage A from those in stages B and C. Median values of $I(\text{N}_2\text{H}^+ (1-0))/I(\text{HNC} (1-0))$ decrease by ~18 % and ~28 % from stage A to B and B to C. Median values of $I(\text{HCO}^+ (1-0))/I(\text{HCN} (1-0))$ decrease by ~28 % and ~25 % from stage A to B and B to C. They could be used to trace evolution from stage A to B and B to C.

Median values of $X(\text{HCO}^+)/X(\text{HNC})$ increase by ~80 % from stage A to B, but show no significant variation from stage B to C. Median values of $X(\text{HCN})/X(\text{HNC})$ increase by ~124 % and ~12 % stage A to B and B to C. They are suitable for distinguishing clumps in stages A from those in stage B and C. Median values of $X(\text{N}_2\text{H}^+)/X(\text{HCN})$ decrease by ~60 % and ~17 % from stage A to B and B to C, it is suitable for distinguishing

Table 8 Summary of properties on different spiral arms

Spiral arm (1)	Property (2)	Stage A (Median) (3)	Stage B (Median) (4)	Stage C (Median) (5)	Each spiral arm source (Median) (6)
Integrated intensity ratios					
1	$I(\text{N}_2\text{H}^+)/I(\text{HCO}^+)$	0.42	0.58	0.59	0.59
	$I(\text{HCO}^+)/I(\text{HNC})$	1.01	2.10	1.80	1.87
	$I(\text{HCO}^+)/I(\text{HCN})$	1.80	1.30	0.98	1.08
	$I(\text{N}_2\text{H}^+)/I(\text{HCN})$	1.33	1.09	0.79	0.90
	$I(\text{N}_2\text{H}^+)/I(\text{HNC})$	1.03	0.58	0.53	0.65
	$I(\text{HCN})/I(\text{HNC})$	0.46	1.81	1.72	1.72
Abundance ratios					
1	$X(\text{N}_2\text{H}^+)/X(\text{HCO}^+)$	4.03	1.74	1.81	1.89
	$X(\text{N}_2\text{H}^+)/X(\text{HCN})$	1.44	0.57	0.48	0.54
	$X(\text{N}_2\text{H}^+)/X(\text{HNC})$	1.89	1.83	1.52	1.67
	$X(\text{HCO}^+)/X(\text{HCN})$	0.39	0.39	0.28	0.31
	$X(\text{HCO}^+)/X(\text{HNC})$	0.61	1.09	1.02	1.02
	$X(\text{HCN})/X(\text{HNC})$	1.51	3.37	3.76	3.51
Integrated intensity ratios					
2	$I(\text{N}_2\text{H}^+)/I(\text{HCO}^+)$	1.14	0.80	0.66	0.77
	$I(\text{HCO}^+)/I(\text{HNC})$	1.00	1.43	1.96	1.44
	$I(\text{HCO}^+)/I(\text{HCN})$	1.37	1.01	1.38	1.19
	$I(\text{N}_2\text{H}^+)/I(\text{HNC})$	1.37	1.11	1.02	1.11
	$I(\text{N}_2\text{H}^+)/I(\text{HCN})$	1.74	1.14	0.95	1.10
	$I(\text{HCN})/I(\text{HNC})$	0.92	0.90	1.53	1.21
Abundance ratios					
2	$X(\text{N}_2\text{H}^+)/X(\text{HCO}^+)$	2.13	2.17	2.11	2.14
	$X(\text{N}_2\text{H}^+)/X(\text{HCN})$	0.74	0.87	0.63	0.84
	$X(\text{N}_2\text{H}^+)/X(\text{HNC})$	1.58	1.89	1.85	1.89
	$X(\text{HCO}^+)/X(\text{HCN})$	0.37	0.28	0.33	0.33
	$X(\text{HCO}^+)/X(\text{HNC})$	0.93	0.73	1.16	0.93
	$X(\text{HCN})/X(\text{HNC})$	2.60	2.34	3.14	2.73
Integrated intensity ratios					
3	$I(\text{N}_2\text{H}^+)/I(\text{HCO}^+)$	0.35	0.38	0.46	0.42
	$I(\text{HCO}^+)/I(\text{HNC})$	1.45	1.62	1.98	1.90
	$I(\text{HCO}^+)/I(\text{HCN})$	1.76	1.39	1.23	1.28
	$I(\text{N}_2\text{H}^+)/I(\text{HCN})$	0.56	0.86	1.00	0.90
	$I(\text{N}_2\text{H}^+)/I(\text{HNC})$	0.52	0.68	0.57	0.61
	$I(\text{HCN})/I(\text{HNC})$	0.85	1.21	1.78	1.51
Abundance ratios					
3	$X(\text{N}_2\text{H}^+)/X(\text{HCO}^+)$	1.34	1.55	1.52	1.54
	$X(\text{N}_2\text{H}^+)/X(\text{HCN})$	0.47	0.61	0.47	0.48
	$X(\text{N}_2\text{H}^+)/X(\text{HNC})$	1.23	1.73	1.71	1.69
	$X(\text{HCO}^+)/X(\text{HCN})$	0.39	0.44	0.33	0.34
	$X(\text{HCO}^+)/X(\text{HNC})$	0.90	1.06	1.16	1.11
	$X(\text{HCN})/X(\text{HNC})$	2.10	2.75	3.77	3.45

Table 8 (Continued)

Spiral arm (1)	Property (2)	Stage A (Median) (3)	Stage B (Median) (4)	Stage C (Median) (5)	Each spiral arm source (Median) (6)
Integrated intensity ratios					
4	$I(\text{N}_2\text{H}^+)/I(\text{HCO}^+)$	0.84	0.50	0.42	0.47
	$I(\text{HCO}^+)/I(\text{HNC})$	0.88	1.79	2.00	1.87
	$I(\text{HCO}^+)/I(\text{HCN})$	0.95	1.09	0.88	0.92
	$I(\text{N}_2\text{H}^+)/I(\text{HCN})$	0.77	0.95	0.76	0.82
	$I(\text{N}_2\text{H}^+)/I(\text{HNC})$	0.86	1.04	0.38	0.51
	$I(\text{HCN})/I(\text{HNC})$	0.94	1.34	2.45	1.87
Abundance ratios					
4	$X(\text{N}_2\text{H}^+)/X(\text{HCO}^+)$	2.37	1.42	1.30	1.37
	$X(\text{N}_2\text{H}^+)/X(\text{HCN})$	0.73	0.64	0.40	0.51
	$X(\text{N}_2\text{H}^+)/X(\text{HNC})$	1.55	2.00	1.40	1.62
	$X(\text{HCO}^+)/X(\text{HCN})$	0.30	0.43	0.29	0.30
	$X(\text{HCO}^+)/X(\text{HNC})$	0.69	1.36	1.12	1.17
	$X(\text{HCN})/X(\text{HNC})$	2.36	3.23	3.91	3.55

This table lists the summary median values of each spiral arm. *Column 1* lists the location of the sources (spiral arm 1, 2, 3 and 4); *Column 2* lists the properties of the sources; *Columns 3 to 5* list the median values of each evolutionary stages; *Column 6* list the median values of each spiral arms (including all evolutionary stages)

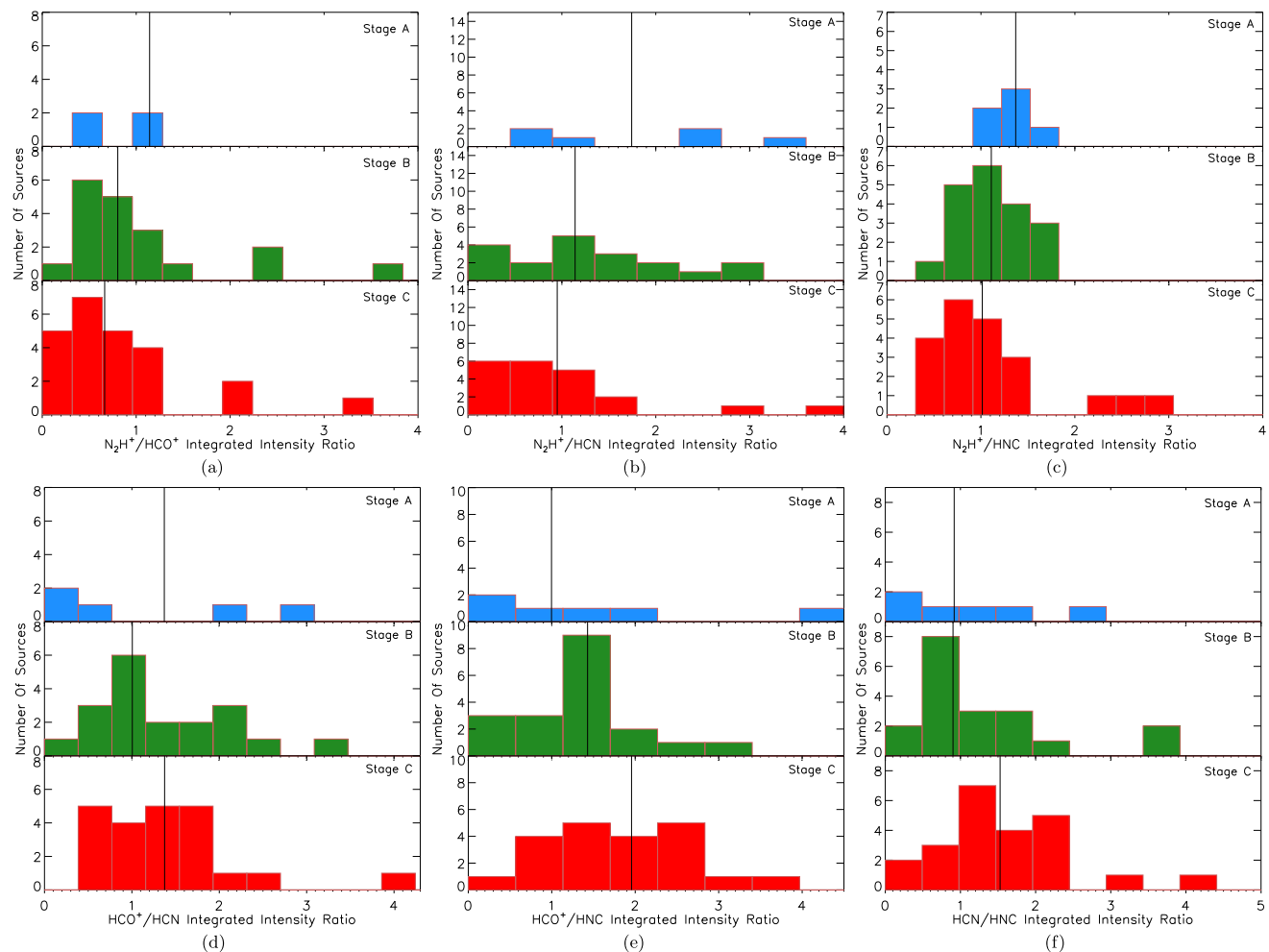


Fig. 13 The histograms of the global averaged integrated intensity ratios of $I(\text{N}_2\text{H}^+)/(1-0)/I(\text{HCO}^+)/(1-0)$, $I(\text{N}_2\text{H}^+)/(1-0)/I(\text{HCN})(1-0)$, $I(\text{N}_2\text{H}^+)/(1-0)/I(\text{HNC})(1-0)$, $I(\text{HCO}^+)/(1-0)/I(\text{HCN})(1-0)$ and $I(\text{HCN})(1-0)/I(\text{HNC})(1-0)$ for the stage A, B and C in the spiral arm 2 of the Galaxy,

respectively. The name of the evolutionary stage is given on the top right corner of each panel. The vertical solid lines indicate the median values of the integrated intensity ratios for each evolutionary stage. The median values are given in Table 8

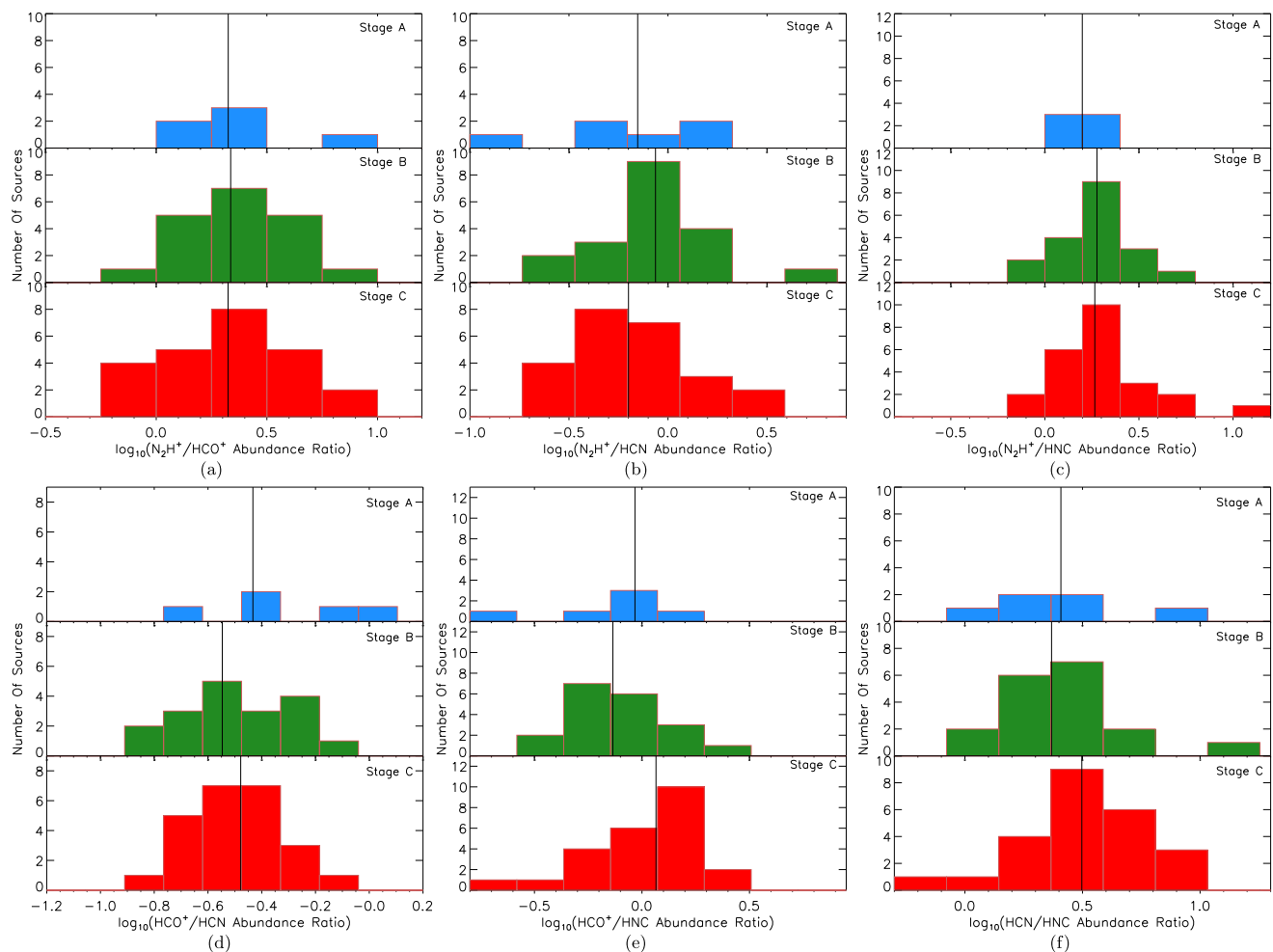


Fig. 14 The histograms of the global averaged abundance ratios (in logarithm) of $X(\text{N}_2\text{H}^+)/X(\text{HCO}^+)$, $X(\text{N}_2\text{H}^+)/X(\text{HCN})$, $X(\text{N}_2\text{H}^+)/X(\text{HNC})$, $X(\text{HCO}^+)/X(\text{HCN})$, $X(\text{HCO}^+)/X(\text{HNC})$ and $X(\text{HCN})/X(\text{HNC})$ for the stage A, B and C in the spiral arm 2 of the Galaxy,

respectively. The name of the evolutionary stage is given on the top right corner of each panel. The vertical solid lines indicate the median values of the abundance ratios for each evolutionary stage. The median values are given in Table 8

clumps in stage A from those in stages B and C. Median values of $X(\text{HCO}^+)/X(\text{HCN})$ show no significant variation from stage A to B, but decrease by $\sim 27\%$ from stage B to C, it could be used to distinguishing clumps in stage A and B from those in stage C.

Figures 13 and 14 show global averaged integrated intensity and abundances ratios for high-mass star forming clumps at different evolutionary stages located in spiral arm 2, and their median values are shown in Table 8. Median values of $I(\text{N}_2\text{H}^+ (1-0))/I(\text{HCO}^+ (1-0))$ decrease by $\sim 30\%$ and $\sim 17\%$ from stage A to B and B to C. Median values of $I(\text{N}_2\text{H}^+ (1-0))/I(\text{HCN} (1-0))$ decrease by $\sim 35\%$ and $\sim 17\%$ from stage A to B and B to C. Median values of $I(\text{HCO}^+ (1-0))/I(\text{HNC} (1-0))$ increase by $\sim 43\%$ and $\sim 37\%$ from stage A to B and B to C. They could be used to trace evolution from stage A to B and B to C. Median values of $I(\text{HCN} (1-0))/I(\text{HNC} (1-0))$ show no significant variation from stage A to B, but increasing

by $\sim 70\%$ from stage B to C, it is suitable for distinguishing clumps in stages A and B from those in stage C. Median values of $I(\text{N}_2\text{H}^+ (1-0))/I(\text{HNC} (1-0))$ decrease by $\sim 19\%$ from stage A to B, but show no significant variation from stage B to C. Median values of $X(\text{N}_2\text{H}^+)/X(\text{HNC})$ increase by $\sim 2\%$ from stage A to B, but show no significant variation from stage B to C. They are suitable for distinguishing clumps in stage A from those in stages B and C.

Figures 15 and 16 show global averaged integrated intensity and abundances ratios for high-mass star forming clumps at different evolutionary stages located in spiral arm 3, and their median values are shown in Table 8. Median values of $I(\text{N}_2\text{H}^+ (1-0))/I(\text{HCO}^+ (1-0))$ increase by $\sim 9\%$ and $\sim 21\%$ from stage A to B and B to C. Median values of $I(\text{HCO}^+ (1-0))/I(\text{HNC} (1-0))$ increase by $\sim 12\%$ and $\sim 22\%$ from stage A to B and B to C. These two ratios are more suitable for distinguishing clumps in

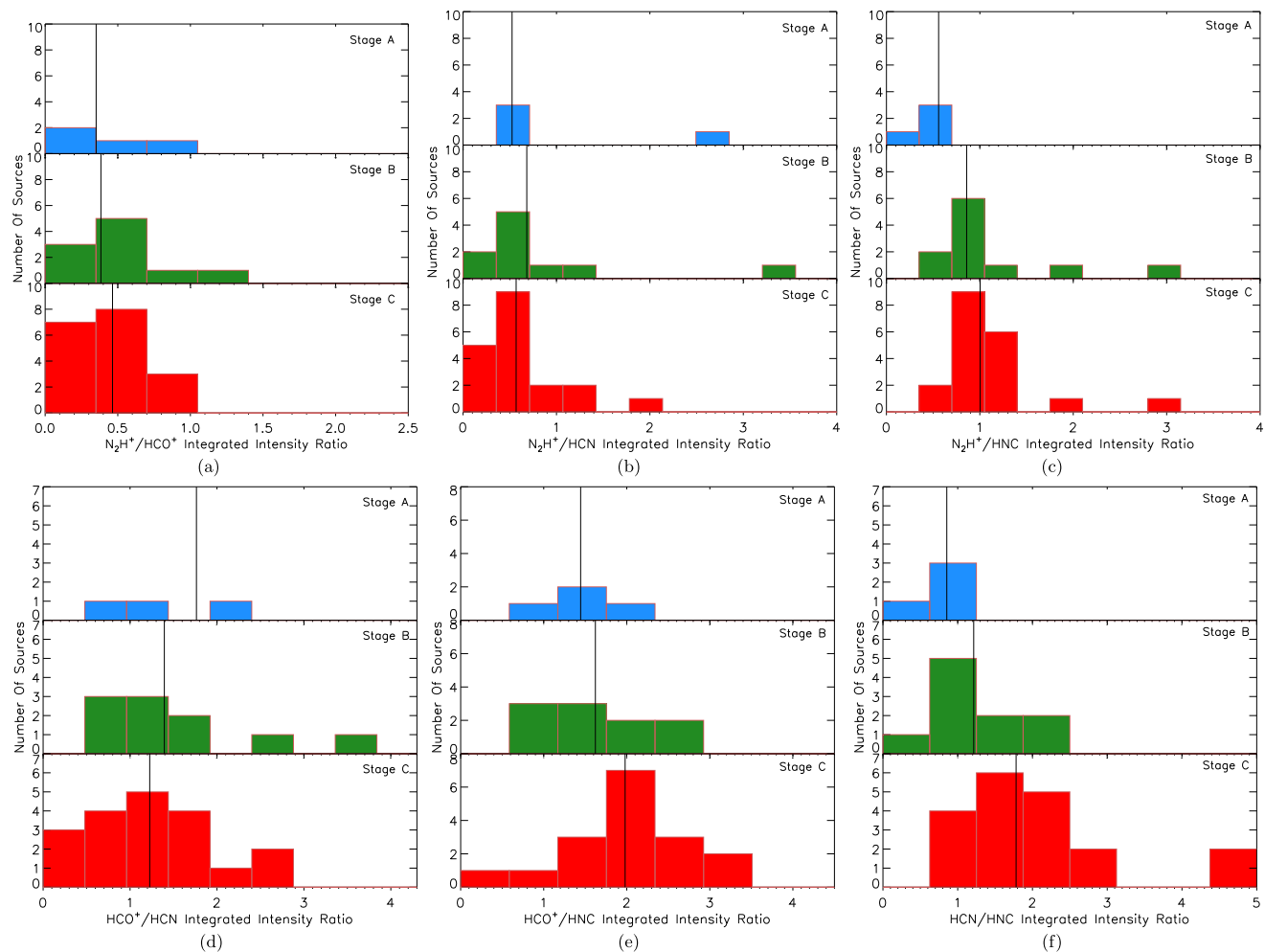


Fig. 15 The histograms of the global averaged integrated intensity ratios of $I(\text{N}_2\text{H}^+ \text{ (1-0)})/I(\text{HCO}^+ \text{ (1-0)})$, $I(\text{N}_2\text{H}^+ \text{ (1-0)})/I(\text{HCN} \text{ (1-0)})$, $I(\text{N}_2\text{H}^+ \text{ (1-0)})/I(\text{HNC} \text{ (1-0)})$, $I(\text{HCO}^+ \text{ (1-0)})/I(\text{HCN} \text{ (1-0)})$, $I(\text{HCO}^+ \text{ (1-0)})/I(\text{HNC} \text{ (1-0)})$ and $I(\text{HCN} \text{ (1-0)})/I(\text{HNC} \text{ (1-0)})$ for the stage A, B and C in the spiral arm 3 of the

Galaxy, respectively. The name of the evolutionary stage is given on the top right corner of each panel. The vertical solid lines indicate the median values of the integrate intensity ratios for each evolutionary stage. The median values are given in Table 8

stage A and B from those in stage C. Median values of $I(\text{HCO}^+ \text{ (1-0)})/I(\text{HCN} \text{ (1-0)})$ decrease by $\sim 21\%$ and $\sim 12\%$ from stage A to B and B to C, it is more suitable for distinguishing clumps in stage A from those in stage B and C. Median values of $I(\text{HCN} \text{ (1-0)})/I(\text{HNC} \text{ (1-0)})$ increase by $\sim 42\%$ and $\sim 47\%$ from stage A to B and B to C. Median values of $I(\text{N}_2\text{H}^+ \text{ (1-0)})/I(\text{HNC} \text{ (1-0)})$ increase by $\sim 54\%$ and $\sim 17\%$ from stage A to B and B to C. These two ratios could be used to trace evolution from stage A to B and B to C.

Median values of $X(\text{N}_2\text{H}^+)/X(\text{HNC})$ increase by $\sim 40\%$ from stage A to B, but show no significant variation from stage B to C, it is suitable for distinguishing clumps in stage A from those in stages B and C. Median values of $X(\text{HCN})/X(\text{HNC})$ increase by $\sim 32\%$ and $\sim 37\%$ from stage A to B and B to C, it could be used to trace evolution from stage A to B and B to C.

Figures 17 and 18 show global averaged integrated intensity and abundances ratios for high-mass star forming clumps at different evolutionary stages located in spiral arm 4, and their median values are shown in Table 8. Median values of $I(\text{N}_2\text{H}^+ \text{ (1-0)})/I(\text{HCO}^+ \text{ (1-0)})$ decrease by $\sim 40\%$ and $\sim 17\%$ from stage A to B and B to C, median values of $I(\text{HCO}^+ \text{ (1-0)})/I(\text{HNC} \text{ (1-0)})$ increase by $\sim 102\%$ and $\sim 12\%$ from stage A to B and B to C, these two ratios are more suitable for distinguishing clumps in stage A from those in stage B and C. Median values of $I(\text{HCN} \text{ (1-0)})/I(\text{HNC} \text{ (1-0)})$ increase by $\sim 42\%$ and $\sim 83\%$ from stage A to B and B to C, it could be used to trace evolution of high-mass star forming clumps.

Median values of $X(\text{N}_2\text{H}^+)/X(\text{HCO}^+)$ decrease by $\sim 40\%$ and $\sim 9\%$ from stage A to B and B to C, it is suitable for distinguishing clumps in stages A from those in stage B and C. Median values of $X(\text{N}_2\text{H}^+)/X(\text{HCN})$ de-

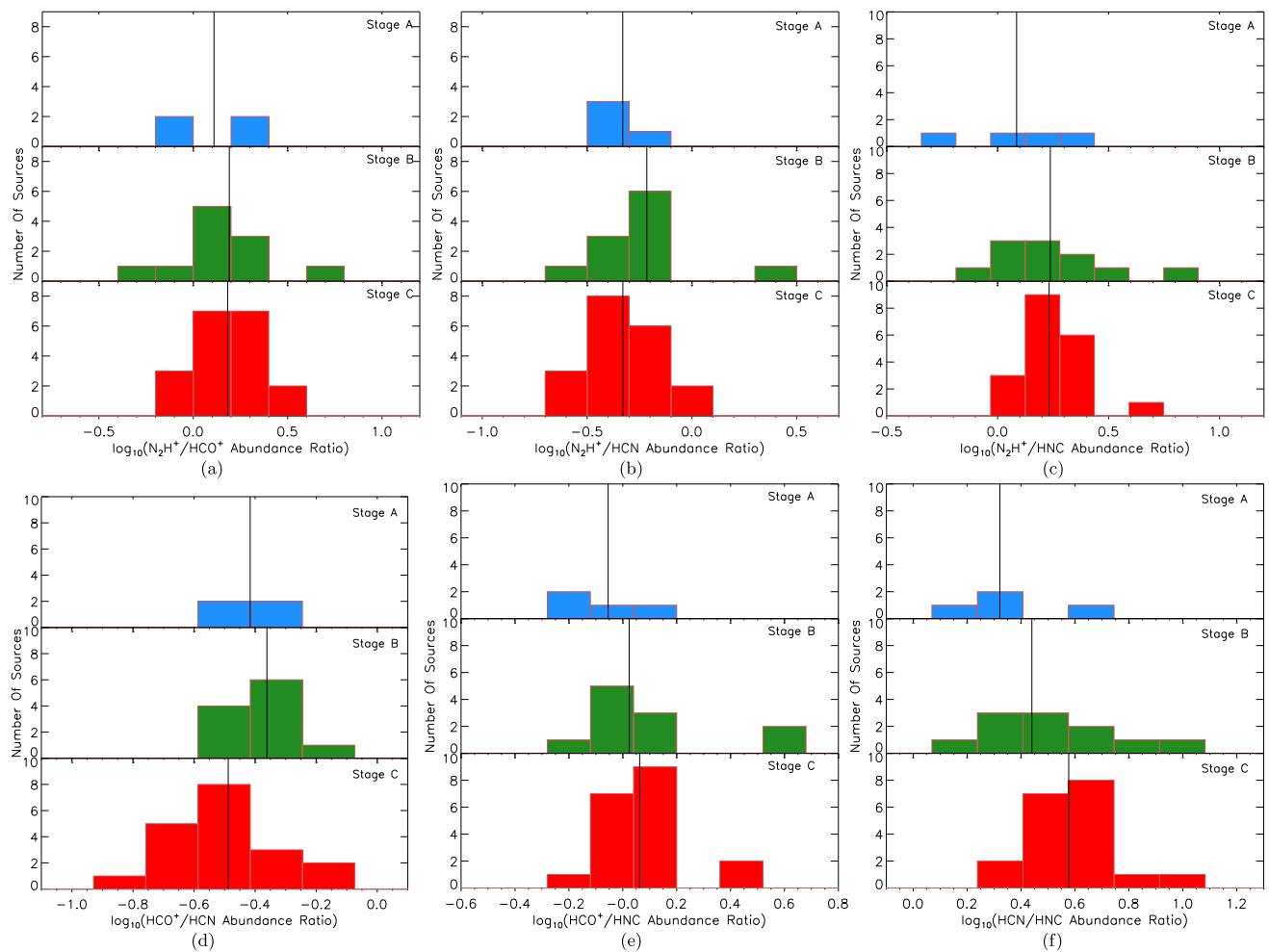


Fig. 16 The histograms of the global averaged abundance ratios (in logarithm) of $X(\text{N}_2\text{H}^+)/X(\text{HCO}^+)$, $X(\text{N}_2\text{H}^+)/X(\text{HCN})$, $X(\text{N}_2\text{H}^+)/X(\text{HNC})$, $X(\text{HCO}^+)/X(\text{HCN})$, $X(\text{HCO}^+)/X(\text{HNC})$ and $X(\text{HCN})/X(\text{HNC})$ for the stage A, B and C in the spiral arm 3 of the

Galaxy, respectively. The name of the evolutionary stage is given on the top right corner of each panel. The vertical solid lines indicate the median values of the abundance ratios for each evolutionary stage. The median values are given in Table 8

crease by $\sim 12\%$ and $\sim 38\%$ from stage A to B and B to C, it is suitable for distinguishing clumps in stages A and B from those in stage C. Median values of $X(\text{HCN})/X(\text{HNC})$ increase by $\sim 37\%$ and $\sim 21\%$ from stage A to B and B to C, it could be used to trace evolution from stage A to B and B to C.

Here we only discuss those ratios that show significant variations, i.e. by more than 15% . These results are significantly different from those derived from the whole sample (Sects. 4.1 and 4.2). One possible reason is that there are too few sources in each spiral arm to provide consistency.

4.3.2 High-mass star forming clumps located in the same spiral arm, near and far from the Galactic Center

High-mass star forming clumps in spiral arms 1 (Sagittarius arm) and 4 (Norma-Outer arm) could be divided into two groups according to their distance from the Galactic Cen-

ter (Fig. 8). In spiral arm 1, there are two groups of clump concentrations, one group locating in the Galactocentric distance range 3.6–4.9 kpc, and the other one at 6–16 kpc. Similarly, in spiral arm 4 there are also two groups of clumps, one at the Galactocentric distances of 3.2 to 4.3 kpc, and the other at 5.1–9.5 kpc. Since more dense gas concentrates near the Galactic center, the probability of high-mass star formation occurring should be higher, and so more high-mass star forming clumps should be in earlier stages of star formation.

From the previous sections, global integrated intensity and abundance ratios $\text{N}_2\text{H}^+/\text{HCO}^+$, HCO^+/HNC and HCN/HNC are sensitive to evolution of high-mass star forming clumps, and so these ratios were compared between the near and far groups.

Figure 19 shows the groups for spiral arm 1. Median values for the near and far groups are 0.61 and 0.55 for $I(\text{N}_2\text{H}^+ (1-0))/I(\text{HCO}^+ (1-0))$, 1.85 and 2.04 for $I(\text{HCO}^+ (1-0))/I(\text{HNC} (1-0))$, 1.37 and 1.47 for

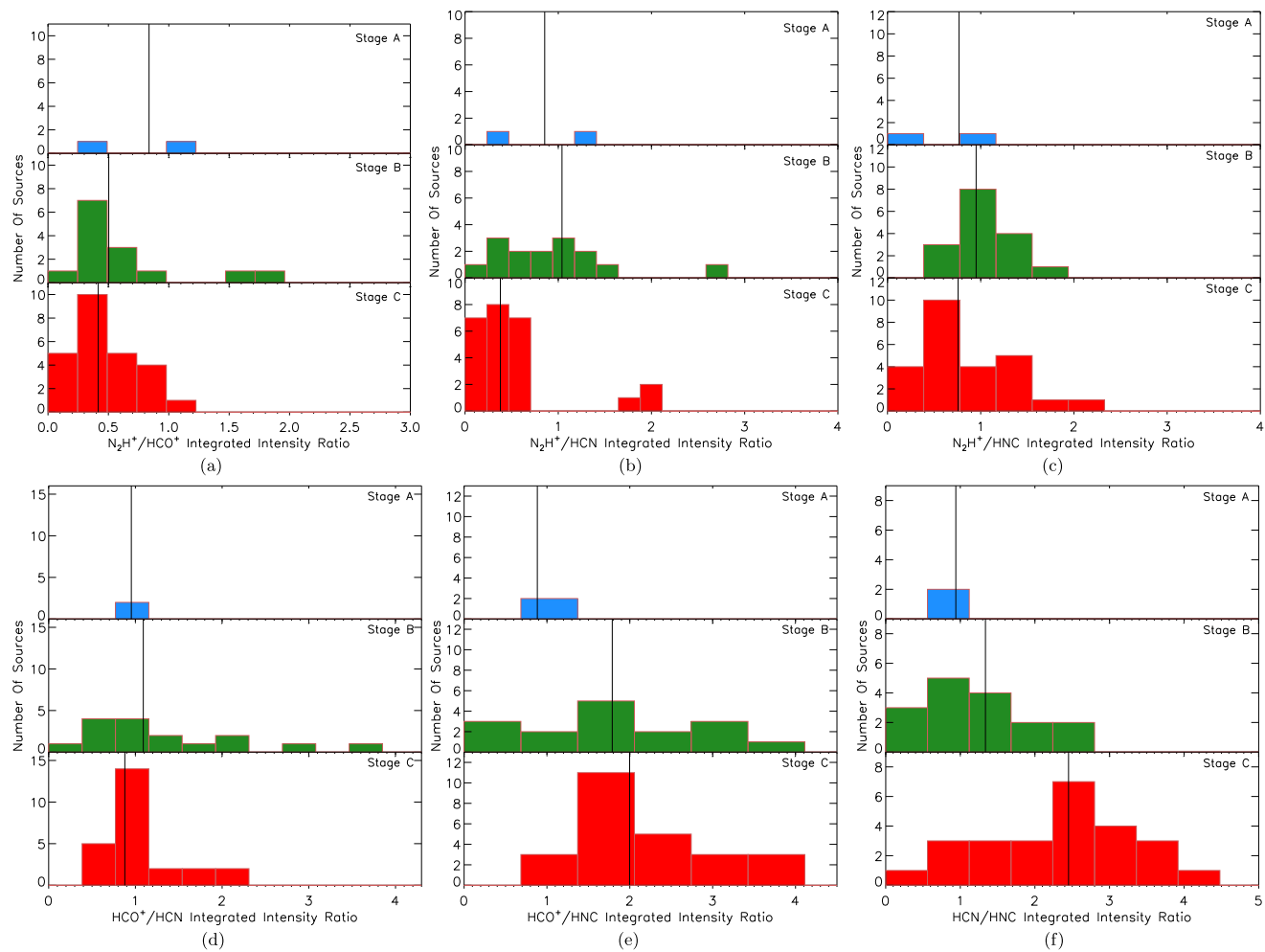


Fig. 17 The histograms of the global averaged integrated intensity ratios of $I(\text{N}_2\text{H}^+ \text{ (1-0)})/I(\text{HCO}^+ \text{ (1-0)})$, $I(\text{N}_2\text{H}^+ \text{ (1-0)})/I(\text{HCN} \text{ (1-0)})$, $I(\text{N}_2\text{H}^+ \text{ (1-0)})/I(\text{HNC} \text{ (1-0)})$, $I(\text{HCO}^+ \text{ (1-0)})/I(\text{HCN} \text{ (1-0)})$, $I(\text{HCO}^+ \text{ (1-0)})/I(\text{HNC} \text{ (1-0)})$ and $I(\text{HCN} \text{ (1-0)})/I(\text{HNC} \text{ (1-0)})$ for the stage A, B and C in the spiral arm 4 of the

Galaxy, respectively. The name of the evolutionary stage is given on the top right corner of each panel. The vertical solid lines indicate the median values of the integrate intensity ratios for each evolutionary stage. The median values are given in Table 8

$I(\text{HCN} \text{ (1-0)})/I(\text{HNC} \text{ (1-0)})$, 2.05 and 1.59 for $X(\text{N}_2\text{H}^+)/X(\text{HCO}^+)$, 0.91 and 1.02 for $X(\text{HCO}^+)/X(\text{HNC})$, and 3.03 and 3.89 for $X(\text{HCN})/X(\text{HNC})$, respectively.

For the near and far groups in the spiral arm 4 (Fig. 20), median values are 0.66 and 0.43 for $I(\text{N}_2\text{H}^+ \text{ (1-0)})/I(\text{HCO}^+ \text{ (1-0)})$, 1.63 and 2.04 for $I(\text{HCO}^+ \text{ (1-0)})/I(\text{HNC} \text{ (1-0)})$, 1.27 and 2.18 for $I(\text{HCN} \text{ (1-0)})/I(\text{HNC} \text{ (1-0)})$, 1.94 and 1.25 for $X(\text{N}_2\text{H}^+)/X(\text{HCO}^+)$, 1.07 and 1.30 for $X(\text{HCO}^+)/X(\text{HNC})$, and 2.72 and 3.78 for $X(\text{HCN})/X(\text{HNC})$, respectively. These results indicate that the near group is younger than the far group overall, and hence support a scenario of more massive stars being formed near the Galactic Center. However, it should be noted that the sample sizes of the near and far groups in spiral arms 1 and 4 are too small to provide a statistically significant result.

5 Summary and conclusions

A total of 197 relatively isolated high-mass star forming clumps were selected from all the MALT90 survey data and classified into prestellar, protostellar, and HII/PDR stages. Their chemical evolution was investigated based on four molecular lines, $\text{N}_2\text{H}^+ \text{ (1-0)}$, $\text{HCO}^+ \text{ (1-0)}$, $\text{HCN} \text{ (1-0)}$ and $\text{HNC} \text{ (1-0)}$. The findings were as follows:

1. Global averaged integrated intensities $I(\text{N}_2\text{H}^+ \text{ (1-0)})$, $I(\text{HCO}^+ \text{ (1-0)})$, $I(\text{HCN} \text{ (1-0)})$, and $I(\text{HNC} \text{ (1-0)})$ of high-mass star forming clumps all showed increasing trends with increased evolutionary stage. Global averaged line ratios $I(\text{HCO}^+ \text{ (1-0)})/I(\text{HNC} \text{ (1-0)})$, $I(\text{HCN} \text{ (1-0)})/I(\text{HNC} \text{ (1-0)})$, $I(\text{N}_2\text{H}^+ \text{ (1-0)})/I(\text{HCO}^+ \text{ (1-0)})$ and $I(\text{N}_2\text{H}^+ \text{ (1-0)})/I(\text{HCN} \text{ (1-0)})$ could be used to trace evolution of high-mass star forming clumps.

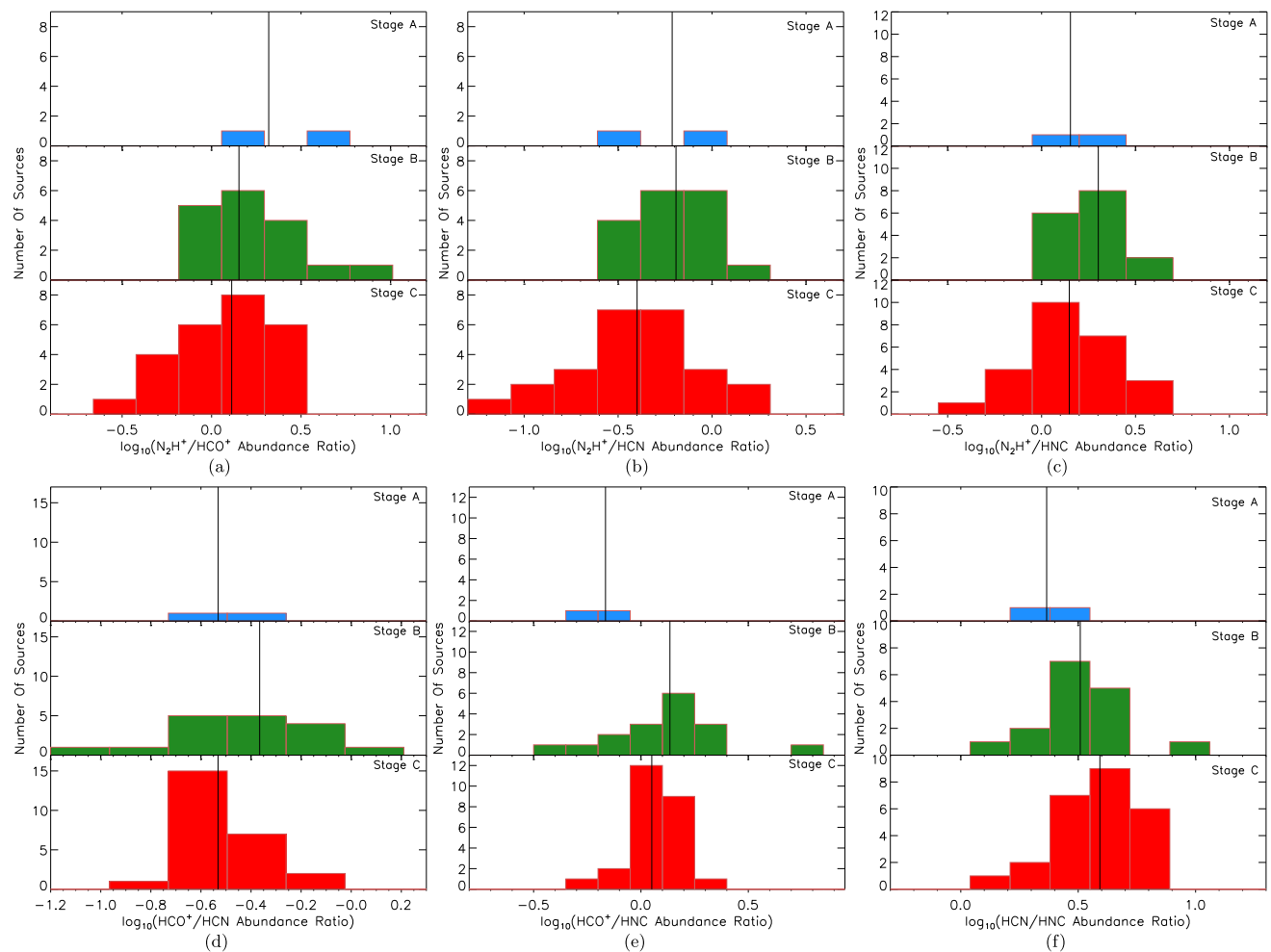


Fig. 18 The histograms of the global averaged abundance ratios (in logarithm) of $X(N_2H^+)/X(\text{HCO}^+)$, $X(N_2H^+)/X(\text{HCN})$, $X(N_2H^+)/X(\text{HNC})$, $X(\text{HCO}^+)/X(\text{HCN})$, $X(\text{HCO}^+)/X(\text{HNC})$ and $X(\text{HCN})/X(\text{HNC})$ for the stage A, B and C in the spiral arm 4 of the

Galaxy, respectively. The name of the evolutionary stage is given on the top right corner of each panel. The vertical solid lines indicate the median values of the abundance ratios for each evolutionary stage. The median values are given in Table 8

2. Global averaged column densities of N_2H^+ , HCO^+ , HCN , and HNC increase as high-mass star forming clumps evolve.
3. Global averaged abundances $X(N_2H^+)$, $X(\text{HCO}^+)$, $X(\text{HCN})$ and $X(\text{HNC})$ increase with evolutionary stage. The abundance ratio $X(\text{HCN})/X(\text{HNC})$ could be used to trace evolution of high-mass star forming clumps, $X(\text{HCO}^+)/X(\text{HNC})$ is more suitable for distinguishing high-mass star forming clumps in stage A from those in stages B and C.
4. Our results suggest that the global averaged line ratios based on the whole clump display more obvious trends with its evolution, and they are suitable for tracing the evolution of high-mass star forming clumps. On the other hand, the global abundance ratios based on the whole clump do not show much more advantages compared to those results derived from the beam-averaged peak data

or single point observation, only $X(\text{HCN})/X(\text{HNC})$ display an obvious trend of increase as clumps evolve.

5. The global chemical properties of high-mass star forming clumps in each spiral arm of the Galaxy are significantly different from those derived from the whole sample. One possible reason is that the sources in each spiral arm are too few to provide consistency, while another possible contributing factor could be that the physical and the chemical properties of each spiral arm are different.
6. For high-mass star forming clumps in spiral arms 1 and 4, the clumps near the Galactic Center appear younger than those far from the Galactic center. One possible reason for this is that the Galactic Center region contains more dense molecular gas, which can lead to an elevated rate of high-mass star formation.

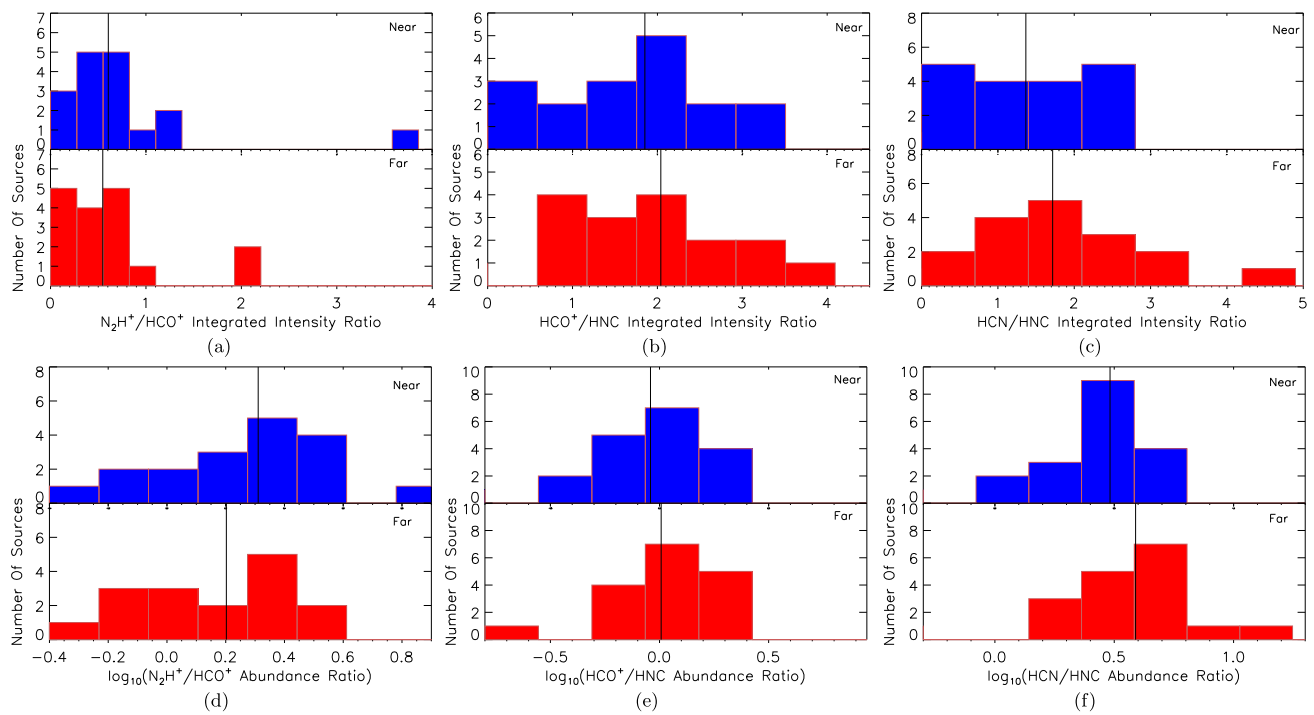


Fig. 19 The histograms of the global averaged integrated intensity ratios $I(N_2H^+ (1-0))/I(\text{HCO}^+ (1-0))$, $I(\text{HCO}^+ (1-0))/I(\text{HNC} (1-0))$ and $I(\text{HCN} (1-0))/I(\text{HNC} (1-0))$ and abundance ratios $X(N_2H^+)$ /

$X(\text{HCO}^+)$, $X(\text{HCO}^+)/X(\text{HNC})$ and $X(\text{HCN})/X(\text{HNC})$ for the high-mass star-forming clumps in the near (in blue) and far (in red) Group in the spiral arm 1 of the Galaxy

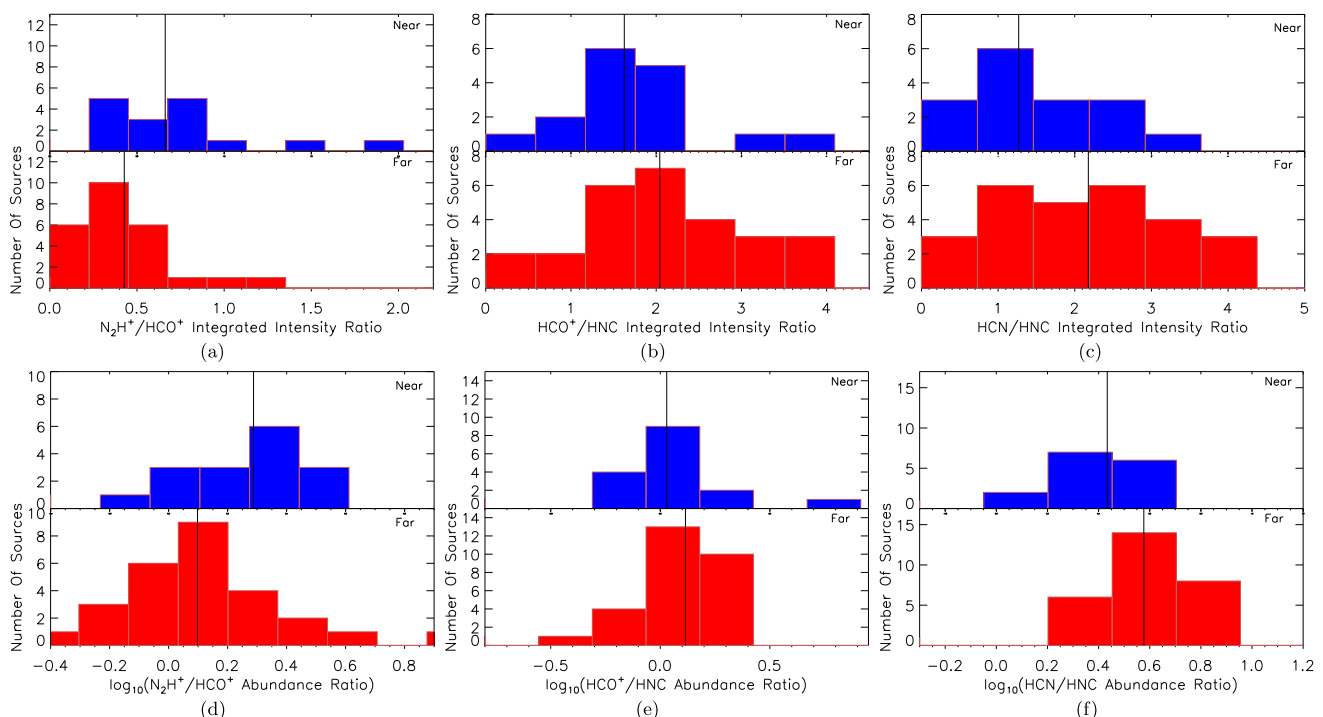


Fig. 20 The histograms of the global averaged integrated intensity ratios $I(N_2H^+ (1-0))/I(\text{HCO}^+ (1-0))$, $I(\text{HCO}^+ (1-0))/I(\text{HNC} (1-0))$ and $I(\text{HCN} (1-0))/I(\text{HNC} (1-0))$ and abundance ratios $X(N_2H^+)$ /

$X(\text{HCO}^+)$, $X(\text{HCO}^+)/X(\text{HNC})$ and $X(\text{HCN})/X(\text{HNC})$ for the high-mass star-forming clumps in the near (in blue) and far (in red) Group in the spiral arm 4 of the Galaxy

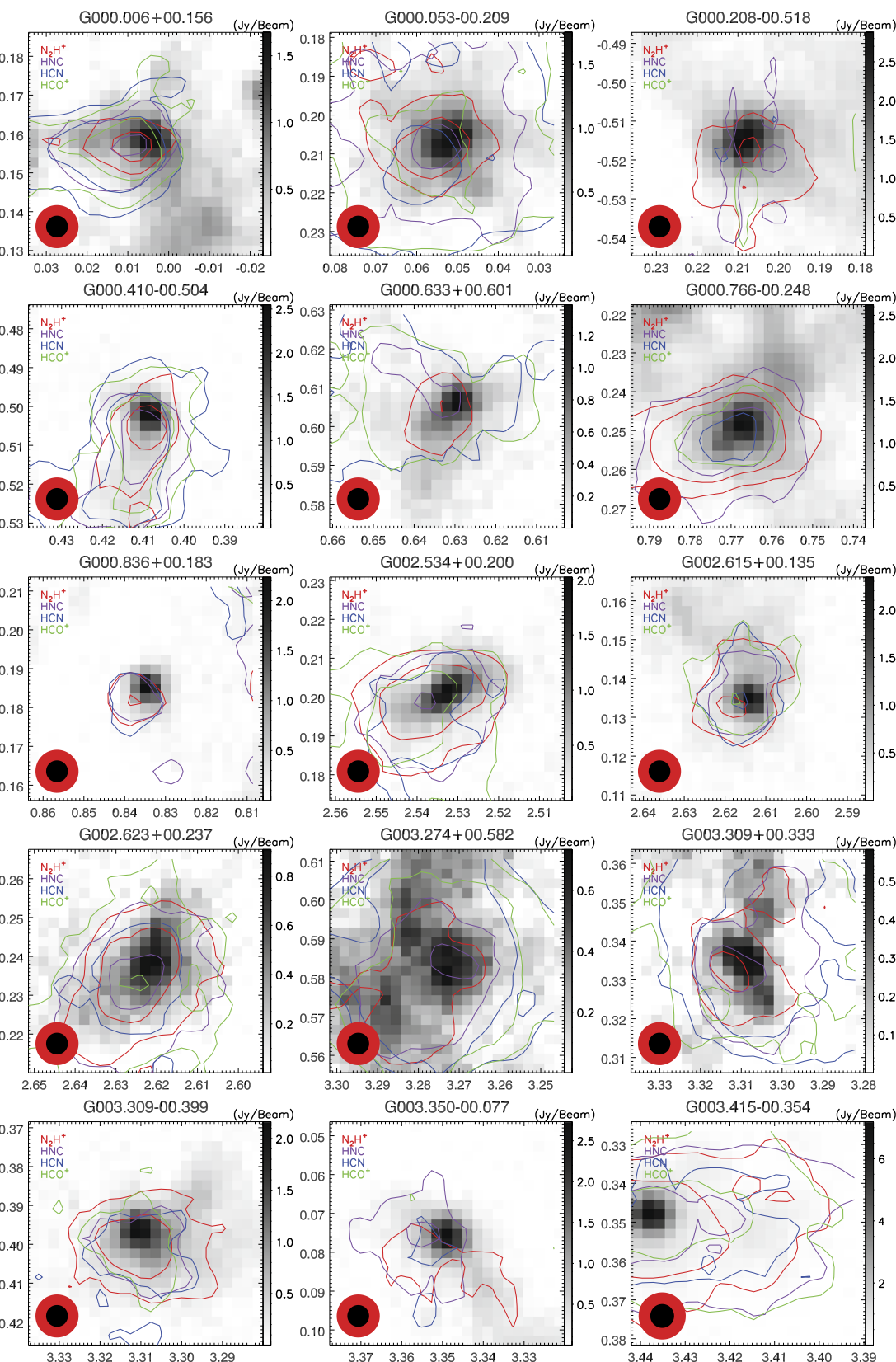
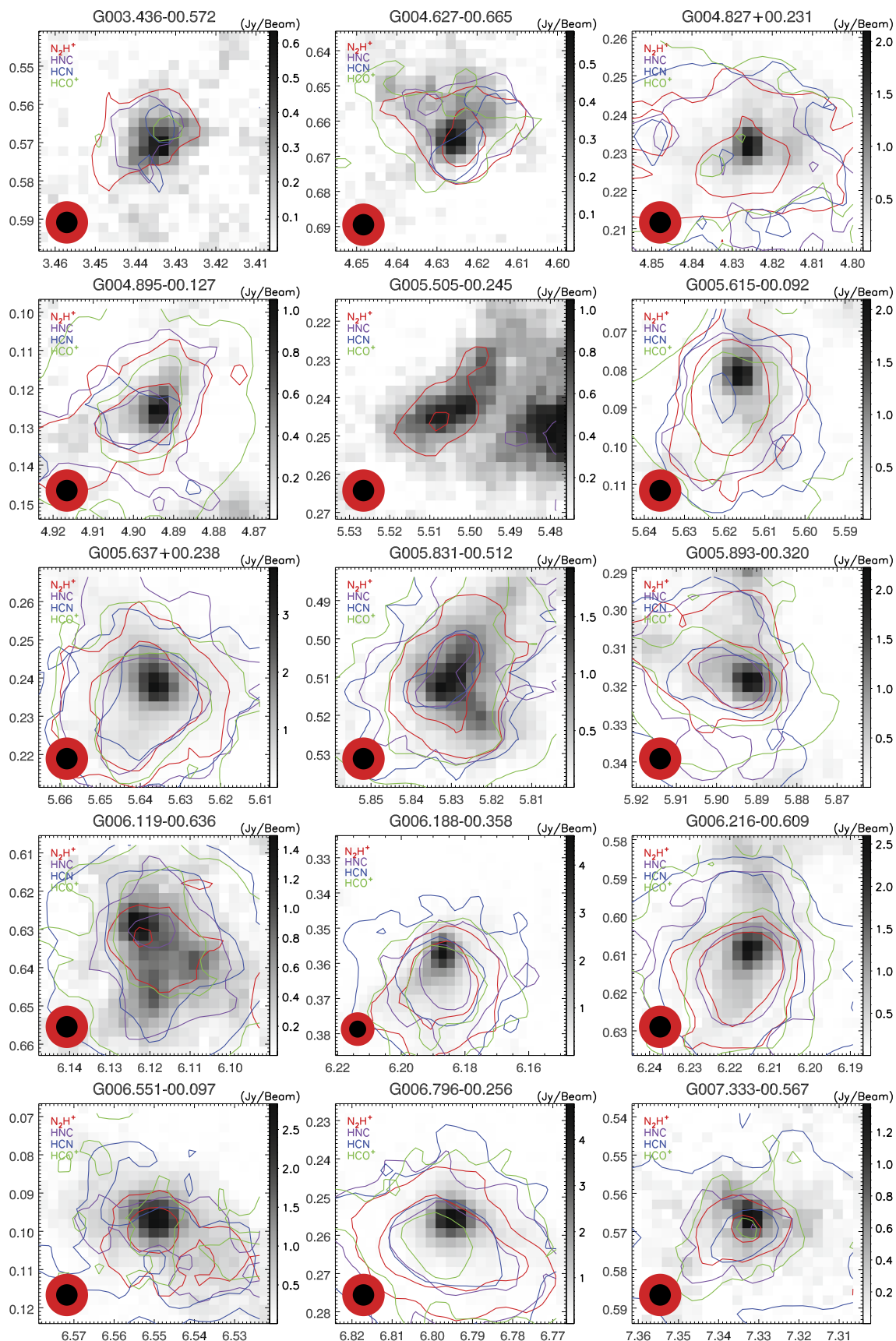
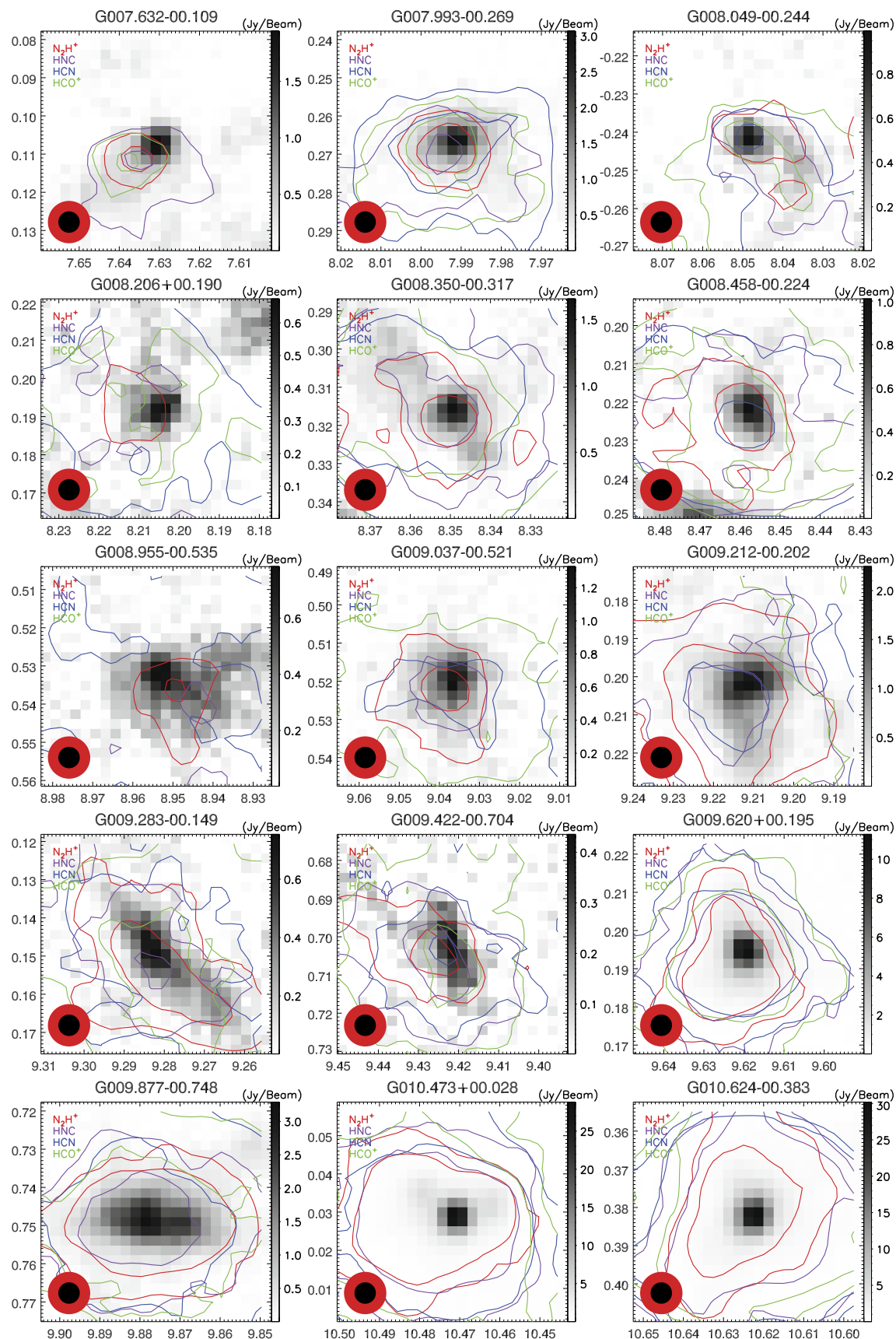
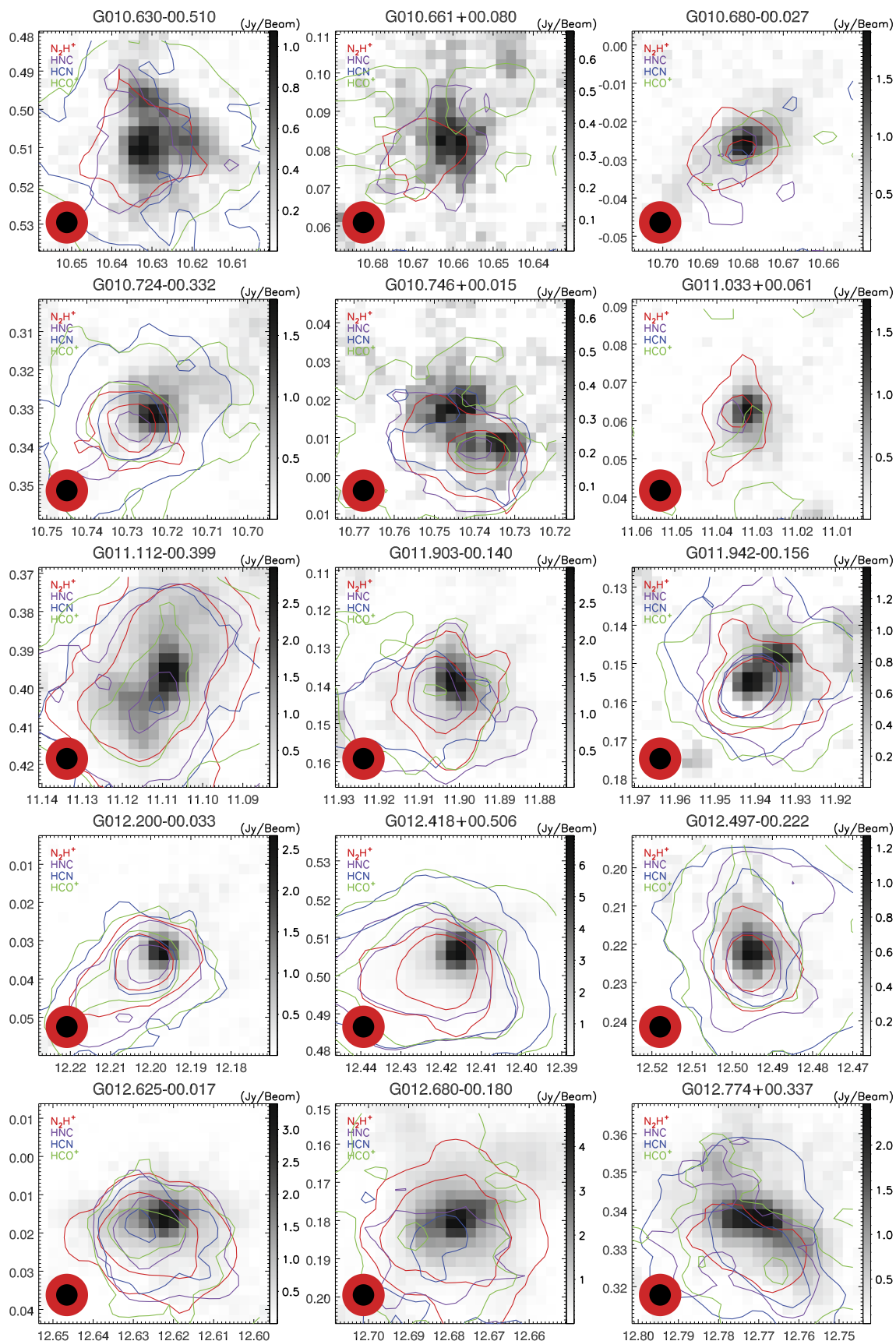


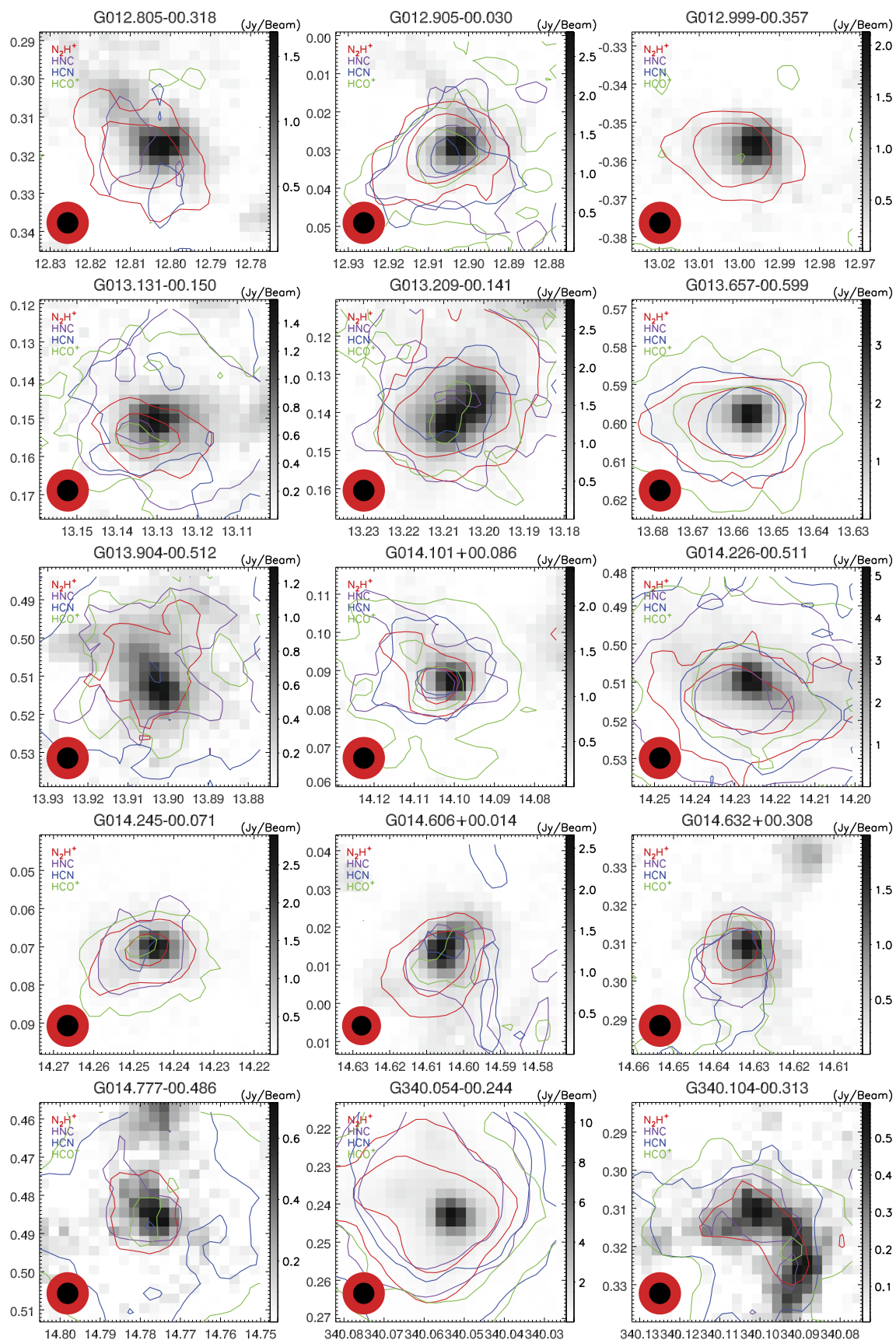
Fig. 21 The contour maps for the integrated intensities of N_2H^+ (1–0), HCO^+ (1–0), HCN (1–0) and HNC (1–0), overlaid on the 870 μm emission for all 197 high-mass star-forming clumps. Levels 1 and 2 of N_2H^+ (1–0), HCO^+ (1–0), HCN (1–0) and HNC (1–0)

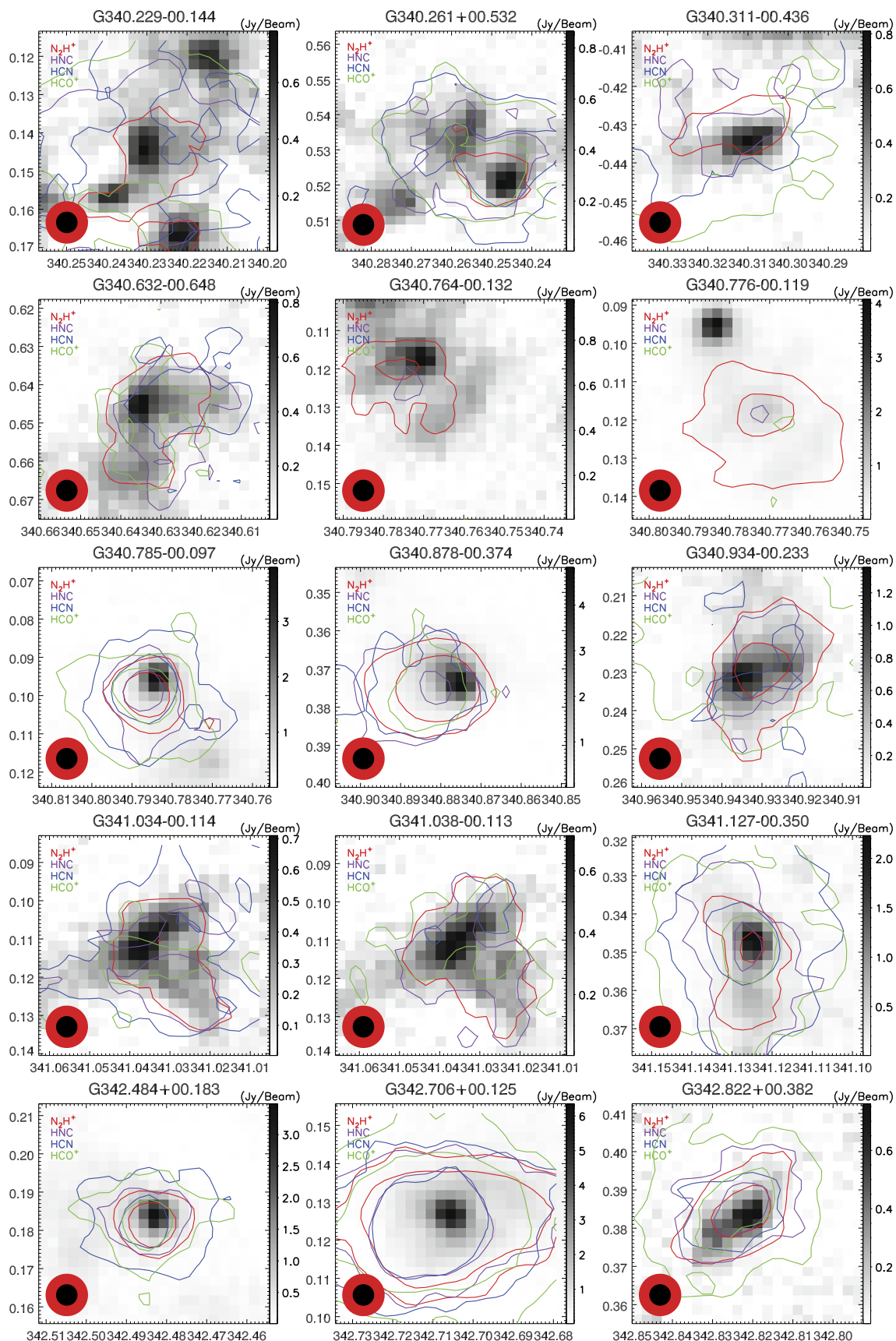
correspond to 3σ and 9σ , respectively. The red circle in the bottom left corner represents the FWHM beam size for molecular lines, the enclosed black circle indicates the FWHM beam size of 870 μm emission observations

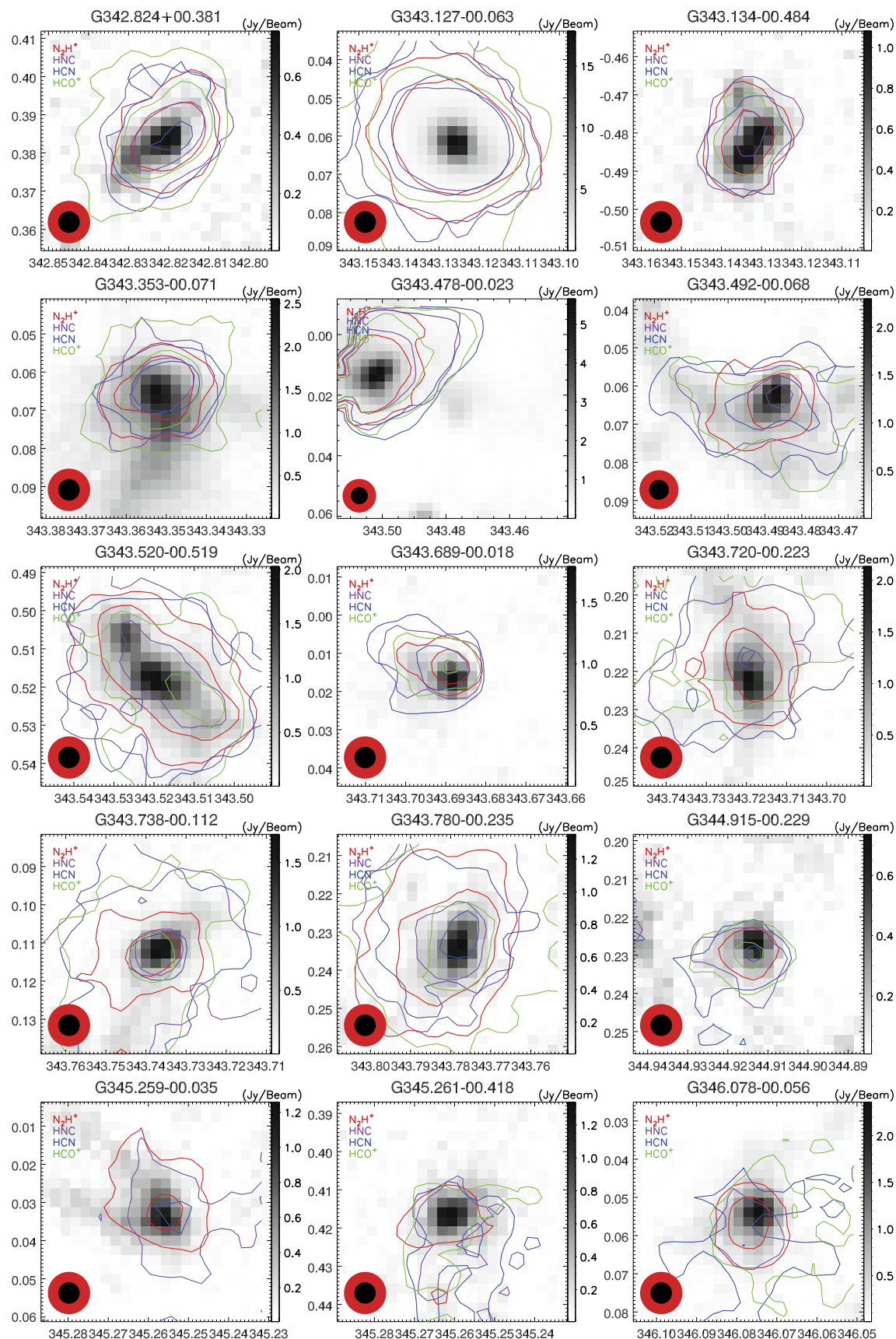
**Fig. 21** (Continued)

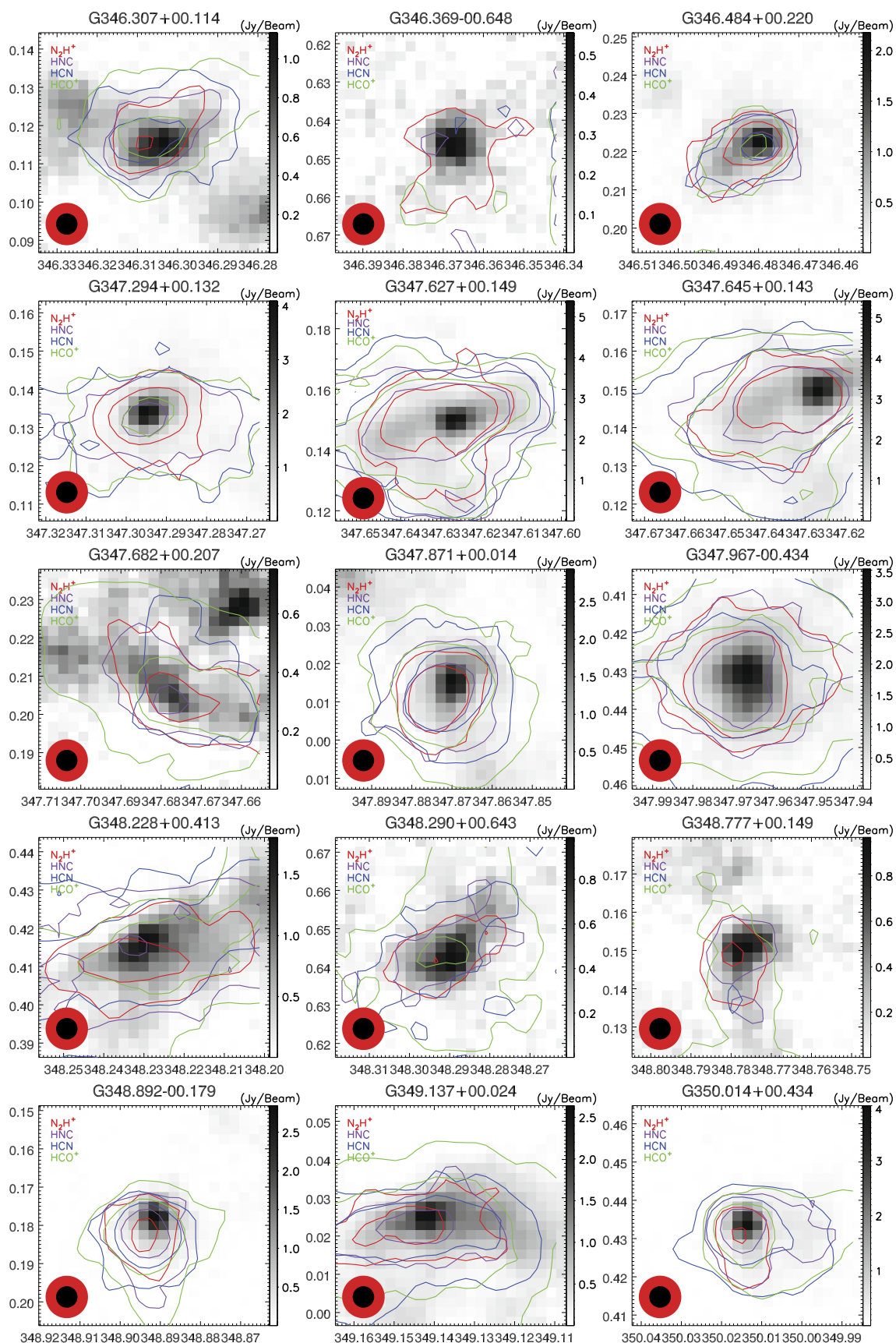
**Fig. 21** (Continued)

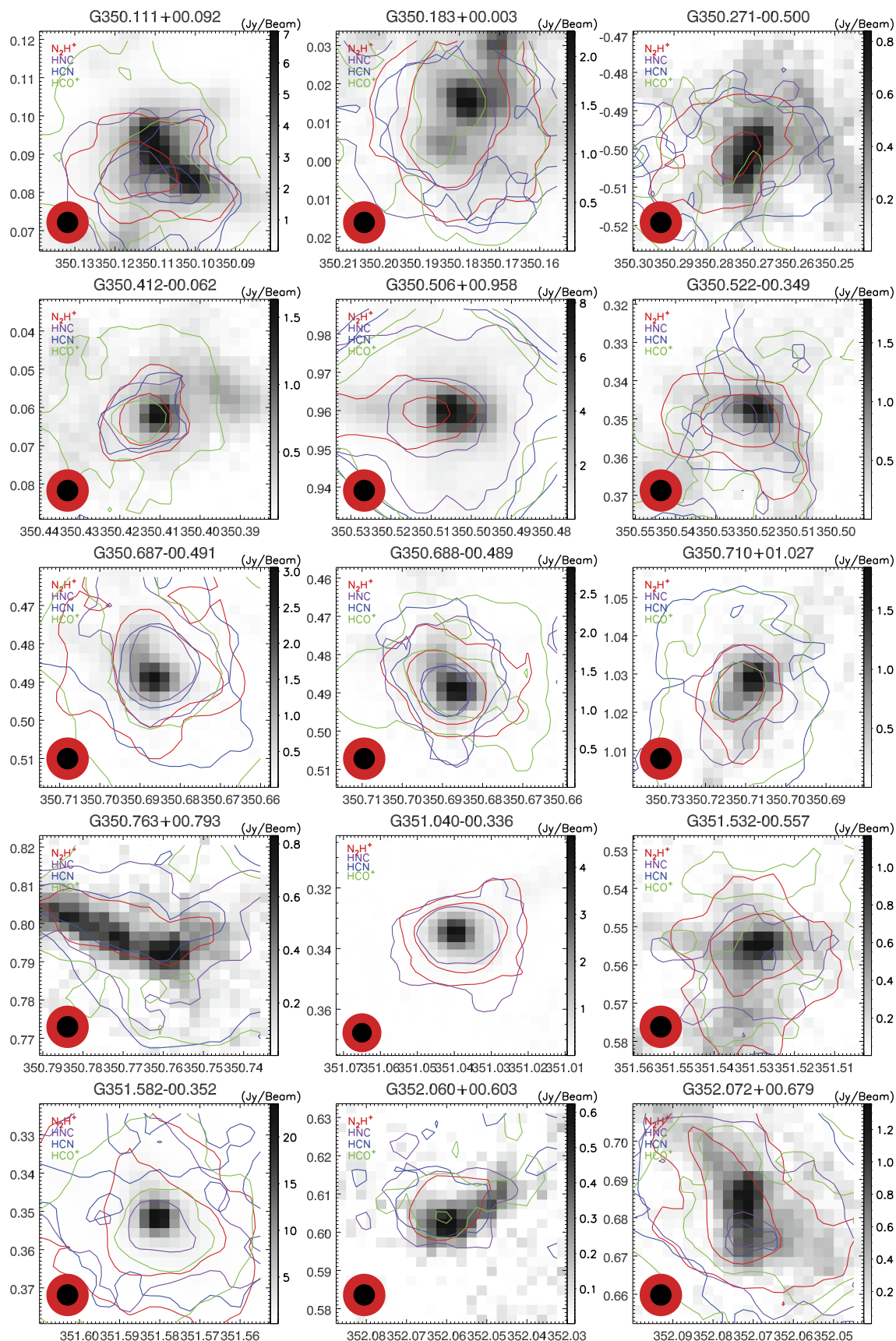
**Fig. 21** (Continued)

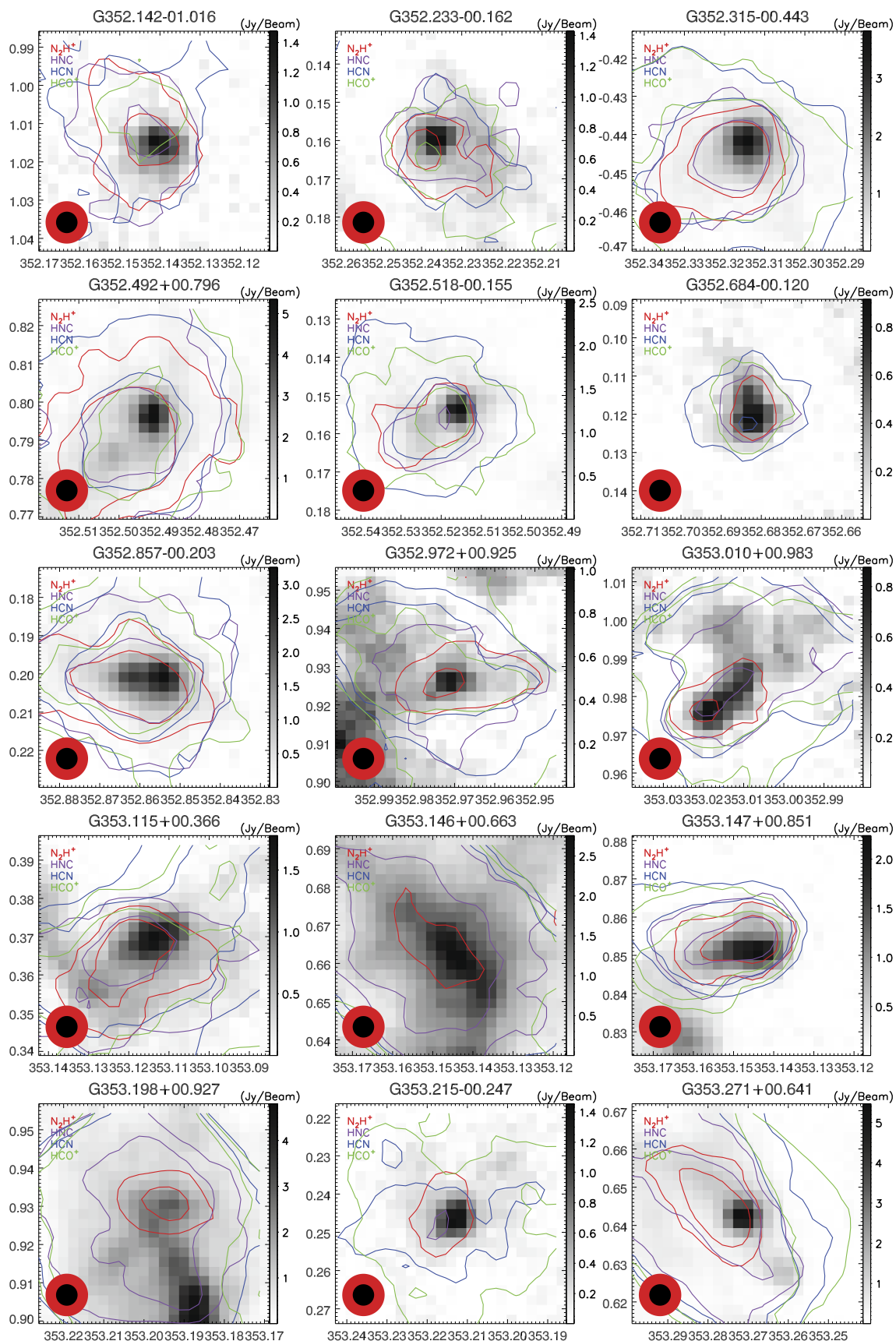
**Fig. 21** (Continued)

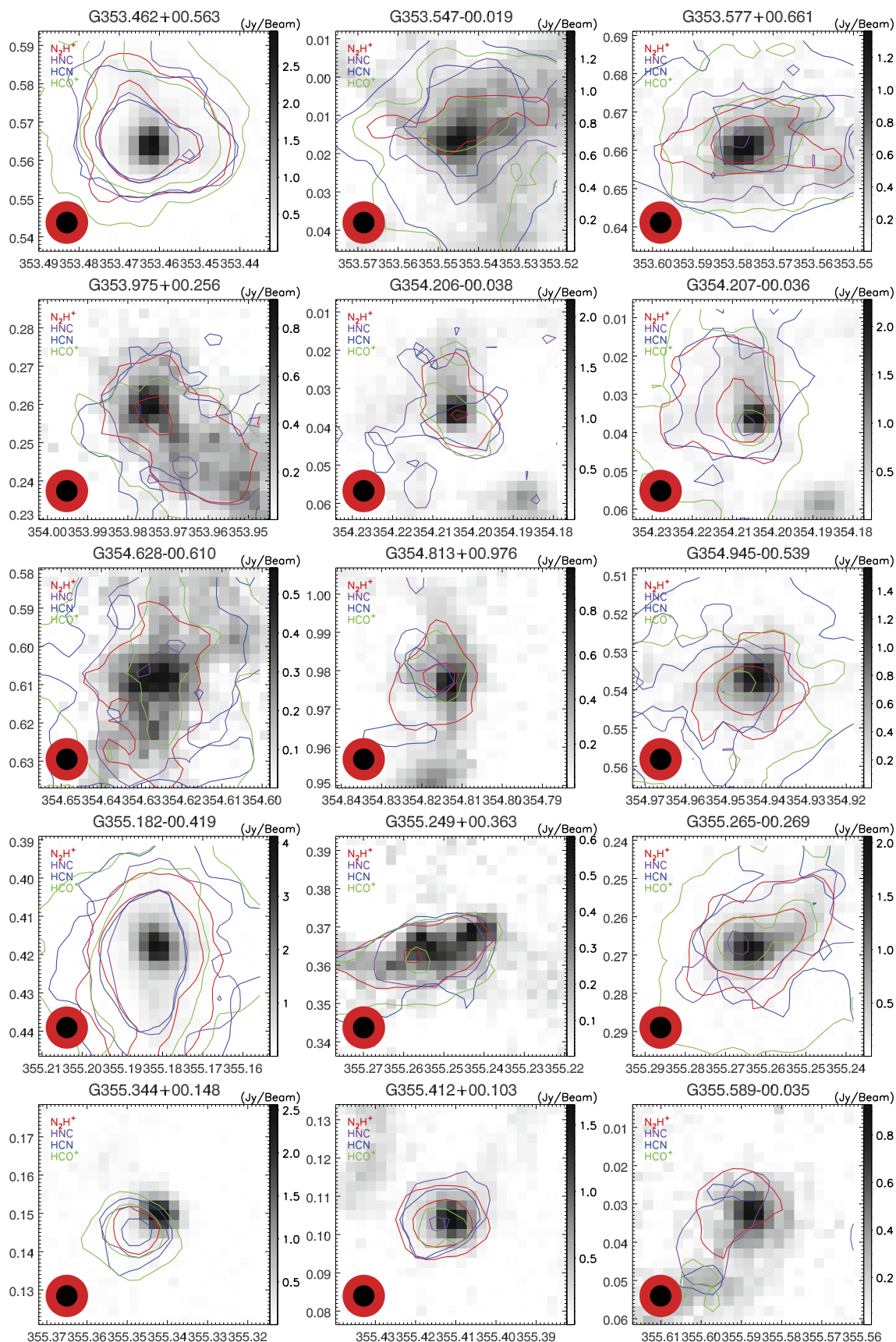
**Fig. 21** (Continued)

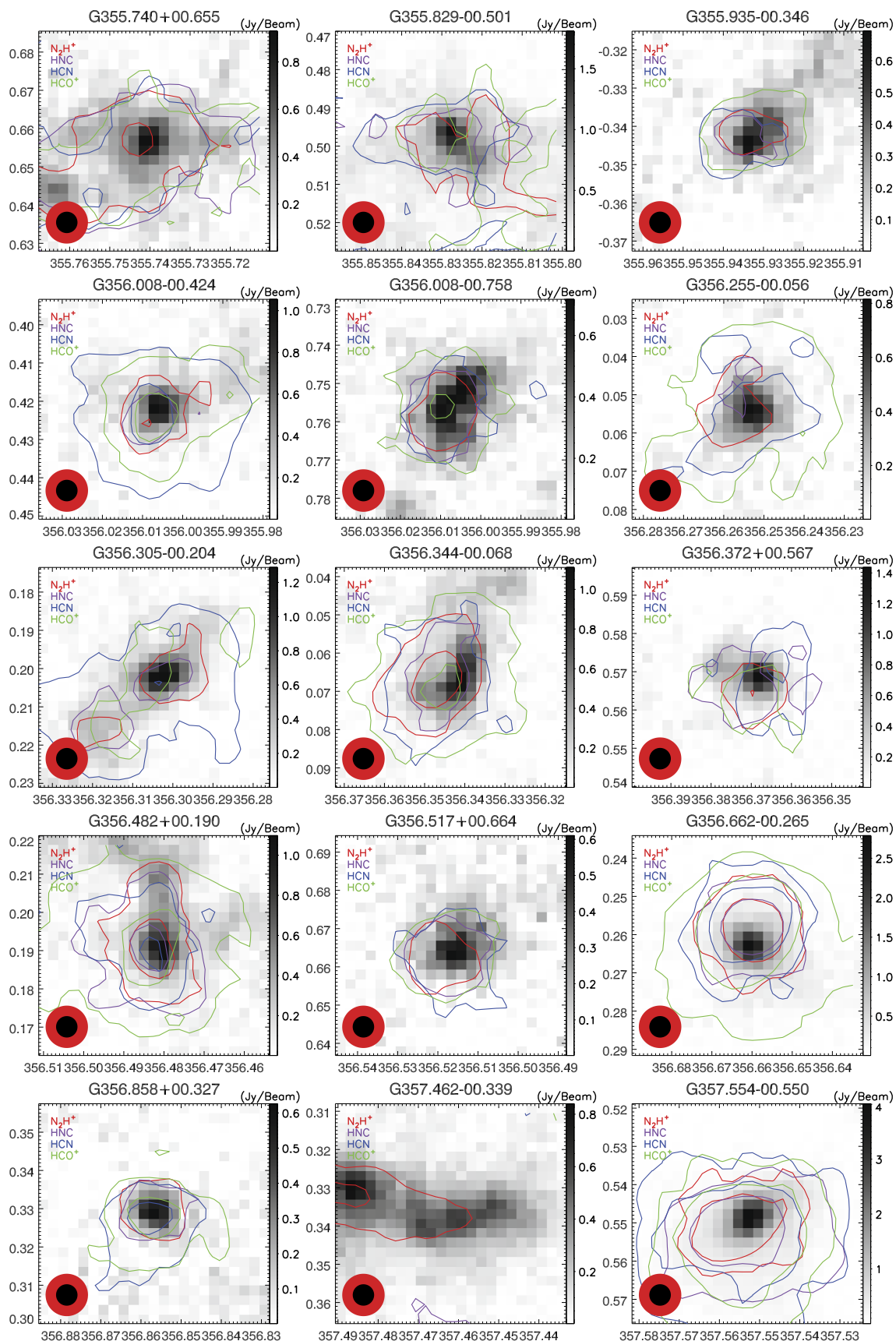
**Fig. 21** (Continued)

**Fig. 21** (Continued)

**Fig. 21** (Continued)

**Fig. 21** (Continued)

**Fig. 21** (Continued)

**Fig. 21** (Continued)

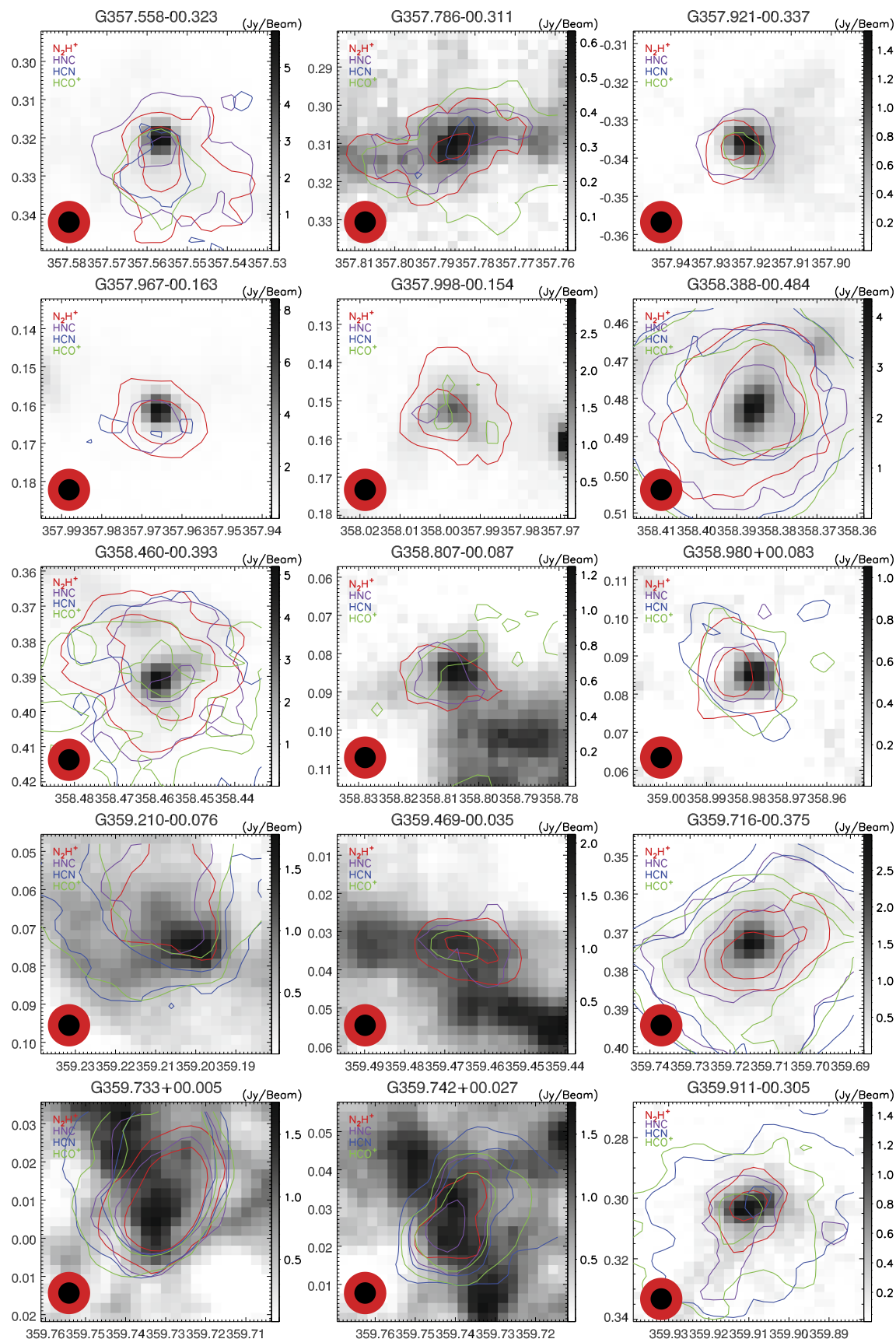
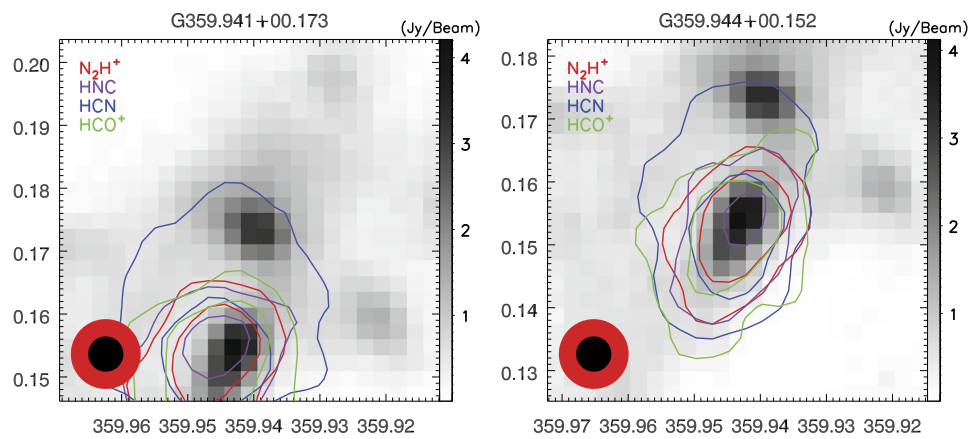
**Fig. 21** (Continued)

Fig. 21 (Continued)

Acknowledgements This research has made use of data products from the Millimeter Astronomy Legacy Team 90 GHz (MALT90) survey, the APEX Telescope Large Area Survey of the Galaxy (ATLASGAL) survey, which is a collaboration between the Max-Planck-Gesellschaft, the European Southern Observatory (ESO) and the Universidad de Chile, and also used NASA/IPAC Infrared Science Archive, which is operated by the Jet Propulsion Laboratory, California Institute of Technology, under contract with the National Aeronautics and Space Administration.

This work was funded by The National Natural Science foundation of China under grant 11433008 and partly supported by National Basic Research Program of China (973 program, 2012CB821802) and the National Natural Science foundation of China under grant 11373062 and 11303081, and The Program of the Light in China's Western Region (LCRW) under grant Nos. RCPY201202 and XBBS-2014-24.

References

- Ahrens, V., Lewen, F., Takano, S., Winnewisser, G., et al.: Z. Naturforsch. **57a**, 669 (2002)
- Benjamin, B.A., et al.: Publ. Astron. Soc. Pac. **115**, 953 (2003)
- Blackman, G.L., Brown, R.D., Godfrey, P.D., Gunn, H.I.: Nature **261**, 395 (1976)
- Botschwina, P.: Chem. Phys. Lett. **107**, 535 (1984)
- Botschwina, P., Horn, M., Flugge, J., Seeger, S.: J. Chem. Soc. Faraday Trans. **623**, 2219 (1993)
- Carey, S.J., et al.: Publ. Astron. Soc. Pac. **121**, 76 (2009)
- Caselli, P., Walmsley, C.M., Tafalla, M., Dore, L., Myers, P.C.: Astrophys. J. Lett. **523**, L165 (1999)
- Cordes, J.M., Lazio, T.J.W.: arXiv:astro-ph/0207156 (2002)
- Cyganowski, C.J., Whitney, B.A., Holden, E., et al.: Astron. J. **136**, 2391 (2008)
- Garden, R.P., Hayashi, M., Hasegawa, T., Gatley, I., Kaifu, N.: Astrophys. J. **374**, 540 (1991)
- Gerner, T., Beuther, H., Semenov, D., et al.: Astron. Astrophys. **563**, A97 (2014)
- Gutermuth, R.A., Heyer, M.: Astron. J. **149**, 64 (2015)
- Han, X.H., Zhou, J.J., Wang, J.Z., et al.: Astron. Astrophys. **576**, A131 (2015)
- Havenith, M., Zwart, E., Leo Meerts, W., Ter Meulen, J.J.: J. Chem. Phys. **93**, 8446 (1990)
- Hirota, T., Yamamoto, S., Mikami, H., Ohishi, M.: Astrophys. J. **503**, 717 (1998)
- Hoq, S., Jackson, J.M., Foster, J.B., et al.: Astrophys. J. **777**, 157 (2013)
- Jackson, J.M., Rathborne, J.M., Foster, J.B., et al.: Publ. Astron. Soc. Aust. **30**, 57 (2013)
- Lattanzi, V., Walters, A., Drouin, B.J., Pearson, J.C.: Astrophys. J. **662**, 771 (2007)
- McClure-Griffiths, N.M., Dickey, J.M., Gaensler, B.M., Green, A.J., et al.: Astrophys. J. Suppl. Ser. **158**, 178 (2005)
- Miettinen, O.: Astron. Astrophys. **562**, A3 (2014)
- Ossenkopf, V., Henning, T.: Astron. Astrophys. **291**, 943 (1994)
- Pagani, L., Daniel, F., Dubernet, M.L.: Astron. Astrophys. **494**, 719 (2009)
- Reid, M.J., Menten, K.M., Zheng, X.W., et al.: Astrophys. J. **700**, 137–148 (2009)
- Sanhueza, P., Jackson, J.M., Foster, J.B., et al.: Astrophys. J. **756**, 60 (2012)
- Schilke, P., Walmsley, C.M., Pineau des Forets, G., Roueff, E., Flower, D.R., Guilloteau, S.: Astron. Astrophys. **256**, 595 (1992)
- Schuller, F., Menten, K.M., Contreras, Y., et al.: Astron. Astrophys. **504**, 415 (2009)
- Siringo, G., et al.: Astron. Astrophys. **497**, 945 (2009)
- Tan, J.C., Beltrán, M.T., Caselli, P., et al.: Protostars and Planets VI, p. 149 (2014)
- Urquhart, J.S., Moore, T.J.T., Csengeri, T., et al.: Mon. Not. R. Astron. Soc. **443**, 1555 (2014)
- van der Tak, F.F.S., Müller, H.S.P., Harding, M.E., Gauss, J.: Astron. Astrophys. **507**, 347 (2009)
- Vasyunina, T., Linz, H., Henning, T., et al.: Astron. Astrophys. **527**, A88 (2011)
- Yamaguchi, Y., Richards, C.A. Jr., Schaefer, H.F. III: J. Chem. Phys. **101**, 8945 (1994)
- Zinnecker, H., Yorke, H.W.: Annu. Rev. Astron. Astrophys. **549**, 425 (2007)